

**Comparative Assessment of HEC-HMS 2D and HEC-RAS 2D Rain-on-Grid for  
Continuous Urban Watershed Modeling**

by

Ashmita Poudel

A thesis submitted to the Graduate Faculty of  
Auburn University  
in partial fulfillment of the  
requirements for the Degree of  
Master of Science in Civil and Environmental Engineering

Auburn, Alabama  
December 13, 2025

Keywords: Distributed hydrologic modeling, rainfall-runoff modeling, overland flow, baseflow modeling

Copyright 2025 by Ashmita Poudel

Approved by

Dr. Jose G. Vasconcelos, Chair, Professor of Civil and Environmental Engineering  
Dr. Xing Fang, Professor of Civil and Environmental Engineering  
Dr. Frances O'Donnell, Associate Professor of Civil and Environmental Engineering

## Abstract

The application of two-dimensional (2D) hydrologic and hydraulic modeling tools is increasing for overland flow simulation as they represent spatial changes in depth, velocity, and flow conditions more accurately. Recently, the US Army Corps HEC-HMS (Hydrologic Engineering Center Hydrologic Modeling System) included the capability of unstructured 2D hydrologic-hydrodynamic modeling. In parallel, HEC-RAS 2D (Hydrologic Engineering Center – River Analysis System), initially applied for river flow simulation, was adapted to include rain-on-grid (RoG) features and infiltration algorithms, providing some hydrological modeling capabilities. HEC-RAS hydrological capabilities are limited to event-based simulations as there are no provisions to represent abstractions such as evapotranspiration or groundwater/baseflow contributions. By contrast, HEC-HMS supports continuous 2D surface modeling and includes baseflow options in both semi-distributed and fully distributed configurations, albeit with simpler hydrodynamic calculation capabilities. Studies performing a direct comparison between HEC-HMS RoG and HEC-RAS RoG approaches in representing urban hydrology remain scarce. This MS thesis aims to fill that gap by assessing their performance in Moore’s Mill Creek Watershed, in Lee County, Alabama, with a focus on long-term continuous rainfall-runoff modeling. Both models run on the same unstructured mesh and use identical rainfall, terrain, land-use, and soil data. Model simulations are compared over an extended period to evaluate simulated depth, velocity, and flow hydrographs against field observations. The comparison shows HEC-HMS superior performance for extended simulation and provides practical guidance on parameter alignment, data needs, and tool selection.

## Artificial Intelligence (AI) Use Disclosure Statement

In the preparation of this thesis / dissertation, the following Artificial Intelligence (AI) tools were used: ChatGPT, Grammarly. These tools were used primarily for grammar correction. The author acknowledges full responsibility for the intellectual content of this work and has ensured that all AI-assisted sections have been reviewed and revised for accuracy and appropriate academic style. All AI-generated content was reviewed and validated for relevance, appropriateness, and accuracy before incorporation into the final document to maintain scholarly integrity of this research.

## Acknowledgments

I wanted to extend my sincere appreciation to my advisor, Dr. Jose G. Vasconcelos, for his mentorship, guidance and support throughout my Masters' journey. His continuous motivation and guidance have been crucial to my development during my master's program. I would also like to thank my committee members, Dr. Xing Fang and Dr. Frances O'Donnell, for their valuable input and suggestions on my research.

Further, I would like to thank my labmates, Michael Alexandar Bragg, Stephanie Iris Graciano Pinto and Celi Cotton, for their help with field data collection and my overall research. I also would like to thank Bruno Jose De Oliveira Sousa, Vitor Gustavo Geller, Luiz Menezes Morgado, Excie Guillot, and Stefano Duarte for their indirect support during my research at Auburn.

I want to acknowledge Alabama Department of Environmental Management (ADEM) for funding this research as a part of Moore's Mill Creek Watershed Management Plan.

Words cannot express my gratitude to my parents, whose selfless love, unconditional support, and countless sacrifices have helped me spread my wings and pursue my dreams. I am also deeply grateful to my sisters and brothers, Bindu, Gunu, Avishkar, and Bigyan, for their love and support. To my roommate, Ajeeta, I couldn't have asked for a better companion with whom to share the challenges of a new place and the beginning of my journey in this foreign land. Lastly, I would like to thank my husband, Bidhan, for his love and support.

## Table of Contents

Abstract.....	ii
Artificial Intelligence (AI) Use Disclosure Statement.....	iii
Acknowledgments.....	iv
List of Tables.....	vii
List of Figures.....	ix
List of Abbreviations.....	xii
Chapter 1: Introduction.....	1
1.1    Background.....	1
1.2    Distributed Hydrological Modeling.....	2
1.3    Objectives of Overall Studies .....	6
1.3.1    Overall Objective .....	6
1.3.2    Specific Objectives .....	6
1.4    Key Investigative Points and Thesis Summary.....	7
Chapter 2: Methodology .....	8
2.1    General Overview of the Study Area .....	8
2.2    Data Collection .....	10
2.2.1    Stream Depth Data Collection .....	11
2.2.2    Rainfall Data Collection .....	12
2.2.3    Stream Velocity Data Collection.....	13
2.3    Event Selection .....	14
2.4    External Data .....	17
2.5    Model Development.....	17
2.5.1    HEC-HMS 2D Overview .....	18
2.5.2    HEC-RAS Overview.....	28
2.6    Scenario Matrix.....	35
2.7    Sensitivity Analysis.....	36
2.8    Analysis and Statistical performance.....	38

Chapter 3: Results.....	42
3.1    HEC-HMS Results.....	42
3.1.1    Calibration Results.....	43
3.1.2    Validation Results .....	49
3.1.3    Sensitivity Analysis in HEC-HMS.....	53
3.2    HEC-RAS Results.....	65
3.2.1    Calibration Results.....	65
3.2.2    Validation Results .....	71
3.2.3    Sensitivity Analysis in HEC- RAS .....	72
3.3    Comparative Analysis between HEC-RAS & HEC-HMS RoG Simulations.....	75
3.3.1    Comparison using Deficit and Constant loss method. ....	75
3.3.2    Comparison using SCS CN loss method .....	76
3.3.3    Cumulative Volume.....	79
Chapter 4: Discussion and Limitations.....	81
4.1    Discussion .....	81
4.2    Limitations .....	84
Chapter 5: Conclusions and Recommendations .....	88
5.1    Conclusions.....	88
5.2    Recommended Future Investigations.....	89
References.....	93
Appendix A: CN Look Up Table .....	C-1
Appendix B: Python Code for Rain Data Extraction from COA.....	C-2
Appendix C: VBA Code for Error Metrics .....	C-3

## List of Tables

Table 1: Field measurement data used for HEC-HMS model calibration and validation.....	16
Table 2: Soil Types and their Available Water Storage (AWS) and Available Water Capacity (AWC) for the study area from Web Soil Survey (WSS) .....	22
Table 3: Soil Types and their saturated Hydraulic Conductivity ( $K_{sat}$ ) for the study area from Web Soil Survey (WSS).....	24
Table 4: Monthly Evapotranspiration Rate for Auburn (NOAA/National Weather Service) .....	27
Table 5: Characteristics of HEC-HMS and HEC-RAS Scenarios .....	36
Table 6: Parameters for Sensitivity Analysis in HEC-HMS .....	37
Table 7: Comparison of depth error for scenarios with and without Baseflow for Hamilton (HAM) and Bent Creek Road (BCR) monitoring sites.....	44
Table 8: Comparison of velocity error for scenarios with and without Baseflow for Hamilton (HAM) and Bent Creek Road (BCR) monitoring sites.....	46
Table 9: Comparison of Total inflow error for scenarios with and without Baseflow for Bent Creek Road (BCR) monitoring site.....	48
Table 10: Error metrics for Validation at HAM using HEC-HMS.....	49
Table 11: Error Metrics at BCR for validation period using HEC-HMS.....	51
Table 12: Comparison of Total inflow error and simulation time for different levels of parallelization in HMS Baseline Condition at Bent Creek Road (BCR) monitoring site.....	65
Table 13: Comparison of depth error for scenarios in HEC-RAS using two different solvers for Hamilton (HAM) and Bent Creek Road (BCR) monitoring sites.....	66

Table 14: Comparison of velocity error for scenarios in HEC-RAS using two different solvers for Hamilton (HAM) and Bent Creek Road (BCR) monitoring sites.....	68
Table 15: Comparison of Total inflow error for scenarios in HEC-RAS using two different solvers for Bent Creek Road (BCR) monitoring site .....	70
Table 16: Error metrics for Validation at HAM using HEC-RAS .....	72
Table 17: Error metrics for Validation at HAM using HEC-RAS .....	74

## List of Figures

Figure 1: Moores Mill Creek Watershed, AL, USA.....	8
Figure 2: Land Cover Classification of MMC .....	9
Figure 3: Monitoring Stations of MMC.....	10
Figure 4: U201-04 Level Logger (Image Source: Onset, 2025).....	12
Figure 5: Onset HOBO RG3 Rain-Gauge (Image Source: Onset, 2025).....	12
Figure 6: Stage-Velocity Rating Curve for Hamilton Bridge (HAM) .....	14
Figure 7: Selected Study Area and Monitoring Stations.....	15
Figure 8: Land Cover Classification of Study Area.....	16
Figure 9: Schematic of Basic Components of Model Development.....	18
Figure 10: Watershed Delineation in HEC-HMS.....	20
Figure 11: Coarse and Fine Mesh Representation in HEC-RAS Model.....	35
Figure 12: Comparison of Depth Hydrographs at for Calibration Period in HEC-HMS at (a) HAM and (b) BCR .....	45
Figure 13: Comparison of Velocity Hydrographs at for Calibration Period in HEC-HMS at (a) HAM and (b) BCR.....	47
Figure 14: Comparison of Total inflow Hydrographs at BCR for Calibration Period in HEC-HMS .....	48
Figure 15: Comparison of (a) Depth and (b) Velocity Hydrographs at HAM monitoring site for Validation Period in HEC-HMS.....	50
Figure 16: Comparison of (a) Depth and (b) Velocity and (c) Total inflow Hydrographs at BCR monitoring site for Validation Period in HEC-HMS.....	52

Figure 17: Sensitivity analysis of simulated Total inflow at BCR for variations in Groundwater coefficients (a) GW1 (b) GW2.....	56
Figure 18: Sensitivity analysis of simulated Total inflow at BCR for variations in Groundwater coefficients (a) GW1 (b) GW2.....	58
Figure 19: Sensitivity analysis of HEC-HMS Baseflow Parameters relative to baseline Total inflow at BCR in terms of NSE.....	59
Figure 20: Sensitivity analysis of HEC-HMS Baseflow Parameters relative to baseline Total inflow in terms of Cumulative Runoff Volume at BCR.....	60
Figure 21: Sensitivity analysis of simulated Total inflow at BCR for variations in Loss Parameter: Constant Rate.....	62
Figure 22: Sensitivity analysis of HEC-HMS Loss Parameter (Constant Rate) relative to baseline Total inflow in terms of NSE at BCR.....	63
Figure 23: Sensitivity analysis of HEC-HMS Loss Parameter (Constant Rate) relative to baseline Total inflow in terms of Cumulative Runoff Volume at BCR.....	64
Figure 24: Comparison of Depth Hydrographs for Calibration Period in HEC-RAS at (a) HAM and (b) BCR.....	67
Figure 25: Comparison of Velocity Hydrographs for Calibration Period in HEC-RAS at (a) HAM and (b) BCR.....	69
Figure 26: Comparison of Total inflow Hydrographs at BCR for Calibration Period in HEC-RAS.....	70
Figure 27: Depth and Velocity hydrographs at HAM for validation period using HEC-RAS.....	71
Figure 28: Sensitivity analysis of Mannings roughness coefficient relative to HEC-RAS baseline scenario for Total inflow in terms of change in NSE at BCR.....	72

Figure 29: Sensitivity analysis of Mannings roughness coefficient relative to HEC-RAS baseline scenario in terms of change in cumulative volume at BCR.....	73
Figure 30: Sensitivity analysis of spatial discretization to Total inflow hydrograph at BCR for RAS model.....	74
Figure 31: Comparison of Discharge Hydrograph between HEC-HMS and HEC-RAS at BCR using Deficit and Constant Loss Method.....	76
Figure 32: Comparison of (a) Depth and (b) Velocity and (c) Total inflow Hydrographs between HEC-HMS and HEC-RAS at BCR monitoring site using CN Loss Method.....	78
Figure 33: Comparison of (a) Cumulative runoff volume and (b) runoff coefficients at BCR monitoring site .....	80

## List of Abbreviations

1D	One-dimensional
2D	Two-dimensional
3D	Three-dimensional
AV	Area-Velocity
AWS	Available Water Storage
AWC	Available Water Capacity
BCR	Bent Creek Road Monitoring Station
COA	City of Auburn
CN	Curve Number
DEM	Digital Elevation Map
GIS	Geographic Information System
GW	Groundwater
GSSHA	Gridded Surface Subsurface Hydrologic Analysis (GSSHA)
HAM	Hamilton Bridge Monitoring Station
HV	Head-Velocity
HEC	US Army Corp of Engineers Hydrologic Engineering Center
HMS	Hydrologic Modeling System
RAS	River Analysis System
MMC	Moore's Mill Creek
NLCD	National Land Cover Database
NRCS	Natural Resources Conservation Service

RMSE	Root Mean Square Error
R <sup>2</sup>	Coefficient of Determination
RoG	Rain on Grid
SCS	Soil Conservation Service
SSURGO	Soil Survey Geographic Database
SWAT	Soil and Water Assessment Tool
SWMM	Storm Water Management Model
USACE	US Army Corps of Engineers
UTM	Universal Transverse Mercator
VBA	Visual Basic for Application
WSS	Web Soil Survey

# Chapter 1: Introduction

## 1.1 Background

Hydrological investigations involve understanding hydrological processes, such as rainfall, interception, infiltration, percolation, evapotranspiration, runoff, channel routing, and groundwater flow. Understanding these processes is essential for planners, engineers, decision-makers and stakeholders to evaluate how a watershed responds to various conditions, including flood risks, droughts, reservoir operations, land-use changes, urbanization, and water quality and ecosystem dynamics. Hydrological models play a critical role in representing these complex interactions within the water cycle. They support practitioners in planning, analysis, design, construction, and operation of projects that control, use, and manage water resources (USGS, 2019).

There are different types of hydrological modeling tools, which are classified based on how they represent spatial variation in their modeling domain. One such classification is lumped, semi-distributed, and distributed models (NASEM, 2023). A lumped model treats the entire basin as a single homogeneous basin and produces a single hydrograph at the outlet (Jones, 2014). They are widely used for tasks such as real-time forecasting in gauged basins and generating design flows. The parameters in these models are not directly related to the basin's physical characteristics, and they struggle when conditions depart from those of the calibration period and when spatial variability matters (Reed et al., 2004). The semi-distributed model divides the basin into smaller subbasins, where each subbasin has the lumped homogeneous parameters, and the flow is routed from one subbasin to another. These models capture heterogeneity to some extent with moderate data and computational resources (Khakbaz et al., 2012). A fully distributed model divides the

landscape into a system of grids cells, assigning modeling parameters to cell and more realistically routing excess rain across cells using physics-based equations through the basin (Kampf & Burges, 2007). The grid size is chosen to be sufficient to capture the spatial variation in land characteristics and hydrological processes. They best reflect spatial variability and are well suited to questions about land-use change, spatially varying inputs, pollutant and sediment transport, and ungauged basins (Beven, 1989; Wolff-Piggott & Gorgens, 1995). However, they require extensive data, careful parameterization, and substantial computing resources.

Similarly, another form of hydrological model classification is based on how the model distributes runoff in spatial dimensions, the most common being: one-dimensional (1D) and two-dimensional (2D) hydrological models. A 1D model is an area-averaged model that represents changes in water to flow in a single dimension, such as in a river reach, canal, or storm sewer, and is well-suited where lateral spread is minor. A 2D model is depth-averaged, representing water motion in both horizontal directions, thus is well-suited for overland flow, floodplain inundation, and spatially variable rainfall and roughness. Some integrated hydrologic models couple 2D surface flow with vertical soil and groundwater processes to represent surface–groundwater interactions, and these are generally regarded as 2D hydrologic models with subsurface routing. A comparative study by Bratton (2017) examining flood extension in a region in California, USA, found that 2D models are better suited for flood mapping and they capture flooding extents more accurately than 1D models.

## **1.2 Distributed Hydrological Modeling**

Over the past decade, distributed 2D hydrologic and hydraulic models have been increasingly used to simulate overland flow due to the availability of high-resolution topographic

data and availability of computational resources enabling the representation of distributed depths, velocities, and flow patterns (Costabile et al., 2015). Among such models, one of the widely adopted models is the Hydrologic Engineering Center – River Analysis System (HEC-RAS, 2016). It is software developed by the US Army Corps of Engineers (USACE) and was initially designed to represent river hydraulics using one-dimensional (1D) formulations. Later, in 2016, the HEC-RAS included two-dimensional (2D) unsteady flow modeling by representing structured and unstructured grid cells in a solution domain. While performing 2D computation, RAS uses either the full shallow-water equations (SWE) or a diffusion-wave (DWE) simplification that disregard local and convective accelerations in the flow routing across computational cells.

A useful feature in 2D HEC-RAS modeling is Rain-on-grid (RoG) capabilities, which applies rainfall directly to a 2D computational mesh, allowing the model to generate runoff and route it over the terrain without a separate lumped hydrological model (Costabile et al., 2021). This approach is popular because it could reduce the need for separate hydrologic calculations, particularly event-based modeling, as the 2D hydraulic model itself handles both runoff generation and flow routing. As an example, a study by Ennouini et al. (2024) for flood risk assessment in Italy showed that it yielded satisfactory results in simulating the flood extension by calibrating only a few parameters, such as Manning's roughness and an infiltration loss, when compared to hydrological models that require more parameters. However, all HEC-RAS 2D studies focus on flood inundation within a single rainfall event.

Event-based modeling tools, such as HEC-RAS 2D, represent the effects of a single rainfall-runoff event and on short-term hydrological processes, disregarding evapotranspiration, baseflow contributions, among other long-term effects. Event-based models provide estimates of

surface runoff, peak flow rates, and flood propagation, typically employing abstraction computation methods such as the NRCS Curve Number for losses and unit hydrographs in the case of lumped models (Odey & Cho, 2025). Since these models disregard long-term processes, they are comparatively less data-intensive, but also have more limited applicability since some key abstractions, such as baseflow contributions, will not be considered.

Even when applied to event-based hydrological simulations, HEC-RAS 2D has limitations stemming from the lack of baseflow representation (Bragg et al., 2025). One workaround is to combine this model with USACE's Hydrologic Engineering Center Hydrologic Modeling System (HEC-HMS) or another hydrological tool that is able to represent extended-simulation hydrology. For instance, base flows from larger watersheds obtained from semi-distributed tools such as HEC-HMS can be added to HEC-RAS 2D RoG through external boundary conditions (Fernando & Galvis, 2023; Zeiger & Hubbart, 2021).

However, in other cases, extended-period simulations are necessary. One example is the study in Colorado River Basin by Miller et al. (2016), who indicated that a significant fraction of streamflow is sustained by baseflow, which is only possible through continuous hydrological modeling. Continuous models simulate hydrologic processes over an extended period (several weeks to years) by accounting for short and long-term hydrological processes (Odey & Cho, 2025). Past research shows a trend toward continuous simulations in semi-distributed models such as the Soil and Water Assessment Tool (SWAT) and the Storm Water Management Model (SWMM) (Hossain et al., 2019; Sánchez-Gómez et al., 2024; Zhang, 2025), which include baseflow or groundwater components. Yet, some models, particularly semi-distributed models, lack the spatial detail of fully distributed physics-based models. To achieve spatial detail and long-term mass

balance, gridded and fully coupled surface–subsurface models like MIKE SHE and Gridded Surface Subsurface Hydrologic Analysis (GSSHA) are used, which couple surface flow and groundwater flow formulations (GSSHA, 2016; MIKE SHE, 2008). However, these models explicitly simulate groundwater flow and require detailed spatial characterization of subsurface properties and boundary conditions, as well as more complex calibration workflows, which can limit their use in many routine engineering and watershed-management applications. For watershed-scale studies that focus primarily on surface runoff and baseflow response at a limited number of outlets, fully distributed HEC-HMS 2D offers a more streamlined alternative, retaining distributed representation of surface processes and conceptual baseflow while avoiding the full complexity of groundwater modeling.

Semi-distributed or fully distributed models of HEC-HMS have been used for applications such as flood forecasting, drainage design, river basin planning, sediment modeling, and impact assessment due to their strong mass-balance performance (Sahu et al., 2023) . When compared to HEC-RAS 2D, the Hydrologic Modeling System (HEC-HMS 2D) is a more versatile hydrologic modeling tool as it can simulate both single-storm and continuous events. It supports the representation of key hydrological processes, including precipitation input, soil infiltration losses, evapotranspiration, canopy interception, surface depression storage, runoff generation from excess precipitation, baseflow derived from groundwater, and overland flow simulation. Recently, HEC-HMS was improved to represent 2D Diffusion Wave transform method (version 4.7 and later) (HEC-HMS User’s Manual, 2020). With this improvement, unlike older HEC-HMS models, overland flow models are directly computed with rain-on-grid (RoG) and surface flow routed through grid cells that can be imported from HEC-RAS. HEC-HMS infiltration is computed using various hydrologic loss models, some of which are able to represent extended period simulations.

Yet, there is currently limited literature exploring the new 2D Diffusion Wave approach in HEC-HMS, which uses the same 2D diffusion-wave solver as HEC-RAS on an unstructured 2D mesh to route excess precipitation from cell to cell. This method has the potential to capture nonlinear runoff processes across a basin with detailed spatial variability and continuous simulation, which forms the basis for the research question addressed in this thesis. In other words, with the improved 2D flow simulation now included in HEC-HMS 2D, it is unclear the benefits of using HEC-HMS 2D over HEC-RAS 2D to represent hydrological processes in a semi-urbanized watershed. Such comparative evaluation between these two modeling approaches is lacking in the current literature and will be explored in the next chapters.

### **1.3 Objectives of Overall Studies**

#### **1.3.1 Overall Objective**

The objective of this study is to evaluate and compare the performance and behavior of HEC-HMS and HEC-RAS RoG for simulating the hydrologic and hydraulic response of the Moore's Mill Creek watershed using observed data for continuous simulation.

#### **1.3.2 Specific Objectives**

- To calibrate and validate the HEC-HMS model using observed rainfall, depth, velocity and discharge, and to analyze how key basin parameters and loss representations affect model performance and total runoff volume compared with a baseline or calibrated configuration.
- To calibrate and validate the HEC-RAS model against observed water levels, velocities and discharges, and to quantify how choices of hydraulic roughness and grid resolution influence simulated flow rates.

- To compare HEC-HMS and HEC-RAS outputs in terms of consistency between hydrologic inputs and hydraulic response, agreement with observations, and the influence of different model setups and loss methods on cumulative runoff volumes and runoff coefficients.

## **1.4 Key Investigative Points and Thesis Summary**

The primary questions addressed by this research are:

- What is the relative performance of HEC-HMS and HEC-RAS in urban hydrological modeling using an unstructured grid?
- How can the models be calibrated to achieve reliable performance?

This thesis is organized into five chapters. Chapter 1 introduces the research background and motivation, reviews relevant literature and states the goals and objectives. Chapter 2 details the methods, including data sources and preprocessing, configuration of the fully distributed 2D HEC-RAS and 2D HEC-HMS models on a common domain, the parameter crosswalk used to ensure comparable process representations, calibration and validation procedures, performance metrics used for hydrographs analysis, sensitivity and uncertainty analyses. Chapter 3 presents the results and sensitivity analysis of individual models and direct comparisons across calibration validation events against observed data, including accuracy in depth, velocity, and flow hydrograph. Furthermore, it also presents the comparison between two models under different scenarios. Chapter 4 discusses the findings, interprets the causes of performance differences between the models, evaluates implications for engineering practice, and notes limitations. Chapter 5 concludes by answering the research questions relative to the stated research objectives, summarizing the principal contributions, offering practical recommendations for model selection and setup in fully distributed applications, and outlining directions for future work.

## Chapter 2: Methodology

### 2.1 General Overview of the Study Area

The Moores Mill Creek watershed (MMC), located in Lee County, Alabama (32.586 degrees latitude and -85.45 degrees longitude using the datum NAD83), drains approximately 29.8 square kilometers (~ 11.5 square miles) and serves as a tributary to Chewacla Creek within the larger Tallapoosa River Basin. The creek originates near the Tiger Town commercial area in Opelika, flows southwest through urban and suburban Auburn, including the Moores Mill Club golf course, and discharges into Chewacla Lake at Chewacla State Park (Figure 1). The watershed lies within the Southern Outer Piedmont ecoregion and is heavily urbanized, with roughly 35–40% of its area developed and impervious surfaces comprising up to 15%. Land cover includes a mix of residential, commercial, and forested areas (Figure 2), creating a flashy hydrologic response to rainfall (Bragg, 2025) .

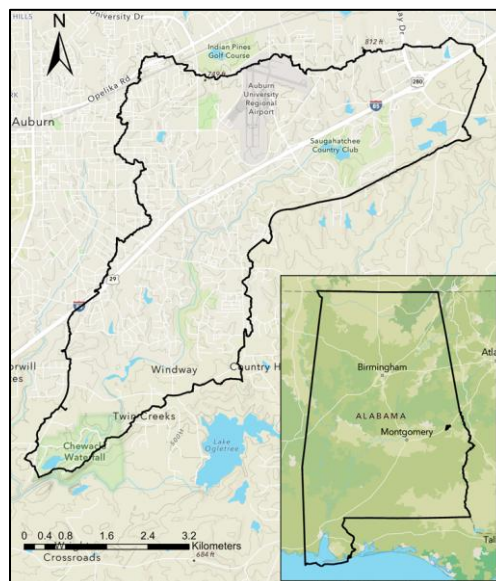
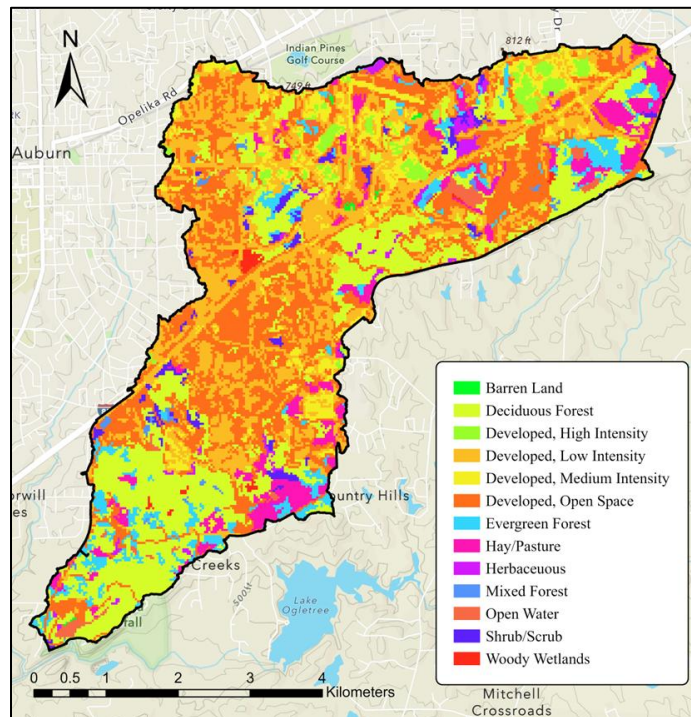


Figure 1: Moores Mill Creek Watershed, AL, USA

The creek is listed on Alabama’s Clean Water Act 303 (d) impaired waters for not meeting Swimming, Fish, and Wildlife uses due to siltation from land development and urban runoff/storm sewers (ADEM, 2024). The regional climate is humid subtropical, with a mean annual precipitation of approximately 1216 mm and a mean annual temperature of about 18 °C (64.3 °F) (US Climate Data, 2025), favoring frequent convective storms in warm seasons that drive short-duration runoff events from impervious surfaces. In response to accelerated growth in Auburn and Opelika, it is necessary to update the 2008 watershed plan (Acer, 2008) and deploy sensors across the basin to observe storm-driven water-level changes and to prioritize erosion and stormwater controls, providing up-to-date context for hydrologic modeling in this watershed. The need for the watershed management plan update, and with it a better understanding of MMC hydrology, triggered the development of the present research.



**Figure 2: Land Cover Classification of MMC**

## 2.2 Data Collection

An effective hydrological modeling study is built on a field data monitoring program. As part of the watershed management plan, the MMC watershed requires extensive data collection to support detailed hydrologic and hydraulic analyses. To facilitate this effort, different sets of data have been collected across different sections of the watershed, including rain data, stream-depth data, and velocity data. The monitoring sites for the watershed are shown in Figure 3 and detailed in the subsections below.

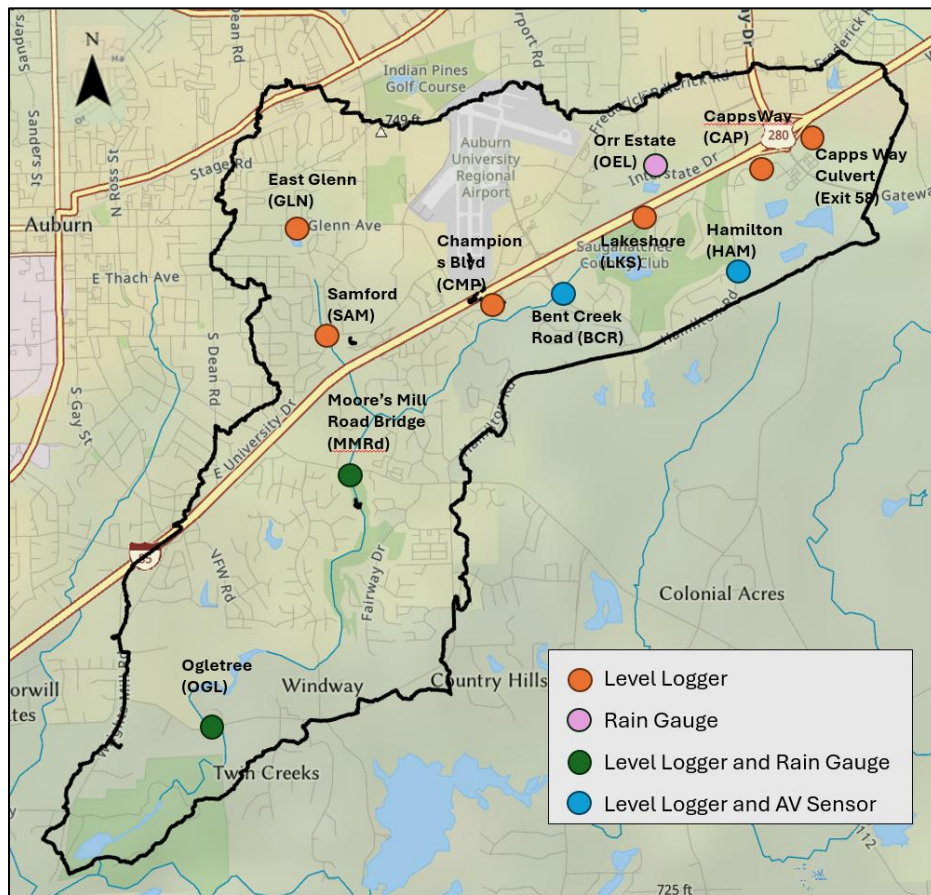


**Figure 3: Monitoring Stations of MMC**

### 2.2.1 Stream Depth Data Collection

Continuous water depth was monitored across the watershed using Onset HOBO U20L-04 pressure loggers (Figure 4) that record absolute pressure. During 2024–2025, seven loggers were deployed at different stream sites where MMC, or its tributaries, crossed a bridge or culvert. From upstream end toward the downstream end of the stream, these were the sites where stream depth data was gathered:

- Capps Way culvert (near Interstate 85N, Exit 58)
- Hamilton Bridge (HAM)
- Bent Creek Road Bridge (BCR)
- East Glenn Avenue near Prather Lake (Auburn’s tributary to MMC) (GLN)
- East Samford Avenue Bridge (Auburn’s tributary to MMC) (SAM)
- Moores Mill Road Bridge (MMRd)
- Ogletree Bridge (OGL).

All instruments were configured to record at 15-minute intervals. A separate pressure logger was installed near the Moores Mill Road Bridge to record atmospheric pressure for barometric compensation for all the in-stream level loggers. An earlier study by (Xiao, 2022) recorded data at five stations: Capps Way (CAP), Hamilton Bridge (HAM), Lakeshore Drive (LKS), Bent Creek Road (BCR), and Champions Boulevard (CMP), with atmospheric pressure recorded at Lakeshore Drive (LKS) during the 2021-2022 study period. Detailed methods for calibration and data processing are documented in prior literature on the same watershed by Bragg (2025) and Xiao (2022).



**Figure 4: U20L-04 Level Logger (Image Source: Onset, 2025)**

## **2.2.2 Rainfall Data Collection**

Rainfall across the watershed was measured using Onset HOB0 RG3 tipping-bucket rain gauges (Figure 5) that record bucket-tip events at a resolution of 0.01 in per tip (0.2 mm for the RG3-M). Gauges were deployed near the Auburn University Airport (AR) for the December 2021 to January 2022 model test period and were subsequently installed at Moore’s Mill Road (MMRd) beginning in November 2023 and near Orr Estates Lake (OEL) beginning in April 2024. Tip events were recorded and processed into 5-minute rainfall depths, which were then exported for use as model input. Detailed methods for calibration, deployment, and data processing have been documented previously for this watershed by Bragg (2025) and Xiao (2022).



**Figure 5: Onset HOB0 RG3 Rain-Gauge (Image Source: Onset, 2025)**

Sometimes, when the HOBO Onset rain gage failed to record data, for example due to battery failure or adverse weather, the missing rainfall values were infilled using data extracted from the City of Auburn online rainfall dashboard with a Python script (City of Auburn, 2025). Although the total rainfall volumes from the City of Auburn (COA) dashboard and the HOBO Onset logger were similar, the City's data showed more intense and short-lived rainfall bursts. However, no City of Auburn rainfall data was used in this study. A Python script developed to extract data for Lake Ogletree at 5-minute intervals from COA is included in the Appendix.

### **2.2.3 Stream Velocity Data Collection**

One Teledyne Isco 2150 area-velocity sensor based on Doppler detection of suspended particles velocity in the water was used. The goal was to measure stream velocity and depth in order to develop rating curves (i.e., relating depth and velocity/flow rates). The sensor was deployed in different field monitoring sites, with the locations and dates for the deployments being:

- Capps Way from November to December 2024
- Hamilton Bridge from December 2024 to January 2025
- Bent Creek from January to April 2025
- East Glenn Avenue since September 2025

Pressure was recorded and converted to depth, and along with recorded velocity. Details of the instrument model and calibration procedures have been documented previously for this watershed by Bragg (2025). Depth and velocity data at each station were processed to develop site-specific stage–velocity rating curves. For illustration, the relationship obtained for the Hamilton site is shown in Figure 6 and was used in subsequent analyses and in comparison with

the hydrological model outputs. Discharge at the monitoring locations was estimated as the product of velocity measured with the AV sensor and cross-sectional area surveyed in the field using a measuring tape. However, these rating curves should be viewed as an approximate attempt to describe the stage–velocity relationship. They are based on a limited number of measurements collected under specific flow conditions, and they are affected by uncertainties in depth, AV sensor velocity readings, and cross-section measurements. As a result, the curves may contain inaccuracies, especially when extrapolated beyond the range of observed data, and the associated discharge estimates should be interpreted with these limitations in mind.

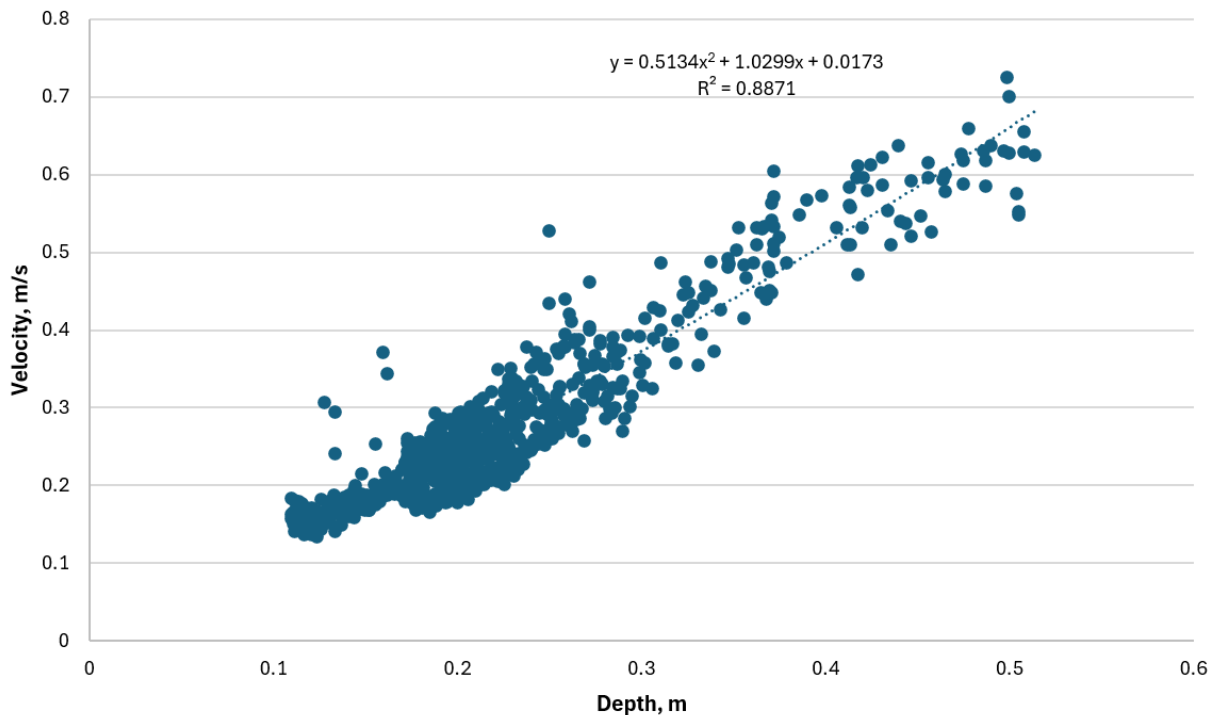


**Figure 6: Stage-Velocity Rating Curve for Hamilton Bridge (HAM)**

### 2.3 Event Selection

This research focused on the upper one-third of the MMC watershed (Figure 7), which includes a mix of land uses: developed, forested, barren, and woody wetlands (Figure 8). The

subarea encompasses parts of Opelika and a small portion of Auburn. Its area is approximately 8 square kilometers (3 square miles). Predominant soils are sandy loam, which confers moderate infiltration capacity and influences storm-event response. A prominent feature that may affect local hydrology and sediment supply is the Interstate 85 (I-85N) crossing. Other prominent sites include the Tiger Town shopping center and Saugahatchee Country Club.

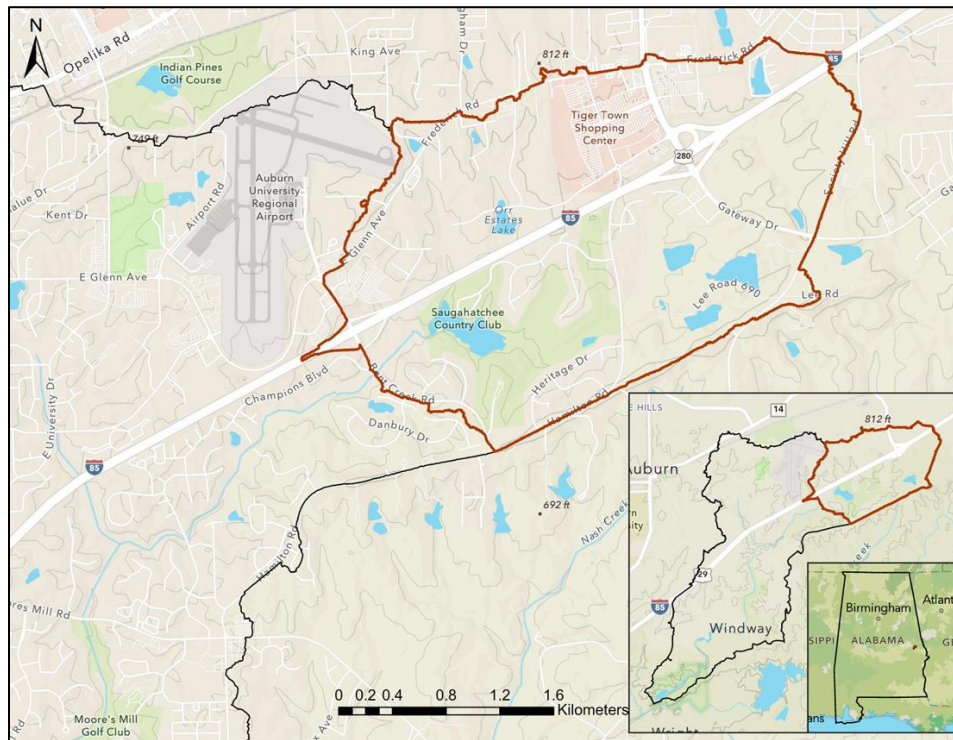


**Figure 7: Selected Study Area and Monitoring Stations**

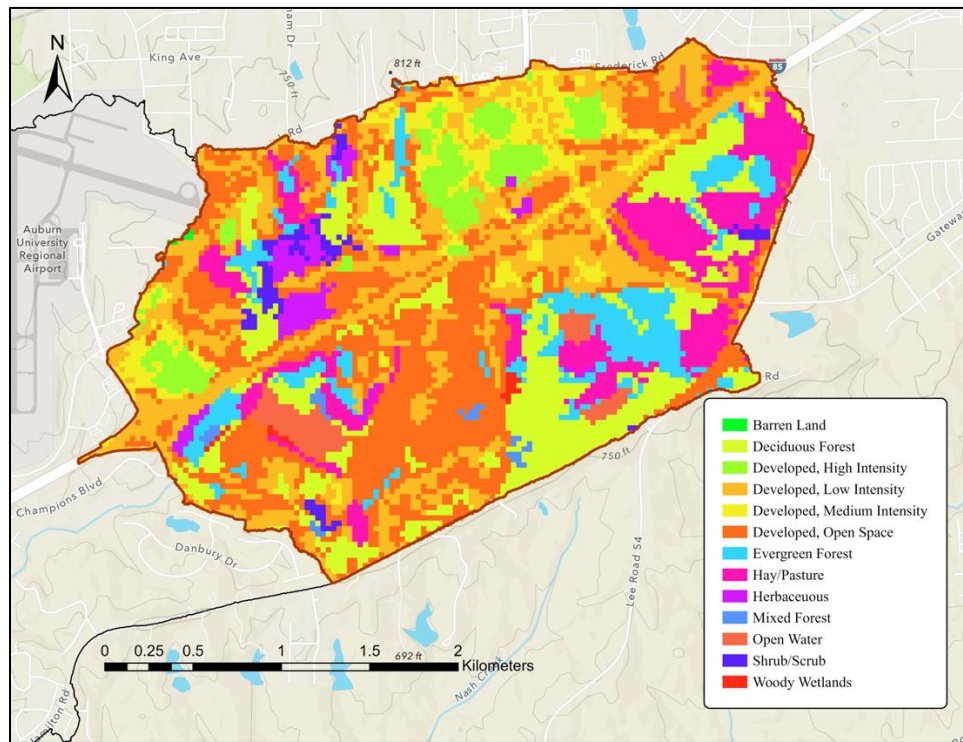


**Figure 8: Land Cover Classification of Study Area**

The monitoring stations and rainfall inputs used for the calibration and validation of the HEC-HMS hydrological models are listed in Table 1.

**Table 1: Field measurement data used for HEC-HMS model calibration and validation**

<b>Station</b>	<b>Parameter</b>	<b>Rain Events selected for Calibration (Rain Gauge Station)</b>	<b>Rain Events selected for Validation</b>
Hamilton Bridge (HAM)	Depth and Velocity	Dec 2021-Jan 2022 (Airport Rain Gauge (AR))	Dec 2024-Jan 2025
Bent Creek Road (BCR)	Depth, Velocity, and Discharge	Dec 2021-Jan 2022 (Moore’s Mill Road Rain Gauge (MMRd))	Mar 2025-Mar 2025

The choice of the validation rainfall event is guided by using stations equipped with AV sensors so that depth and velocity are measured at the same cross-section. By contrast, the earlier calibration used a stage-velocity curve derived at a location slightly offset from the HOBO logger deployments.

## **2.4 External Data**

For the development of HEC-HMS and HEC-RAS model, external datasets that were used in this study include, a digital elevation model (DEM) of 1 m resolution, obtained from the USDA Geospatial Data Gateway (USDA, 2025), which provided the underlying topography for basin delineation, flow direction analysis and generation of the 2D rain-on-grid computational mesh. The City of Auburn (COA) high contrast basemap was used to refine the stream network extracted from the DEM and to locate smaller channels and culvert crossings that are not clearly represented in the elevation data (City of Auburn Map, 2025). Soil information was derived from the gSSURGO database (USDA 2024), which provided hydrologic soil groups and associated soil properties. Land-use and land-cover information was taken from the National Land Cover Database (NLCD) (USGS 2024) to assign spatially distributed hydrologic parameters such as surface roughness and representative loss characteristics, along with soil data, for each grid cell.

## **2.5 Model Development**

In this study, numerical models were developed to represent the rainfall-runoff response of the Moore's Mill Creek Watershed and to evaluate the two-dimensional rain-on-grid simulations in HEC-HMS and HEC-RAS software. The quick overview of the model development is summarized in Figure 9 and will be explained in detail in subsequent subsection.

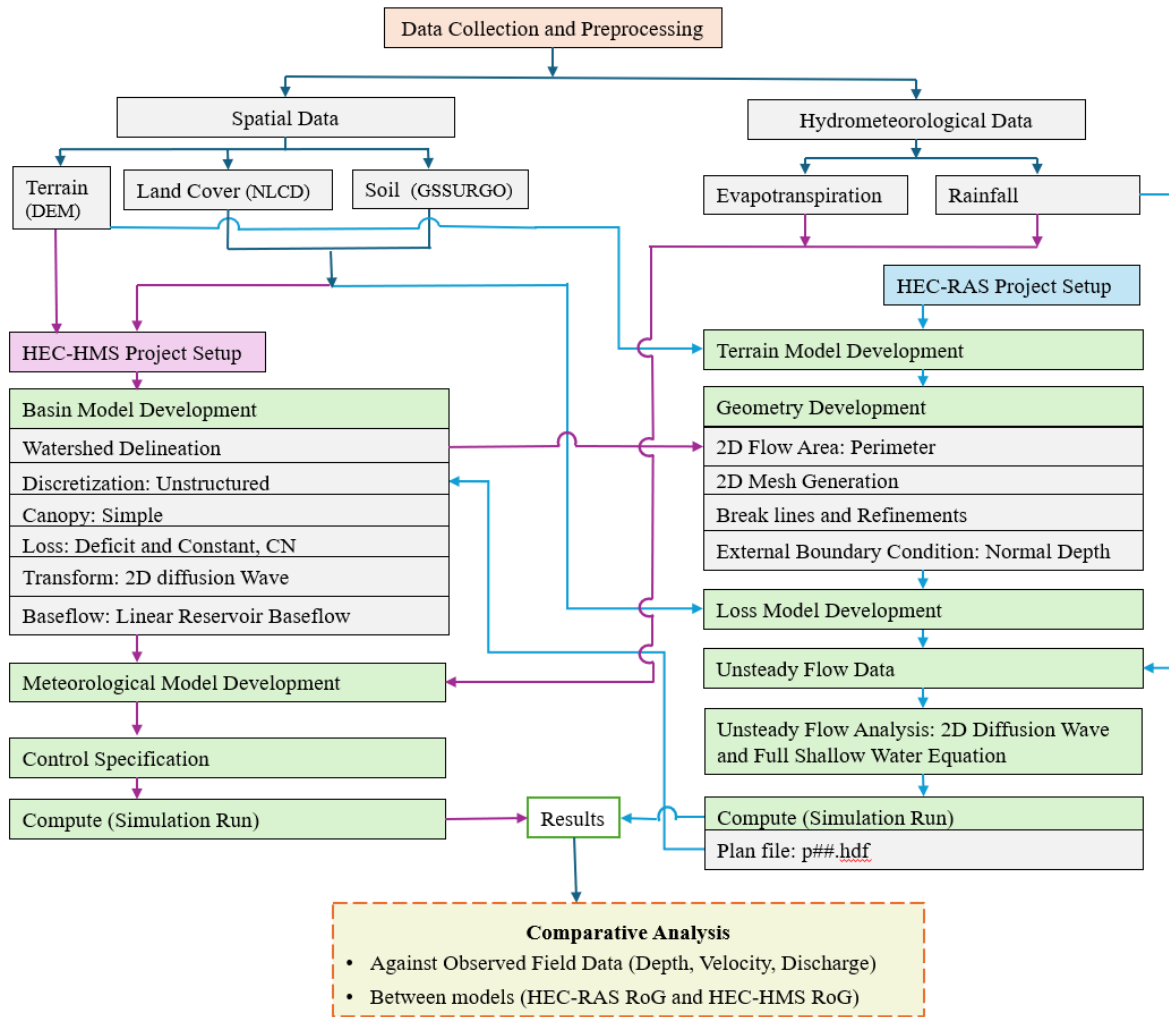


**Figure 9: Schematic of Basic Components of Model Development**

### 2.5.1 HEC-HMS 2D Overview

For this study, HEC-HMS Version 4.12 was used to simulate hydrologic responses to rainfall events in MMC. Like other hydrological models, this model can simulate the rainfall-runoff process by including precipitation, losses, routing, baseflow, canopy, surface, and parameter estimation in its package, focusing on overall water balance (Singh & Jain, 2015). Key inputs include the terrain elevation (DEM) to define the topography and watershed boundaries,

hyetograph time series to throw the precipitation in the area, and land and soil data to assign roughness and loss parameters.

In this study, rainfall–runoff transformation and overland flow routing were simulated using the two-dimensional (2D) rain-on-grid capabilities of HEC-HMS, which solve a simplified form of the shallow-water (diffusion wave) equation (Section 2.5.2, Equation 7) on an unstructured computational mesh. The model was developed to represent the combined effects of surface runoff generation, losses, 2D flow routing over the terrain, evapotranspiration, and groundwater release under continuous simulation. The precipitation model in a software package supplies rainfall to the catchment, while the loss method allows a portion of this rainfall to infiltrate into the soil and computes the remaining excess. The 2D transform method then routes the excess precipitation as overland flow across the unstructured grid to the outlet. Infiltrated water contributes to subsurface storage, from which the baseflow method releases groundwater as delayed flow to the surface. The canopy method, coupled with the evapotranspiration method, extracts water from canopy and soil storage, allowing soil moisture to recover and vary realistically between storm events.

HEC-HMS requires three basic model components to run a simulation: Basin Model, Meteorologic model, and Control Specification. Careful parameterization is important to ensure physically consistent runoff generation and routing. For brevity, only the elements of the model development that are specific to this study are described here; full details of the underlying numerical formulation and default process representations can be found in the HEC-HMS Technical Reference Manual (2024).

### 2.5.1.1 HEC-HMS Basin Model Development

**Watershed delineation:** Basin model represents the physical description of the watershed. To develop it, the DEM was hydro-conditioned at culvert locations crossing I-85 road using ArcGIS Pro (Desktop 10.3.2), the location of which was confirmed from COA maps. The hydro-conditioned DEM was then imported into HEC-HMS to create the terrain model. The GIS tools in HEC-HMS were used to set the projection system to UTM Zone 16N for the study area. The basin model was linked to the terrain model, and the Preprocess Sink tool was used to fill the minor depressions in the terrain. The Preprocess Drainage tool was used to compute flow accumulation and flow direction for each grid cell in the terrain raster data. The Identify Streams tool was used to generate the stream network. The Break Point Creation tool was used to create the outlet point at the Bent Creek Road (BCR) monitoring station. Then, the Delineate Elements tool was used to delineate the watershed boundaries. Multiple subbasins generated after delineation were merged into a single basin, and all reach elements were deleted to set up the model for a fully overland-flow condition, with a basin and outlet junction, as shown in Figure 10.

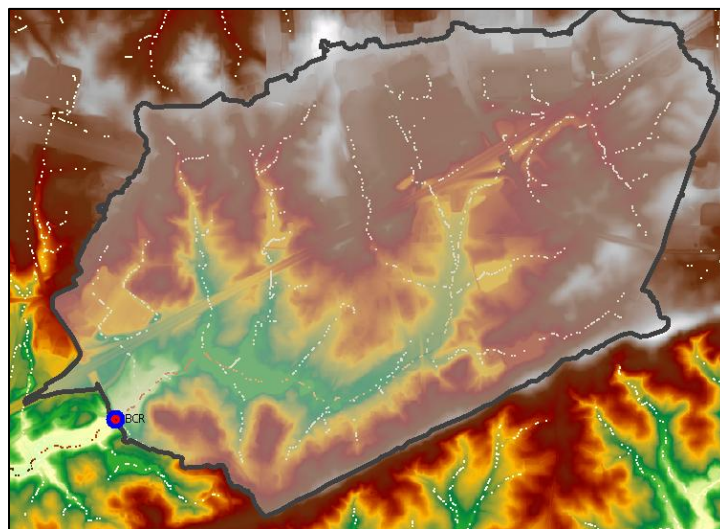


**Figure 10: Watershed Delineation in HEC-HMS**

**Estimation of Loss Parameters:** HEC-HMS version 4.12 includes the following loss methods: Deficit and Constant, Exponential, Green and Ampt, Gridded Deficit and Constant, Gridded Green and Ampt, Gridded SCS Curve Number, Gridded Soil Moisture Accounting, Initial and Constant, Layered Green and Ampt, Linear Deficit and Constant, SCS Curve Number, Smith Parlange, and Soil Moisture Accounting. Among these, methods suitable for continuous simulation include Deficit and Constant (and its gridded form), Soil Moisture Accounting (and its gridded form), Layered Green and Ampt, and Linear Deficit and Constant; by contrast, Gridded Green and Ampt and Gridded SCS Curve Number are recommended for event-based applications (HEC-HMS Technical Guide, 2024).

This study uses the Deficit and Constant method as the primary loss representation for HEC-HMS RoG because the objective is to evaluate the continuous simulation performance of HEC-HMS RoG against HEC-RAS. The choice also maintains consistency with HEC-RAS RoG infiltration options, which include SCS Curve Number, Green and Ampt, and Deficit and Constant.

The SCS Curve Number method, although designed for event-based, is widely used in hydrologic practice because it is relatively simple and less data intensive (Fanta & Tadesse, 2022). In this study, SCS Curve Number is therefore applied only in supplementary simulations as an alternative loss formulation to examine how the model behaves under a widely used, event-based loss method, rather than as the main continuous loss method.

**Deficit and Loss parameter estimates:** For the Deficit and Constant loss method in HEC-HMS, four parameters are required: maximum deficit, initial deficit, impervious percentage, and constant loss rate. Each subbasin uses one parameter set for loss computation. Since this study involved a single subbasin, one parameter set was estimated. The maximum deficit and constant rate were

derived from NRCS Web Soil Survey (WSS) data by importing the basin shapefile into WSS and examining soil physical properties (Web Soil Survey, 2025). The soils within the study area were identified as sandy loam, loamy sand, and silt loam. The maximum deficit was calculated following the approach outlined in the HEC-HMS Technical Reference Manual (2025), which defines it as (Equation 1),

$$\text{Maximum Deficit} = (\text{Effective Porosity} - \text{Wilting Point}) \times \text{Soil Depth} \quad (1)$$

Soil depth was estimated using Available Water Storage (AWS) and Available Water Capacity (AWC) attributes from WSS, where AWS represents the equivalent depth of plant-available water in the soil profile (cm), and AWC is the ratio of available water per unit soil depth (cm/cm) (Web Soil Survey, 2025). Soil depth was computed as:

$$\text{Soil Depth} = \frac{\text{Available Water Storage (AWS)}}{\text{Available Water Capacity (AWC)}} \quad (2)$$

Available Water Storage and Available Water Capacity were calculated as weighted averages of predominant soil types (>10%) across the entire basin.

**Table 2: Soil Types and their Available Water Storage (AWS) and Available Water Capacity (AWC) for the study area from Web Soil Survey (WSS)**

Soil Type	AWS (cm)	AWC (cm/cm)	Percent Area
Blanton loamy sand, 0 to 5 percent slopes	16.46	0.10	0.5%
Cartecay silt loam, 0 to 1 percent slopes	20.87	0.11	5.1%
Marvyn loamy sand, 6 to 10 percent slopes	22.76	0.12	0.5%
Orangeburg loamy sand, 1 to 6 percent slopes	18.63	0.11	0.6%

Pacolet sandy loam, 1 to 6 percent slopes	13.32	0.13	16.6%
Pacolet sandy loam, 6 to 10 percent slopes	21.00	0.14	56.8%
Pacolet sandy loam, 10 to 15 percent slopes	14.17	0.13	5.0%
Pacolet-Urban land complex, 1 to 10 percent slopes	14.40	0.13	0.2%
Pits			0.1%
Toccoa sandy loam, 0 to 2 percent slopes, frequently flooded	22.33	0.11	0.8%
Uchee loamy sand, 0 to 6 percent slopes	22.58	0.11	6.1%
Uchee loamy sand, 6 to 10 percent slopes	18.21	0.11	3.6%
Water			4.0%

$$AWS = \frac{56.8 * 21 + 16.6 * 13.32}{56.8 + 16.6} \text{ cm} * 10 * \frac{\text{mm}}{\text{cm}} \approx 193 \text{ mm}$$

$$AWC = \frac{56.8 * 0.14 + 16.6 * 0.13}{56.8 + 16.6} \frac{\text{cm}}{\text{cm}} \approx 0.14 \frac{\text{mm}}{\text{mm}}$$

Therefore, the approximate soil depth was calculated using equation 2 from AWS and AWC.

Since the predominant soil type was sandy loam, the effective porosity and wilting point were estimated according to the methodology described in the HEC-HMS Tutorials and Guide for sandy loam as 0.41 and 0.1, respectively. Maximum deficit was then approximated using equation 1.

The constant rate was estimated from the saturated hydraulic conductivity ( $K_{\text{sat}}$ ) parameter from WSS using area-weighted values for the predominant soils in the study area.

**Table 3: Soil Types and their saturated Hydraulic Conductivity ( $K_{sat}$ ) for the study area from Web Soil Survey (WSS)**

Soil Type	$K_{sat}$ ( $\mu\text{m/s}$ )	Percent Area
Pacolet sandy loam, 1 to 6 percent slopes	11.7941	16.6%
Pacolet sandy loam, 6 to 10 percent slopes	10.0000	56.8%

$$\text{Constant rate} = \frac{56.8 \times 10 + 16.6 \times 11.79}{56.8 + 16.6} \times 10^{-3} \times 3600 \approx 37.5 \text{ mm/hr}$$

Percent imperviousness was estimated from the NLCD Percent Imperviousness grid, consistent with prior studies by Bragg et al. (2025) for overland flow, by performing an area-weighted summary in ArcGIS Pro. The initial deficit parameter was the calibrated variable, adjusted until the simulated hydrograph peak and volume matched the observed hydrograph.

**SCS Curve Number (CN) Estimation:** CN values were obtained from earlier studies on the same watershed by Xiao and Vasconcelos (2022). A CN lookup table is provided in the dissertation Appendix A.

**Estimation of Baseflow Parameters:** For this study, the Linear Reservoir Baseflow Method was used because it was compatible with the 2D diffusion wave transform method through either a baseflow or an interflow. Parameterization comprised the number of groundwater layers, specification of discharge per unit area, partition fractions to allocate percolation among layers with any remainder treated as deep aquifer recharge and a groundwater storage coefficient (hours) for each layer and the number of routing steps that control attenuation.

Initial values were assigned by setting the “initial discharge per unit area” to the observed pre-event flow per drainage area of the basin, selecting two layers to represent a faster interflow

(GW1) and a slower baseflow (GW2), choosing preliminary partition fractions consistent with these roles, and starting with a single routing step. Storage coefficients were then estimated from the observed hydrograph recession behavior using the equation for watershed storage (Clark, 1945),

$$O(t) = C_a I(t) + C_b O(t - 1) \quad (3)$$

Where,

$$C_a = \frac{\Delta t}{R + 0.5\Delta t}, C_b = 1 - C_a = \text{Routing Coefficients}$$

$O(t)$  = Ordinate of outflow hydrograph at time  $t$

$O(t - 1)$  = Ordinate of outflow hydrograph at time  $t - 1$

$I(t)$  = Ordinate of inflow hydrograph at time  $t$

$R$  = Storage Coefficient for linear reservoir

$\Delta t$  = Time interval for which the hydrograph is defined

Calibration proceeded manually by jointly adjusting the baseflow parameters and evaluating fit against observed discharge hydrograph using the Nash–Sutcliffe efficiency (NSE) as the sole objective function, as defined in Section 2.8. Groundwater coefficients, reservoir fractions, and routing steps were iteratively refined until NSE indicated satisfactory performance and the simulated baseflow timing, volume, and recession behavior visually matched observations. Coefficient of Determination ( $R^2$ ) and Root Mean Square Error (RMSE), as defined in Section 2.8, were calculated for post-calibration model evaluation.

**Canopy:** The Simple Canopy method was used because of its simplicity and fewer parameters.

**Transform:** The 2D Diffusion Wave method was used for this study because of its suitability to be applied to unstructured grids to simulate distributed surface runoff.

### **2.5.1.2 HEC-HMS Meteorological Model Development**

The meteorological model in HEC-HMS serves to define the time-varying atmospheric inputs to the basin model, including precipitation, temperature, wind speed, pressure, dew point, and evapotranspiration (HEC-HMS User's Manual, 2024). For each of these meteorological variables, different specification methods can be selected in HEC-HMS. There are eight different ways to assign the precipitation. In this study, the Specified Hyetograph method was used due to the available data format. The basin was set to the precipitation time series data created in the Time Series Manager for the precipitation gauges. Three precipitation series were created: one for calibration, one for validation at Hamilton (HAM), and one for validation at Bent Creek Road (BCR). The precipitation time series was sampled at 5-minute intervals. Wind speed, pressure, and dew point were set to None because they were not a concern for this research study. For evapotranspiration, the Monthly Average method was used for its simplicity and data availability compared to other empirical approaches. Furthermore, previous simulations without explicit calibration using the Monthly Average Method produced satisfactory results in terms of hydrograph behavior for our study area. Hence, it is chosen over widely used Penman Monteith method, which is less parsimonious and requires many meteorological boundary conditions (HEC-HMS Technical Reference Manual, 2025). The monthly evapotranspiration rate was assigned from 20-year pan evaporation averages for the Auburn site (Southeast Ag Weather Service Center, Auburn University) (Table 4), and the crop coefficient was assumed to be 1 for simplicity. The evapotranspiration method was included in the continuous simulation for this study because it

represents the mechanism by which infiltrated water is returned to the atmosphere from the canopy and the surface in the chosen Deficit and Constant loss method.

**Table 4: Monthly Evapotranspiration Rate for Auburn (NOAA/National Weather Service)**

<b>Month</b>	<b>Rate (MM/MONTH)</b>
January	51.3
February	68.3
March	115.8
April	154.6
May	186.4
June	195.8
July	181.1
August	165.1
September	143.0
October	111.7
November	73.4
December	51.8

### **2.5.1.3 HEC-HMS Control Specifications Development**

Control Specifications are required to define the simulation time window. Three Control Specifications were created for this model: the calibration set from December 26, 2021 to January 26, 2022, the validation at HAM from December 24, 2024 to January 23, 2025, and the validation set for BCR from Mar 3, 2025 to Mar 21, 2025, each using a 15-minute computation interval and

covering the full period of the rain series. Each period was selected to include at least three substantial storm events with continuous rainfall values, and stream depth observations at both stations. A Simulation Run was configured and linked to the created Basin Model, Meteorological Model, and Control Specifications, and Spatial Results were enabled at a 15-minute interval.

Calibration efforts in HEC-HMS included manually adjusting the baseflow parameters (groundwater fractions and coefficients) and evaluating model fit against observed discharge using NSE. Loss-parameter adjustments were made during the HEC-RAS calibration, discussed in the next section, by refining the initial values estimated in Section 2.5.1.1. The parameters calibrated in HEC-RAS were kept the same in HEC-HMS. No canopy parameters were modified in this study.

## 2.5.2 HEC-RAS Overview

For this study, HEC-RAS Version 6.3.1 was used to simulate hydrologic responses in MMC. HEC-RAS is a physics-based hydraulic model that solves the one-dimensional or two-dimensional Saint-Venant equations or shallow water equations for unsteady open-channel flow. In the two-dimensional formulation, the model applies a finite-volume scheme on an unstructured computational mesh, where each cell represents a control volume over which mass and momentum are conserved (HEC-RAS Hydraulic Reference Manual, 2025).

The depth-integrated continuity, or mass conservation, equation for a control volume  $\Omega$  can be written in integral form as Equation 4 (HEC-RAS Hydraulic Reference Manual, 2025),

$$\frac{\partial}{\partial t} \iiint_{\Omega} d\Omega + \iint_s (V \cdot n) dS = Q \quad (4)$$

where the first term represents the rate of change of water volume within the cell, the second term represents fluxes across cell faces, and  $Q$  denotes external sources and sinks. In the finite-volume discretization used by HEC-RAS, this equation becomes (Equation 5),

$$\frac{\Omega_i^{n+1} - \Omega_i^n}{\Delta t} + \sum_{k \in K(i)} (V_k \cdot n_{ik}) A_k = Q_i \quad (5)$$

Where,

$\Omega_i$  = the water volume in cell  $i$ ,

$\Delta t$  = the time step,

$A_k$  = the area of face  $k$ ,

$v_k$  = the face-normal velocity,

$n_{ik}$  = the outward face-normal unit vector, and

$Q_i$  = the net source or sink in cell  $i$ .

Momentum conservation is expressed through the depth-averaged shallow water momentum equation in the form of Equation 6 (HEC-RAS Hydraulic Reference Manual, 2025),

$$\frac{\partial V}{\partial t} + (V \cdot \nabla)V + f_c k \times V = -g \nabla z_s + \frac{1}{h} \nabla \cdot (v_t h \nabla V) - \frac{\tau_b}{\rho R} + \frac{\tau_s}{\rho h} \quad (6)$$

Where,

$V$  = the depth-averaged velocity vector,

$f_c$  = the Coriolis parameter,

$k$  = the vertical unit vector,

$g$  = gravitational acceleration,

$z_s$  = water-surface elevation,

$h$  = flow depth,

$\nu_t$  = the horizontal eddy viscosity,

$\tau_b$  and  $\tau_s$  = bed and wind shear stresses,

$\rho$  = water density, and

$R$  = hydraulic radius.

The terms on the left-hand side of equation 6 represent temporal, advective, and Coriolis accelerations, and the terms on the right-hand side represent pressure gradient, internal momentum diffusion, bed friction, and wind stress, respectively.

Unlike HEC-HMS, which can solve only 2D diffusion wave equations, HEC-RAS can use either the full shallow water equations or a simplified diffusion wave formulation to simulate surface water dynamics across a flexible computational mesh. The diffusion wave equation is obtained by neglecting the local and advective acceleration terms, the Coriolis term, and momentum diffusion, and by expressing velocity in terms of the water-surface gradient using a Mannings relationship. Substituting this velocity expression into the continuity equation yields a diffusion-wave equation of the form (Equation 7) (HEC-RAS Hydraulic Reference Manual, 2025),

$$\frac{\partial h}{\partial t} = \nabla \cdot (\beta \nabla z_s) + q \quad (7)$$

Where,

$\beta$  = hydraulic coefficient that depends on depth, roughness, and slope, and

$q$  = external sources and sinks.

In HEC-RAS, the diffusion wave formulation is the default two-dimensional solver, although the full shallow water equations can be activated when acceleration and dynamic wave effects are important. In this study, the diffusion wave solver was selected to represent overland and channel flow on the two-dimensional rain-on-grid mesh.

A 2D grid model divides the terrain into small computational elements called grid cells. For development of 2D rain-on-grid models in HEC-RAS, the model requires comprehensive geometric data, boundary and unsteady-flow data, plan data, and supporting GIS layers such as terrain, land cover, and soils. The geometric data defines the physical system and computation grid, including the 2D flow area, mesh, breaklines, and roughness zones, which control where and how water can move. The unsteady-flow data provide time-varying inputs such as inflow hydrographs, stage levels, and rainfall applied over the grid, which drive the runoff response. Downstream boundary conditions (e.g. normal depth) are also required to define how water exits the model domain. The plan data link a specific geometry with specific unsteady-flow data and set the simulation period and numerical options, controlling how the model is executed. GIS layers, including terrain, land cover, and soil maps, supply elevations, surface roughness, and infiltration parameters, which determine how rainfall is partitioned between infiltration and runoff and how that runoff is routed across the landscape. Each grid cell is assigned elevation data, hydraulic properties, such as Manning's roughness coefficient from underlying DEM, Land cover and soil layer.

### 2.5.2.1 HEC-RAS Model Development

HEC-RAS RoG model development involved the use of same DEM used in HEC-HMS 2D configuration for basin model development. In addition to this, to facilitate the infiltration modeling in HEC-RAS, NLCD Land Cover and GSSURGO soil data were used. The same precipitation time series used in the meteorological model development in HEC-HMS was used to set up unsteady flow data.

First, the same hydro conditioned DEM from 2.5.1.1 was imported to RAS Mapper for mesh generation. The watershed boundary obtained from the prior basin delineation in HEC-HMS was used to define a 2D flow area for catchment. The basin was then discretized into a grid size of 60 m × 60 m because earlier research done on the same watershed by Bragg et al. (2025) showed a satisfactory result in this mesh size. The mesh was further refined at complex locations such as ridges, stream centerlines, and lake boundaries to preserve flow paths and elevation gradients. Breaklines and local refinements with target cell sizes between 10 and 20 m were applied, resulting in a total of approximately 15,000 cells. Each cell is characterized by detailed elevation–volume and elevation–area relationships precomputed from the terrain. Land Cover Data from NLCD was incorporated to parameterize spatially varying surface roughness and imperviousness, the values were assigned based on NLCD recommendations in the HEC-RAS User Manual.

The infiltration layer was created using the Land Cover and Soil Layer for the Deficit and Constant Loss method, to make an identical loss for both models. For each land cover type and soil group, the same loss parameters were assigned for the entire basin. This is because HEC-HMS supports a single value per basin for each parameter in a current model setup.

Precipitation time series for the same time interval as HEC-HMS were uniformly applied over the 2D mesh. A downstream external boundary condition was defined to represent the watershed outlet. A normal depth was set with a friction slope value assigned using the measurement tool in Ras Mapper near the watershed outlet. In this study, no internal boundary condition was added to create a model similar to HEC-HMS, as the HEC-HMS 2D framework currently does not support them. To establish initial water levels and simulate the first peak in the stream, an artificial rainfall of 30 mm was added to both HEC-HMS and HEC-RAS models prior to four days of the storm based on methodology adopted in HEC-HMS Tutorials and Guide because earlier simulation results showed poor response to first peak.

The HEC-RAS 2D model was run using the Diffusion Wave equation to maintain consistency with the HEC-HMS 2D approach. A maximum Courant number of 1 and a computational time step of 10 seconds were used, and the model was simulated continuously for one month. Calibration requirements were minimal and involved adjusting the initial deficit parameter, maximum deficit parameter, modifying Manning's roughness, and refining breaklines near critical locations while keeping all other parameters constant. Manning's roughness values were increased or decreased by 10 percent until the simulated peaks and the depth and velocity hydrographs aligned closely with observations. In addition, terrain adjustments were made using the Terrain Modification Tool to correct areas which caused unrealistic water retention, even though the prominent features like culverts and bridges had already been burned into the terrain in ArcGIS Pro. Furthermore, because the original DEM did not include bathymetry for the ponds, terrain elevations were lowered using the Terrain Modification tool in HEC-RAS to represent the pond and lake bottoms.

The resulting model gave a plan file with p###.hdf format which was then exported to previously developed HEC-HMS model using deficit and loss method for simulation in fully distributed setup. These two models in HEC-RAS and HEC-HMS served as baseline or calibrated model. It is important to note that all the common parameters between the two models were kept similar to maintain consistency, including loss parameters, mesh configuration, Mannings roughness and impervious percentage.

Furthermore, to assess the impact of HEC-RAS parameters on hydrologic outputs, two tests were conducted. First, the calibrated model was re-simulated using the full shallow water equation solver while keeping all other parameters constant. Second, the effect of average grid-cell size on overland flow was evaluated by comparing simulations with 60 m and 120 m cells as shown in Figure 11. These grid sizes refer only to the overland mesh and do not apply to the refined cells used to represent stream channels, culverts, and other conveyance features. Third, the calibrated model was run for the SCS CN infiltration method, with the same values as mentioned earlier in HEC-HMS Section 2.5.1.1. These scenarios were then compared with the baseline model. The characteristics of all scenarios created in HEC-RAS and HEC-HMS are summarized in the next section.

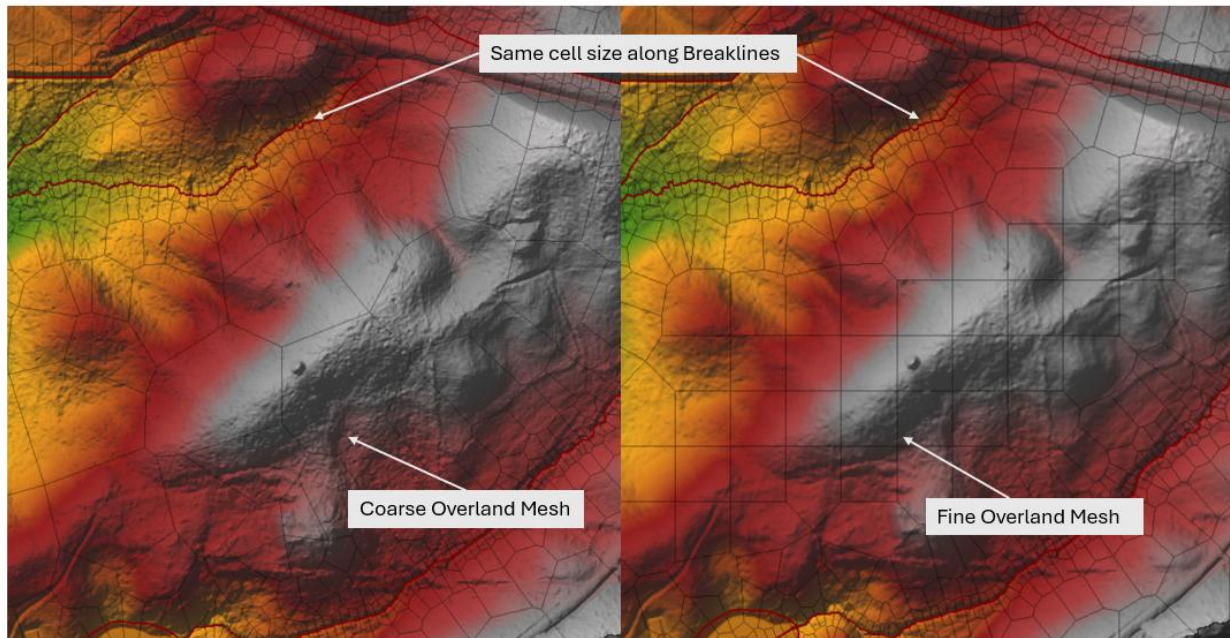


**Figure 11: Coarse and Fine Mesh Representation in HEC-RAS Model**

## 2.6 Scenario Matrix

To evaluate the effect of model structures in assessing the hydrologic and hydraulic behavior in a watershed, seven scenarios were defined by combining alternative loss methods, baseflow settings, and transform methods. The scenarios are labeled according to the modeling software (HEC-HMS or HEC-RAS), the presence of baseflow (BF), the loss method (Deficit and Constant or SCS CN), and the transform method (2D Diffusion Wave or Full Shallow Water Equation), and grid size (coarse or fine). Table 5 summarizes the configuration of each scenario.

Scenarios HMS - No BF and HMS - BF represent the baseline HMS configurations using the Linear Deficit and Constant loss method, with and without baseflow. Scenarios HMS - No BF - CN and HMS - BF - CN are included to examine how the SCS CN loss method alters model behavior when applied to the same grid and rainfall inputs. The RAS, RAS - SWE, RAS - CN and

RAS – Low Resolution scenarios broaden the evaluation by testing alternative solvers, loss formulations and grid sizes in HEC-RAS, supporting this thesis objective of comparing model performance under different hydrologic and hydraulic assumptions.

**Table 5: Characteristics of HEC-HMS and HEC-RAS Scenarios**

Scenario Name	Loss Method	Baseflow	Transform Method
HMS – No BF	Deficit and Constant	Off	2D Diffusion Wave
HMS – BF	Deficit and Constant	On	2D Diffusion Wave
HMS – No BF - CN	SCS Curve Number	Off	2D Diffusion Wave
HMS – BF – CN	SCS Curve Number	On	2D Diffusion Wave
RAS	Deficit and Constant	Off	2D Diffusion Wave (Grid size = 60 m).
RAS – SWE	Deficit and Constant	Off	Full Shallow Water Equation
RAS – CN	SCS Curve Number	Off	2D Diffusion Wave
RAS – Low Resolution	Deficit and Constant	Off	2D Diffusion Wave (Grid size = 120 m).

## 2.7 Sensitivity Analysis

To assess the uncertainty in key parameters in simulating the discharge hydrograph at the basin outlet point, sensitivity analysis of key parameters was carried out. For both models, selected parameters were varied within a range from –40 % to +40 %, with an increment of 20 %, of their calibrated values, while all other parameters were kept constant. The resulting changes in simulated hydrographs, change in NSE and runoff volume were used to identify the most influential parameters.

For HEC-HMS, the sensitivity analysis was performed around the calibrated scenario (HMS – BF) defined in scenario matrix. Table 6 lists the parameters considered in the HEC-HMS sensitivity analysis.

**Table 6: Parameters for Sensitivity Analysis in HEC-HMS**

Parameter Group	Parameter	Description	Variation Range
Groundwater	GW1 Coefficient	Upper Groundwater reservoir Coefficient	-40 % to +40 %
	GW2 Coefficient	Lower Groundwater reservoir Coefficient	
	GW1 Fraction	Fraction of percolation assigned to reservoir 1	
	GW2 Fraction	Fraction of percolation assigned to reservoir 2	
Loss	Constant Rate	Constant Loss rate	
Transform	Number of cores	Number of computational cores used for the transform	4, 8, and 16

While varying the baseflow parameters in the selected range, it is important to note that, groundwater fractions (GW1 and GW2 Fraction) are constrained such that their sum is less than or equal to 1, and groundwater coefficients (GW1 and GW2 Coefficients) are constrained such that GW1 coefficient is less than GW2 Coefficient. The  $\pm 40$  percent perturbations were applied around the calibrated values while preserving these constraints, ensuring that  $\text{GW1 Fraction} + \text{GW2 Fraction} \leq 1.0$  and that the configuration consistently represented a faster interflow reservoir (GW1 Coefficient) and a slower baseflow reservoir (GW2 Coefficient).

For HEC-RAS, sensitivity analysis was carried out for the “RAS” configuration from the scenario matrix. Manning’s roughness coefficients were varied within  $\pm 40$  percent of their

calibrated values. A  $\pm 40\%$  band was used to represent a relatively wide but still realistic uncertainty range for Manning's roughness. As mentioned earlier in section 2.5.2.1, the average two-dimensional grid cell size for overland areas was doubled from the baseline resolution to assess its influence on model performance.

## **2.8 Analysis and Statistical performance**

The performance of the HEC-HMS and HEC-RAS models was evaluated over a representative rainfall–runoff event by comparing simulated and observed hydrographs of water depth, flow velocity, and discharge over calibration and validation period. Hydrographs were generated from model outputs at two monitoring locations, HAM and BCR and were compared with field observations.

To quantify overall water balance, flow hydrographs were further analyzed to compute runoff volumes. For each location, the total runoff volume over the event was calculated by integrating the area under the discharge hydrograph. This total outflow volume was then compared against the incident rainfall volume over the catchment for that event, enabling calculation of an effective runoff coefficient (the ratio of runoff volume to rainfall volume). The runoff coefficient provides insight into the fraction of rainfall that was converted to streamflow (Machado et al., 2022). Runoff coefficients were computed for each storm event bounded by an inter-event dry period of 6 hours and plotted as a time series by assigning each event's coefficient to the time corresponding to the end of that storm on the x-axis. By comparing the runoff coefficients and volumetric totals between the models, it was assessed how different model setups yielded varying catchment responses.

Two types of tools were used to analyze the modeling results: error metrics and graphs. Error metrics were used to compare model results with measurements, and graphs were used to visualize the effects of model parameters. Metrics used were NSE (Nash-Sutcliffe efficiency),  $R^2$  (coefficient of determination), and RMSE (root mean square error); graphs used were hydrographs, and cumulative volume graphs.

NSE is a normalized statistic widely used in hydrologic studies. The method equally weighs errors over the entire simulation and is a good indicator of how well the model reproduces the overall shape of the hydrograph (HEC-HMS Technical Reference Manual, 2025). It compares the variance of the differences between the model results and the observations to the variance of the observations about their mean. The value of NSE ranges from  $-\infty$  to 1, and values closer to 1 indicate that the model represents the measured values more accurately. NSE is calculated as (Equation 8):

$$NSE = 1 - \frac{\sum(OBS_i - SIM_i)^2}{\sum(OBS_i - \overline{OBS})^2} \quad (8)$$

Where,

$OBS_i$  = measured value at time  $i$ ;

$SIM_i$  = model value at time  $i$ ;

$\overline{OBS}$  = mean of measured values.

According to (Moriassi et al., 2007), model simulation can be judged as, Very good if  $0.75 < NSE \leq 1.00$ , Good if  $0.65 < NSE \leq 0.75$ , Satisfactory if  $0.50 < NSE \leq 0.65$  and Unsatisfactory if  $NSE \leq 0.50$ . This classification will be used to evaluate the performance metrics in the subsequent

section. Furthermore, NSE will always be performed between field data and modeled data throughout the studies.

The coefficient of determination ( $R^2$ ) was another statistic which can quantify the fraction of variance in the observed discharge that is reproduced by the model. It is derived from the correlation between simulated and observed values. Conceptually,  $R^2$  reflects how closely the simulated hydrograph follows the trajectory of the measured response, with values approaching 1 indicating that the model explains most of the variance in the observed hydrograph and that the scatter points show minimal deviation from the best-fit linear regression line in scatter space. In this study,  $R^2$  was used as an indicator of linear agreement between the two hydrographs, providing an immediate sense of how well the model tracks observed dynamics. At the same time, we recognize that  $R^2$  alone cannot diagnose systematic underestimation or overestimation and is sensitive to influential outliers (HEC-HMS Technical Reference Manual). For this reason,  $R^2$  was interpreted alongside complementary performance metrics that resolve biases and volumetric errors more explicitly.  $R^2$  is calculated as (Equation 9),

$$R^2 = \left[ \frac{\sum_i^n (OBS_i - \overline{OBS})(SIM_i - \overline{SIM})}{\sqrt{\sum_i^n (OBS_i - \overline{OBS})^2} \sqrt{\sum_i^n (SIM_i - \overline{SIM})^2}} \right]^2 \quad (9)$$

Where,

$\overline{SIM}$  = mean of simulated values.

n = the total number of data points.

The root mean square error (RMSE) is another statistic used in this model which indicates the average magnitude of model error by taking the square root of the mean squared difference

between simulated and observed values, preserving the physical units of discharge. RMSE reflects the typical deviation of the model from observed conditions, with the squaring step amplifying the influence of larger errors. In this study, RMSE was used to provide an error metric that is particularly influenced by periods in which the simulation diverges most strongly from measured responses, such as during peak flows and the recession limb of the hydrograph. Lower RMSE values indicate closer correspondence between simulated and observed discharge, whereas higher RMSE indicates greater overall error. RMSE is calculated as (Equation 10),

$$RMSE = \sqrt{\frac{\sum(OBS_i - \overline{OBS})^2}{n}} \quad (10)$$

## Chapter 3: Results

This chapter presents the modeling results from HEC-HMS and HEC-RAS and is organized into three main sections aligned with the study objectives:

1. HEC-HMS calibration and validation results are evaluated against observed data using standard performance metrics and diagnostic hydrographs, and a sensitivity analysis is used to examine how key basin model parameters influence simulated flow rates. It also evaluates the percent bias in NSE and cumulative runoff volume when parameters are changed from the baseline model.
2. HEC-RAS calibration and validation are assessed against observations in an analogous way, followed by a sensitivity analysis that evaluates how hydraulic roughness and grid resolution affect the flow rates.
3. Outputs from the two models are compared to assess consistency between hydrologic inputs and hydraulic responses and to quantify agreement with observations, with particular emphasis on how different models set up and loss methods affect cumulative runoff volume and runoff coefficients.

Together, these sections provide the basis for interpreting model performance and for comparing the utility of HEC-HMS and HEC-RAS in the study basin.

### 3.1 HEC-HMS Results

This section includes calibration and validation results, along with a limited sensitivity analysis for the basin model parameters in HEC-HMS. The calibration and validation focus on how well the simulated hydrographs reproduce observed conditions at the monitoring stations,

while the sensitivity analysis examines how variations in selected parameters influence hydrograph shape, recession behavior, and overall water balance in the continuous simulations.

### **3.1.1 Calibration Results**

This section compares simulated depth, velocity, and discharge hydrographs at the HAM and BCR monitoring stations for the calibration period from December 29, 2021, to January 26, 2022, and evaluates hydrograph behavior using performance metrics (NSE,  $R^2$ , and RMSE). The calibrated HEC-HMS model was obtained by manually adjusting baseflow parameters (GW1 Coefficient, GW2 Coefficient, GW1 Fraction, and GW2 Fraction), while loss parameters (initial deficit, maximum deficit, and constant rate) were adopted from the previously calibrated HEC-RAS model setup in the same 2D Diffusion Wave solver to maintain consistency between the two modeling frameworks.

#### **3.1.1.1 Depth Hydrograph**

During the one-month continuous simulation, including a baseflow component produced better agreement with the observed depth hydrographs than the no-baseflow configuration at both stations, particularly for flow magnitude, volume, recession behavior, and sustained low flow as shown in Figure 12. In addition, it also showed markedly good performance statistics as shown in Table 7.

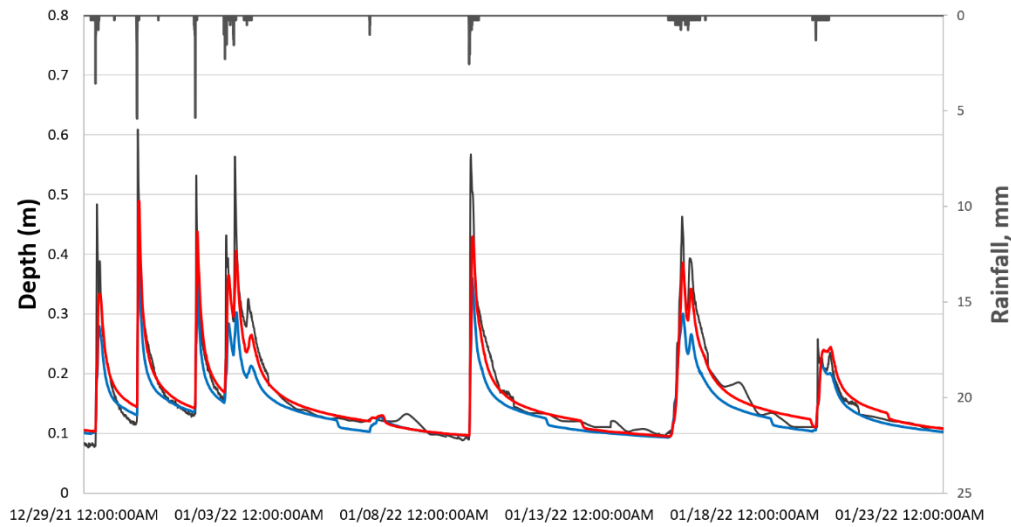
For the HAM Station, the model run with baseflow achieved an NSE of 0.89 and RMSE of 0.02, compared to an NSE of 0.70 and RMSE of 0.03 without baseflow. This indicates a substantial improvement in overall accuracy when baseflow is included, even though the correlation ( $R^2$ ) with observations remained equally high in both cases.

For BCR Station, the inclusion of baseflow raised NSE from 0.40 (no baseflow) to 0.83 and improved  $R^2$  from 0.81 to 0.88; the RMSE dropped from 0.05 to 0.02. Thus, the baseflow scenario matched the observed hydrograph far better at BCR, whereas the no-baseflow run performed unsatisfactorily ( $NSE < 0.5$ ) due to large errors in simulated flow volumes.

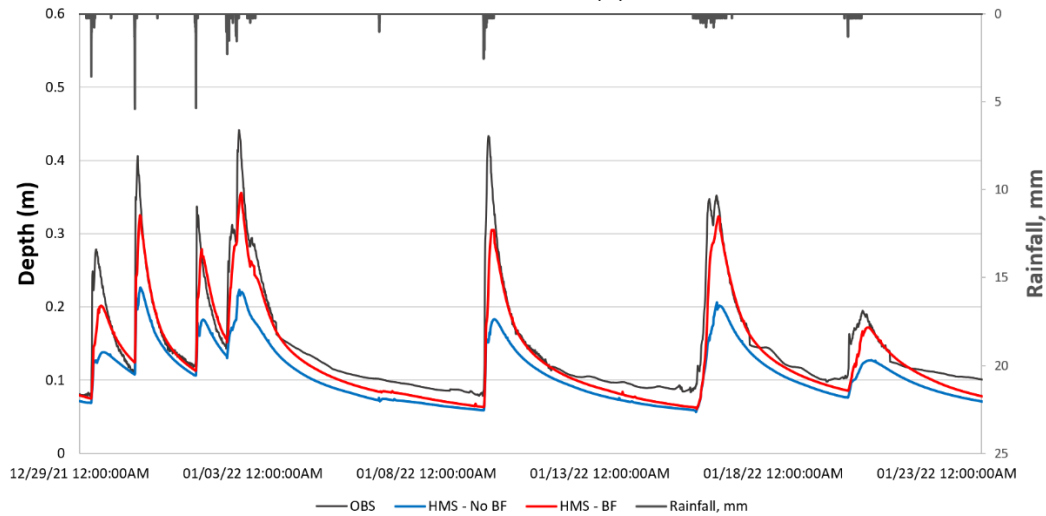
The high  $R^2$  ( $\sim 0.8$ – $0.9$ ) in both cases suggests that both configurations captured the timing of runoff or peak occurrence reasonably well, but the NSE differences indicate that the baseflow configuration achieves somewhat better overall agreement with the observed hydrograph than the no-baseflow configuration. The configurations with baseflow maintained higher flows during inter-event periods and exhibited more gradual recessions after storm peaks, closely mirroring the observed streamflow behavior. In contrast, the no-baseflow showed comparatively steeper recessions, deviating from the observed flow decay.

**Table 7: Comparison of depth error for scenarios with and without Baseflow for Hamilton (HAM) and Bent Creek Road (BCR) monitoring sites.**

HMS-Scenario	$NSE_{\text{Depth}}$		$R^2_{\text{Depth}}$		$RMSE_{\text{Depth}} \text{ (m)}$	
	HAM	BCR	HAM	BCR	HAM	BCR
HMS - No BF	0.74	0.41	0.90	0.81	0.04	0.05
HMS - BF	0.89	0.83	0.90	0.88	0.02	0.03



(a)



(b)

**Figure 12: Comparison of Depth Hydrographs at for Calibration Period in HEC-HMS at (a) HAM and (b) BCR**

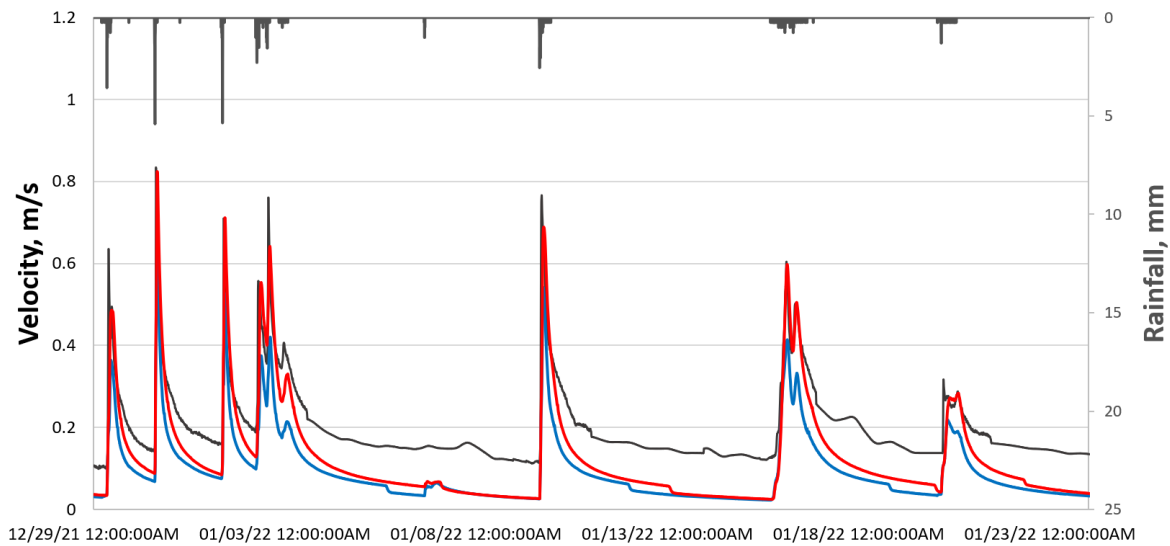
### 3.1.1.2 Velocity Hydrograph

Similar to the depth hydrograph, adding a baseflow component produced higher inter-event velocities and more prolonged recession at both stations compared to the no-baseflow case, as shown in Figure 13. Also, the evaluation metrics, NSE,  $R^2$  and RMSE improved with the addition of baseflow as shown in Table 8. Peak timing was comparable between scenarios. However, the main differences across the stations were in the persistence of velocities between storms.

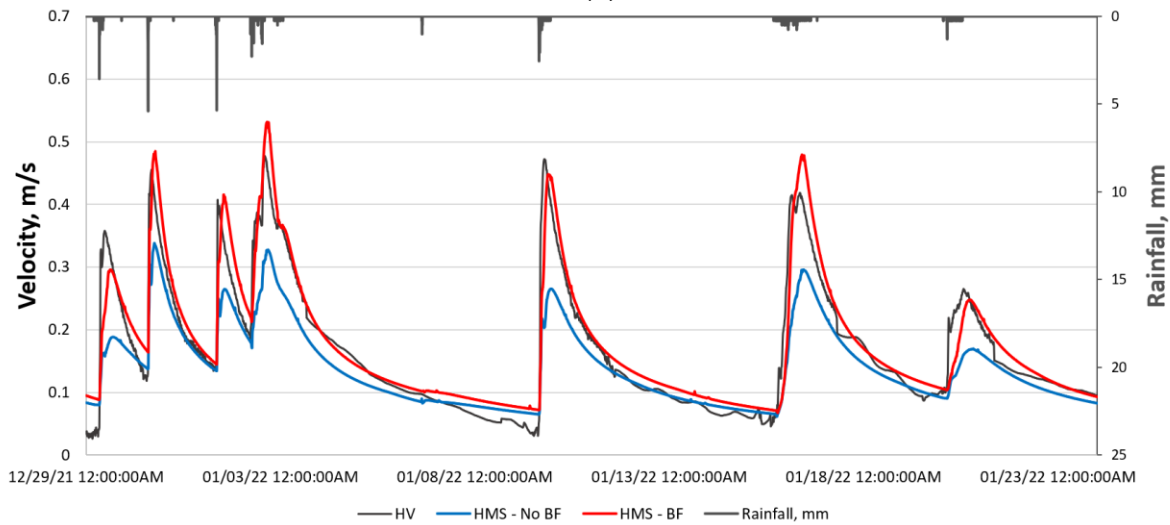
**Table 8: Comparison of velocity error for scenarios with and without Baseflow for Hamilton (HAM) and Bent Creek Road (BCR) monitoring sites.**

HMS-Scenario	NSE <sub>Velocity</sub>		R <sup>2</sup> <sub>Velocity</sub>		RMSE <sub>Velocity</sub> (m/s)	
	HAM	BCR	HAM	BCR	HAM	BCR
HMS - No BF	-0.36	0.73	0.89	0.89	0.11	0.89
HMS - BF	0.15	0.90	0.89	0.91	0.09	0.91

With the addition of baseflow, the HAM station captured the peak and showed a slightly improved baseline velocity compared to without baseflow, but it still tends to remain below the observed baseline during extended dry periods (Figure 13(a)). At the same time, this is not visible at the BCR station, which also used the same rain event for the simulation. This discrepancy is likely due to the HOBO water logger and the AV Sensor at HAM not being collocated, resulting in different cross-sections at the two deployments. The HOBO Logger recording the water level was deployed a few meters away from the AV Sensor measuring the velocities. While this is the same for the BCR, the cross-section at the two deployments was almost identical for the BCR compared to the HAM. This was verified in the field: the HAM Hobo Logger deployment, only a few meters away, had deeper cross sections than the AV Deployment Location, which had comparatively shallower cross sections. Furthermore, the velocity rating curve was developed during a different time frame (year 2024) than the calibration time frame (year 2021/22). Over time, there could be changes in streambed elevation due to sediment deposition and wash-off, and such a rating curve developed from the limited deployments might not be a good representation for this calibration set.



(a)



(b)

**Figure 13: Comparison of Velocity Hydrographs at for Calibration Period in HEC-HMS at (a) HAM and (b) BCR**

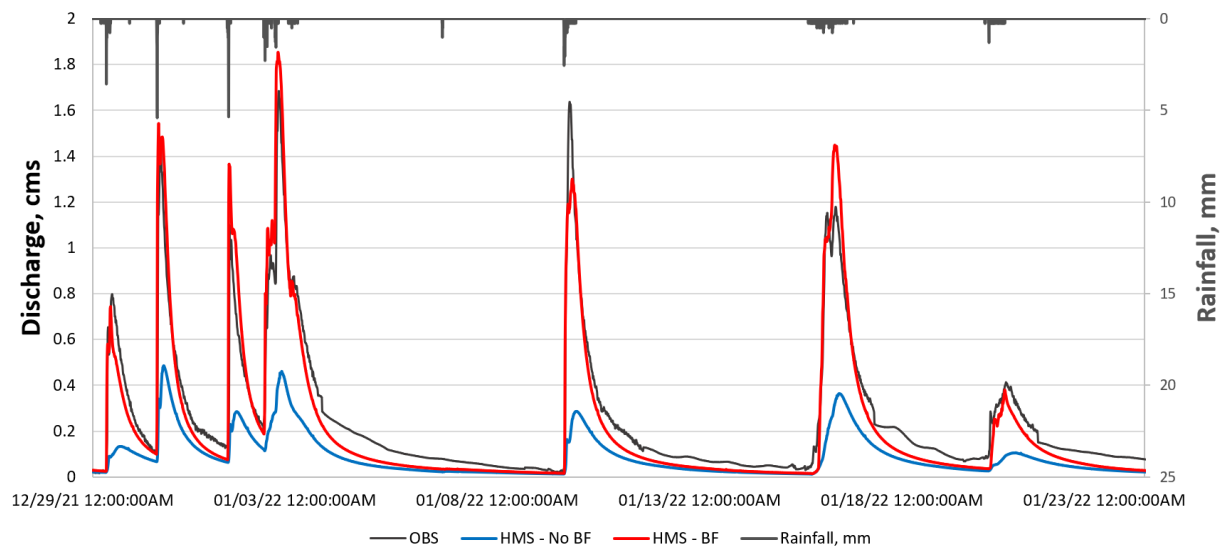
### 3.1.1.3 Discharge Hydrograph

Figure 14 shows the comparison of discharge hydrographs at the BCR station. Because the HEC-HMS model was configured with a single outlet at BCR, discharge time series were available only at that outlet. In contrast, HEC-RAS 2D can report flows at internal locations by extracting along user-defined profile lines within the mesh.

**Table 9: Comparison of Total inflow error for scenarios with and without Baseflow for Bent Creek Road (BCR) monitoring site.**

HMS-Scenario	$NSE_{Discharge}$	$R^2_{Discharge}$	$RMSE_{Discharge}$ (m <sup>3</sup> /s)
HMS - No BF	0.18	0.80	0.26
HMS - BF	0.91	0.94	0.09

Similar to the depth and velocity results, adding the baseflow component improved both peak and recession behavior (Figure 14). Peak flow rates increased by about 3.5 times on average relative to the no-baseflow run, inter-event discharge was sustained, and the recession limbs were longer and smoother. Peak timing remained comparable between scenarios. These changes are consistent with the very good metrics in Table 9 (higher NSE and R<sup>2</sup>, lower RMSE) and indicate that, over the study period, the BCR reach is heavily influenced by baseflow.



**Figure 14: Comparison of Total inflow Hydrographs at BCR for Calibration Period in HEC-HMS**

### 3.1.2 Validation Results

This section compares simulated hydrographs with the observed hydrographs at the HAM and BCR monitoring stations for the validation period. For HAM, the validation period extends from December 26, 2024 to January 23, 2025, which corresponds to the timeframe when the AV sensor was installed to record water level and velocity. Unlike the calibration period, when the HOBO water logger and AV sensor were not collocated, the validation analysis uses depth and velocity extracted directly from the AV sensor location instead of the HOBO logger location. For BCR, the validation period spans March 3, 2025 to March 21, 2025, matching the sub-interval when the AV sensor was installed at that site.

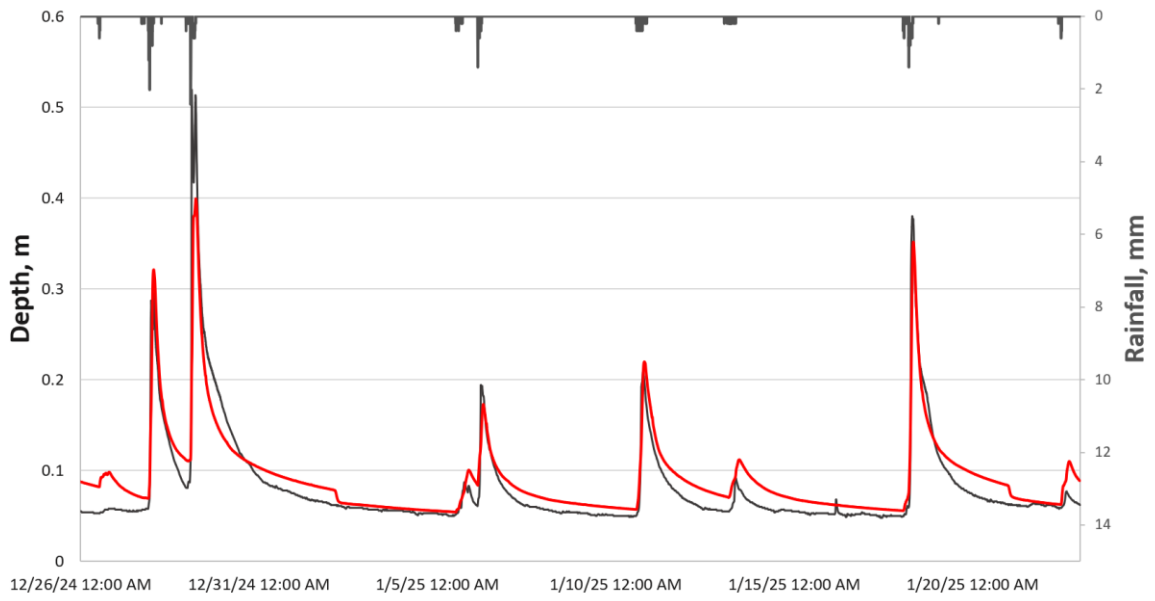
At HAM, depth and velocity hydrographs are compared against observed data for the scenario with baseflow. At BCR, depth, velocity, and discharge hydrographs are compared against observations. Model performance is evaluated using the metrics NSE,  $R^2$ , and RMSE.

#### 3.1.2.1 Validation Results at HAM

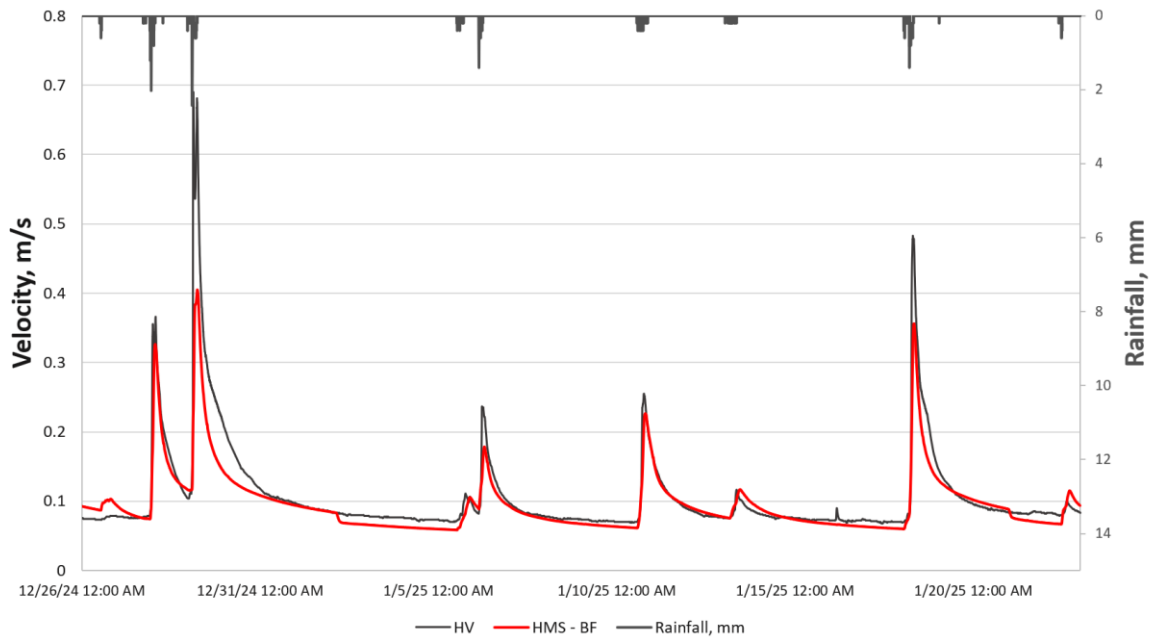
Figure 15 shows that the model aligns with the observed data most of the time in terms of time to peak, recession behavior, and overall volume. Table 10 also shows strong statistical performance for the validation range at Hamilton.

**Table 10: Error metrics for Validation at HAM using HEC-HMS**

HMS-Scenario	NSE	$R^2$	RMSE
HMS - BF (Depth)	0.91	0.92	0.02 m
HMS - BF (Velocity)	0.83	0.91	0.04 m/s



(a)



(b)

**Figure 15: Comparison of (a) Depth and (b) Velocity Hydrographs at HAM monitoring site for Validation Period in HEC-HMS**

### 3.1.2.2 Validation Results at BCR

Figure 16 shows that while the validation at BCR roughly estimated the observed depth, velocity, and discharge hydrographs, it failed to accurately capture the time to peak. This discrepancy is likely due to spatial variation in rainfall patterns across MMC locations. The rain data used for validation was from the Moore’s Mill Road station, and it is possible that the rain started slightly later at this station than at the BCR location, causing a shift in timing. Another reason might be due to an attempt to average out the irregularities in observed data collected from AV Sensor at this location which caused the observed data to shift ahead as shown in Figure 16. The high spike in the first peak might be due to an attempt to add additional precipitation prior to the storm event. The additional precipitation values that performed well during the calibration phase seem ineffective during the validation phase, but they might need to be recalibrated to adjust them to the validation storm scenario. However, Table 11 shows that the statistical performance is within a satisfactory range for velocity and depth, although it has degraded compared to the calibration period, especially for discharge.

**Table 11: Error Metrics at BCR for validation period using HEC-HMS**

HMS-Scenario	NSE	R <sup>2</sup>	RMSE
HMS - BF (Depth)	0.59	0.58	0.04 m
HMS - BF (Velocity)	0.67	0.65	0.10 m/s
HMS - BF (Discharge)	0.21	0.28	0.97 m <sup>3</sup> /s

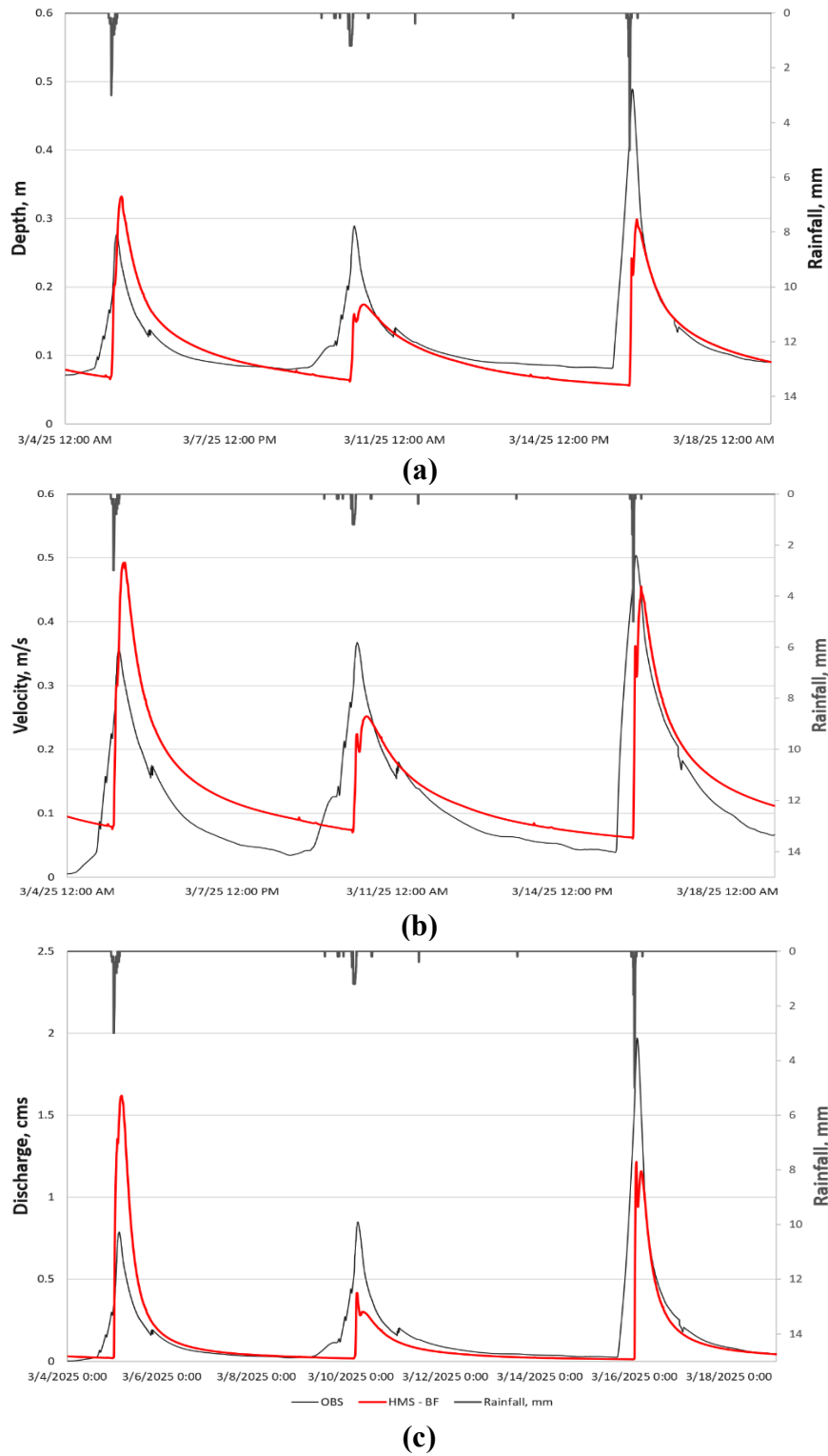


**Figure 16: Comparison of (a) Depth and (b) Velocity and (c) Total inflow Hydrographs at BCR monitoring site for Validation Period in HEC-HMS**

### 3.1.3 Sensitivity Analysis in HEC-HMS

This section reports the sensitivity analysis performed by systematically varying key hydrologic parameters to quantify their effects on model behavior. The analysis evaluates how variations in each parameter affect hydrograph timing, peak discharge, and total runoff volume, and it assesses overall performance using the change in Nash-Sutcliffe efficiency (NSE) and cumulative runoff volume compared to the baseline. The baseline scenario used in this study was the calibrated HEC-HMS model configured with the Deficit and Constant Loss method and the addition of baseflow. The results identify the parameters that exert the greatest control over the model and inform the interpretation of subsequent calibration results.

#### 3.1.3.1 Sensitivity of Baseflow Parameters

This study used the Linear Reservoir baseflow method in HEC-HMS with two groundwater layers and a single routing step in each layer. A sensitivity analysis was performed on four baseflow parameters: the GW1 and GW2 Fractions (dimensionless) and the GW1 and GW2 Coefficients (hours).

In the HEC-HMS linear reservoir formulation, GW1 Fraction represents the portion of infiltrated water that enters the faster, shallow groundwater (or interflow) reservoir (GW1), while GW2 Fraction controls the portion entering the slower, deeper reservoir (GW2). The sum of these two fractions must be less than or equal to 1 and any remainder is deep aquifer recharge (HEC-HMS Technical Reference Manual, 2025).

GW1 Fraction + GW2 Fraction  $\leq$  1, and

$$1 - (\text{GW1 Fraction} + \text{GW2 Fraction}) = \text{Deep aquifer recharge.} \quad (11)$$

In this study, since we have two linear reservoirs, and if  $I(t)$  is a total amount of infiltrated water or inflow into the linear reservoir, then the volume of infiltrated water that reaches the GW1 and GW2 reservoirs are respectively,

$$I_1(t) = \text{GW}_1 \text{ Fraction} \times I(t) \quad (12)$$

$$I_2(t) = \text{GW}_2 \text{ Fraction} \times I(t)$$

The Linear Reservoir model combines the continuity equation with a linear storage–outflow relationship:

$$\frac{dS}{dt} = I(t) - O(t), \quad S(t) = \text{GW Coefficient} * O(t) \quad (13)$$

Where,  $S(t)$  is the storage volume in the reservoir,  $I(t)$  and  $O(t)$  are the inflow and outflow from the linear reservoir.

For each groundwater layer, GW1 and GW2, the linear reservoir equations can be written as,

$$\begin{aligned} \frac{dS_1}{dt} = I_1(t) - O_1(t), \quad O_1(t) &= \frac{S_1(t)}{\text{GW}_1 \text{ Coefficient} (t)} \\ \frac{dS_2}{dt} = I_2(t) - O_2(t), \quad O_2(t) &= \frac{S_2(t)}{\text{GW}_2 \text{ Coefficient} (t)} \end{aligned} \quad (14)$$

And the Total baseflow at the subbasin outlet is then,

$$O(t) = O_1(t) + O_2(t) \quad (15)$$

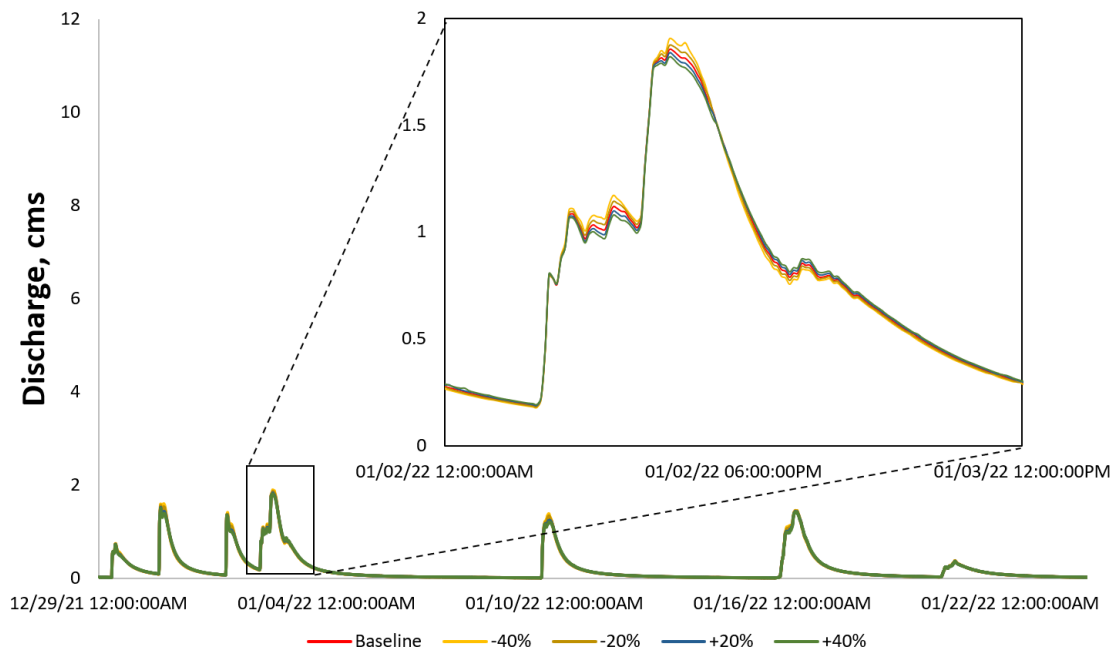
In summary, GW1 and GW2 Fractions only control how the inflow is split between the fast (GW1) and slow (GW2) groundwater reservoirs, while GW1 and GW2 Coefficients control how quickly each reservoir releases its stored water.

### GW1 and GW2 Coefficients

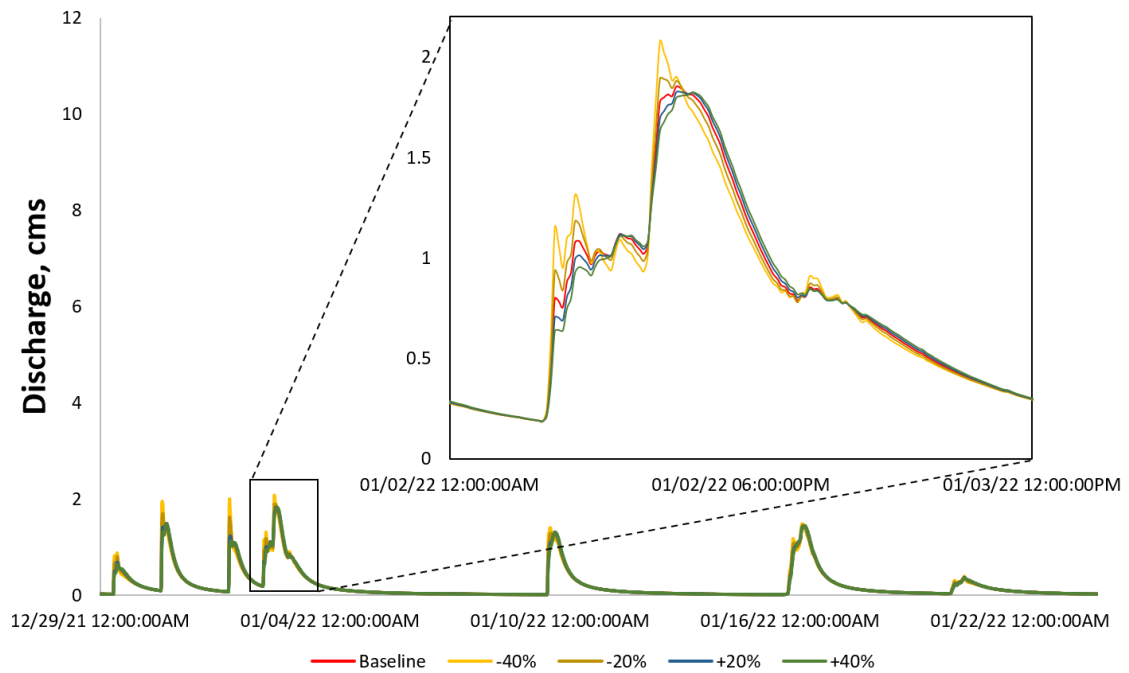
Figure 17 shows that varying GW1 and GW2 coefficients by  $\pm 20$  and  $\pm 40$  percent from their calibrated values produces systematic but modest changes in the simulated hydrograph. For both coefficients, lower values yield slightly higher peak discharges and higher values attenuate the peak, consistent with the linear reservoir equation (14) in which the coefficients are inversely related to outflow. The time of the main peak remains essentially unchanged for all runs, in line with the HEC-HMS formulation and guidance that these coefficients primarily control magnitude rather than timing.

For GW1, even a  $\pm 40$  percent change causes only minor deviations from the baseline, and the recession limbs are nearly coincident across scenarios. By contrast, GW2 produces a much stronger response: in Figure 17 (b), the  $\pm 40$  percent variations generate a wider spread in peak flows and in the falling limb than the corresponding GW1 conditions (Figure 17 (a)). Lower GW2 values yield higher peaks and faster recessions, whereas higher GW2 values produce lower peaks, more prolonged recessions, and slightly smoother secondary peaks, indicating that this groundwater layer 2 exerts greater control on both peak magnitude and baseflow persistence. Consequently, GW2 should be treated as a priority parameter during calibration, with GW1 used mainly to fine-tune the hydrograph once GW2 has been constrained.

Although the variation in recession patterns and peak attenuation appears modest within the  $\pm 40$  percent range, earlier calibration with much larger departures from the final values produced strongly attenuated peaks and substantially longer recessions.



(a)



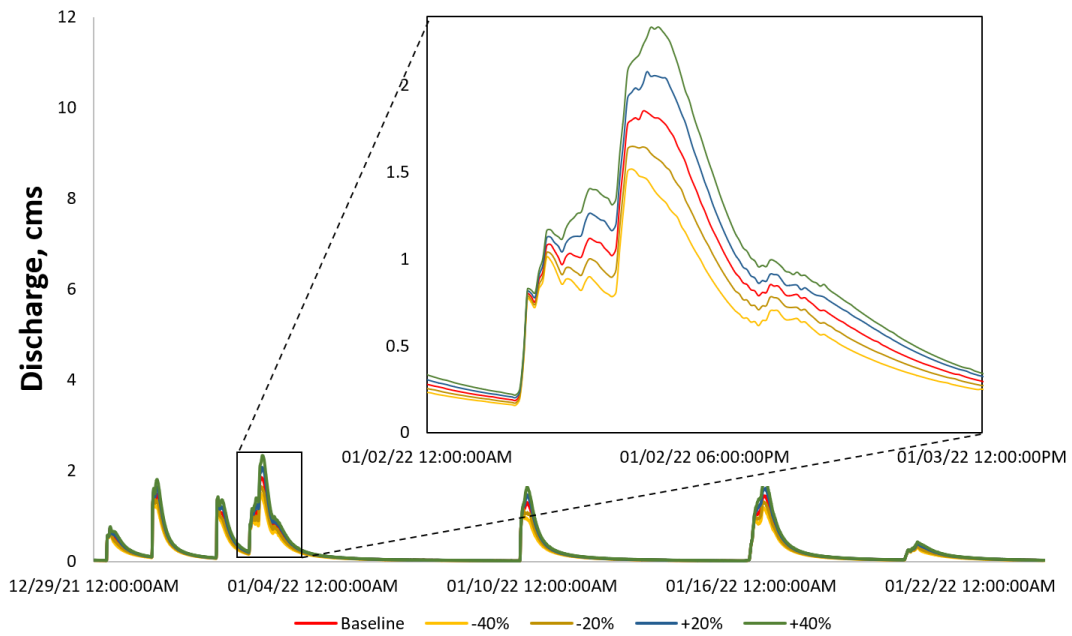
(b)

**Figure 17: Sensitivity analysis of simulated Total inflow at BCR for variations in Groundwater coefficients (a) GW1 (b) GW2**

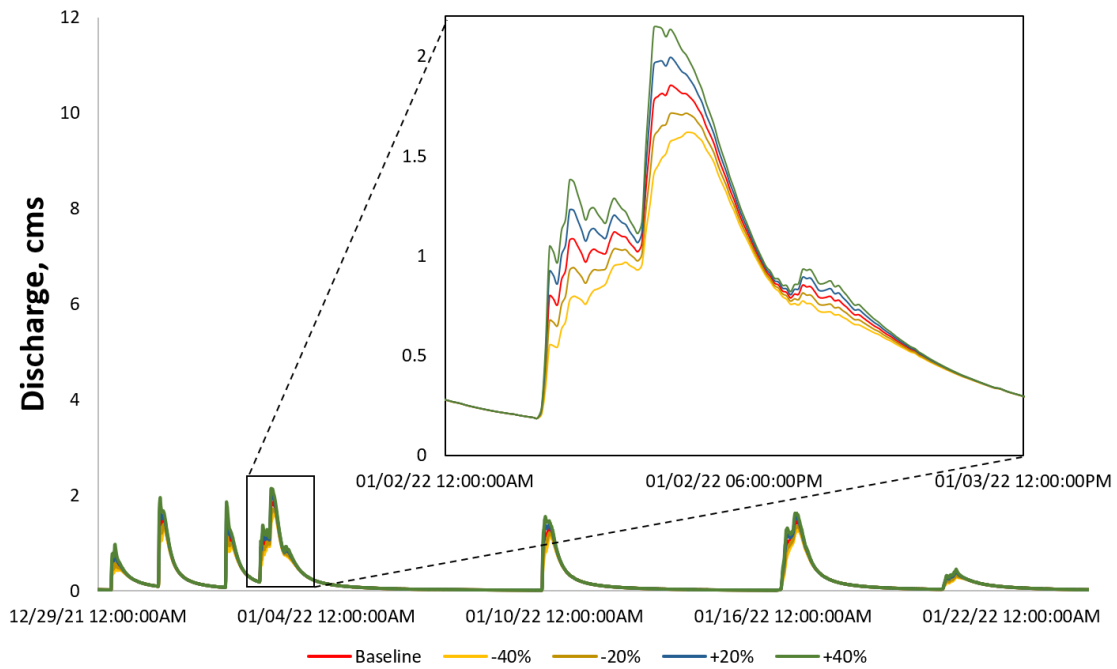
### GW1 and GW2 Fraction

Figure 18 shows that increasing either GW1 or GW2 Fraction shifts a larger share of infiltrated water into the linear reservoir baseflow system, so peak discharge rises and attenuation decreases. The effect is clearly stronger for GW1 (Figure 18 (a)): the +40% GW1 Fraction shows a much higher peak and a steeper initial recession than the -40% case, whereas the same  $\pm 40\%$  change in GW2 Fraction produces a smaller separation between peaks and a slight change in the falling limb. This indicates that the quick groundwater pathway represented by GW1 exerts primary control on runoff, while GW2 acts as a slower modulator of the hydrograph shape.

These trends are consistent with the linear-reservoir formulation, where each reservoir outflow is proportional to its storage (Equation 12). Raising GW1 Fraction feeds more water into the fast reservoir (due to lesser GW1 coefficient) which returns flow rapidly to the channel, increasing the peak and reducing the fraction that percolates to unrecoverable deep storage, so the event runoff volume increases. Increasing GW2 Fraction instead might have directed more water into the slower reservoir (due to higher GW2 coefficient): this still increases the peak, but to a lesser degree, and mainly lengthens the recession and slightly elevates inter-event baseflow. Consequently, it seems like GW1 Fraction is the more influential parameter for matching peak magnitude and early recession, whereas GW2 Fraction is better used to adjust total runoff volume and sustained baseflow during calibration.



(a)



(b)

**Figure 18: Sensitivity analysis of simulated Total inflow at BCR for variations in Groundwater Fractions (a) GW1 (b) GW2**

Figure 19 shows the percent change in NSE when each baseflow parameter is changed from -40% to +40% relative to its calibrated value. The NSE of the HEC-HMS model is clearly more sensitive to the groundwater fraction parameters than to the groundwater storage coefficients. Increasing the shallow groundwater fraction (GW1 Fraction) by 40% produces the largest deterioration in performance, with NSE decreasing by about 14–15%. A similar 40% increase in the deep groundwater fraction (GW2 Fraction) yields an NSE reduction of roughly 10%. In contrast, an equivalent  $\pm 40\%$  change in the groundwater coefficients cause only minor changes in NSE. The GW1 coefficient has a negligible effect across the tested range, and the GW2 coefficient exhibits only a mild influence: a 40% decrease in this parameter reduces NSE by about 6%, whereas  $\pm 20\%$  and +40% changes have little impact.

Although groundwater coefficients play a significant role in shaping the recession and peak, their sensitivity is slightly lower compared to groundwater fractions for same range of variations from calibrated value in terms of NSE.

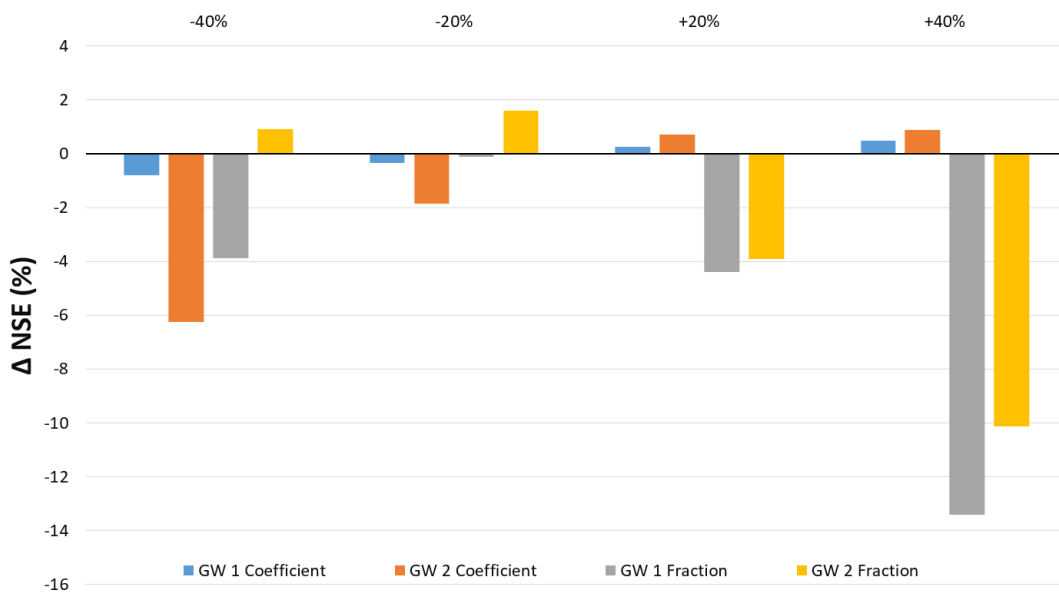


**Figure 19: Sensitivity analysis of HEC-HMS Baseflow Parameters relative to baseline Total inflow at BCR in terms of NSE.**

Figure 20 highlights how the baseflow parameters affect the simulated water balance. The results show that changes in GW1 Fraction and GW2 Fraction have a pronounced impact on cumulative runoff volume, whereas changes in the GW1 and GW2 Coefficients have almost no effect. When GW1 Fraction is reduced by 40%, the cumulative flow volume decreases by about 15–16%, and a 40% reduction in GW2 Fraction produces a reduction of roughly 9–10%. These decreases might be due to a smaller share of infiltrated water being routed to the modeled groundwater reservoirs, so more water is effectively lost to deep aquifer storage instead of contributing to streamflow.

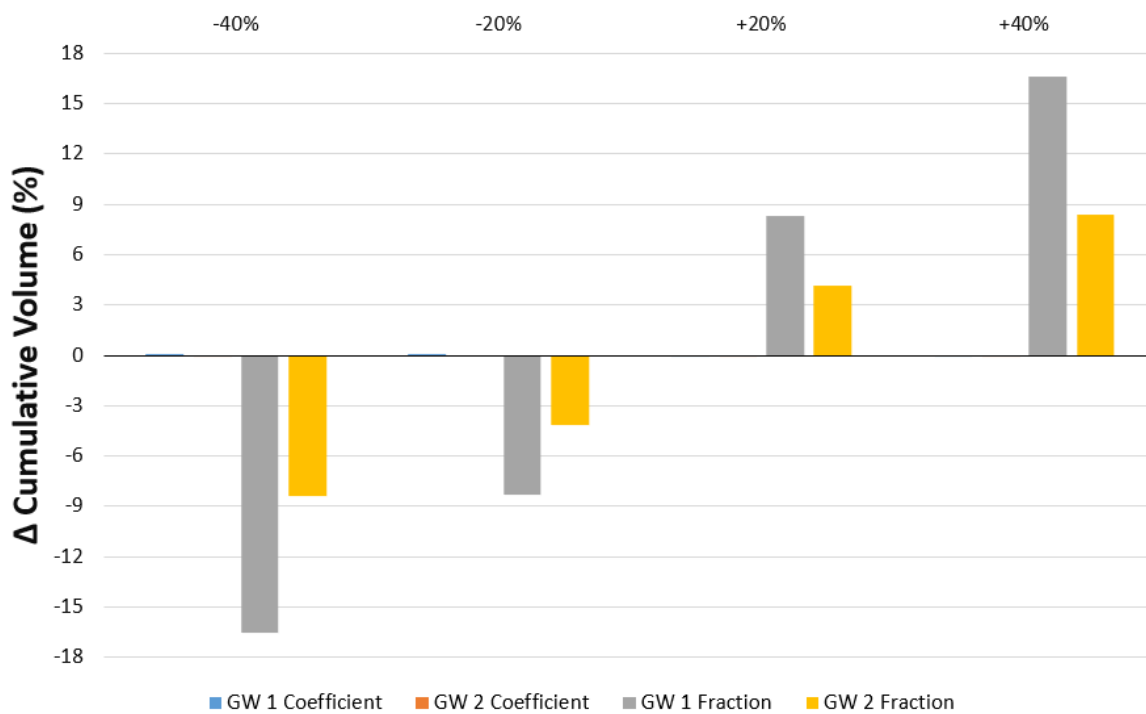


**Figure 20: Sensitivity analysis of HEC-HMS Baseflow Parameters relative to baseline Total inflow in terms of Cumulative Runoff Volume at BCR.**

In the HEC-HMS linear reservoir formulation, since the GW1 Fraction represents the portion of percolated water that enters the faster, shallow groundwater (or interflow) reservoir, and

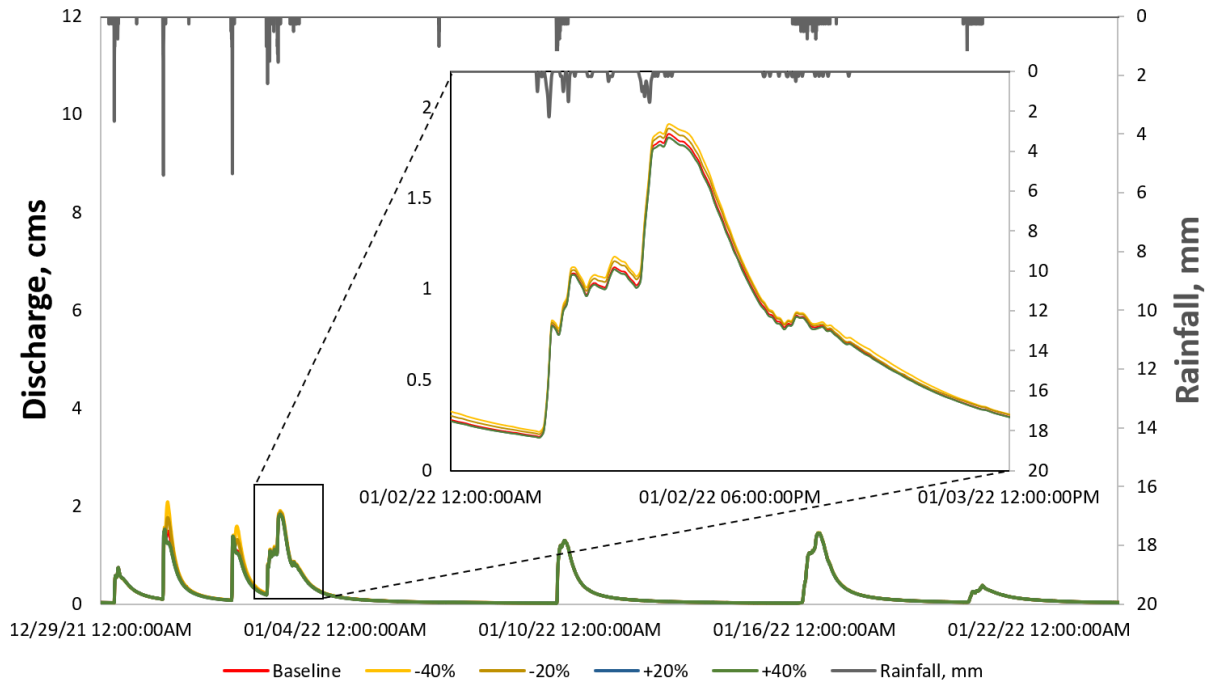
GW2 Fraction controls the portion entering the slower, deeper reservoir. Adjusting these fractions, therefore, changes how much water is available for baseflow and, consequently, the total runoff volume. By contrast, the GW1 and GW2 Coefficients primarily control the rate at which stored groundwater is released, so their variation mainly affected the timing of baseflow and recession rather than the overall volume over the one-month simulation period.

### **3.1.3.2 Sensitivity to Loss Parameter: Constant Rate**

Figure 21 shows that lowering the constant loss rate produced higher peak discharges and larger runoff volumes during the early storms. For example, the -40% conditions yields the largest peak and a slightly steeper rising limb than the calibrated baseline. This behavior might reflect the reduced infiltration capacity and once the event rainfall has filled the soil moisture deficit, any additional rainfall more readily exceeds the lower constant loss rate, and resulting in more excess transfer to streamflow. In contrast, increasing the constant loss rate (+20% and +40%) slightly attenuates the hydrograph, likely due to a greater portion of rainfall infiltrates and less water is available for direct runoff. The timing of the peak flow is nearly unchanged among the scenarios, which indicates that event timing is controlled primarily by the rainfall pattern and routing characteristics of the watershed rather than by the loss parameter.

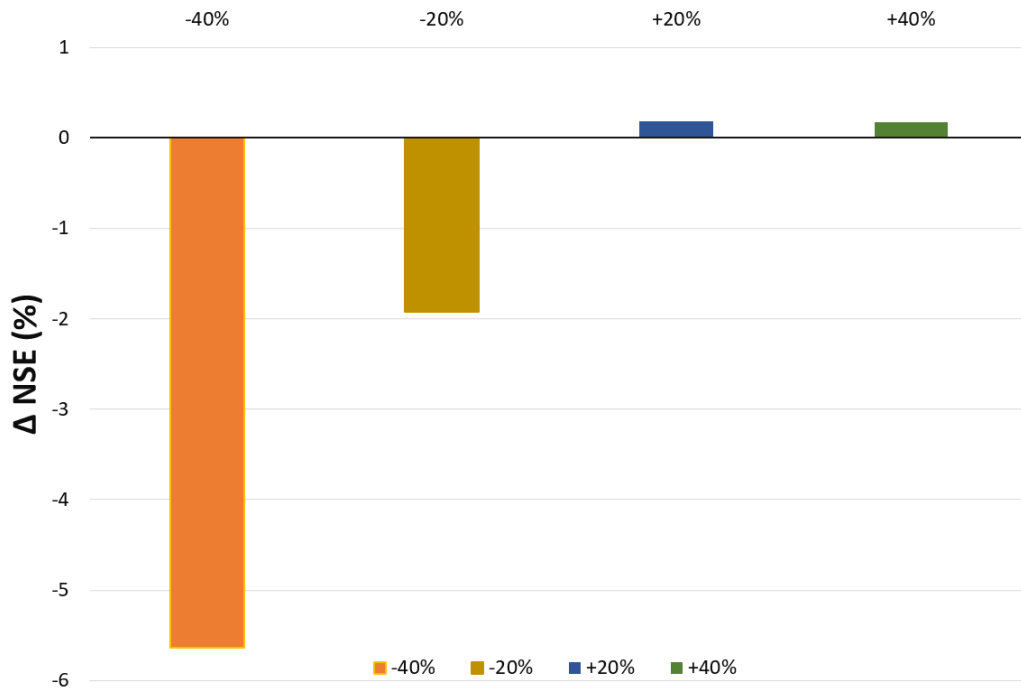
In contrast, variations in the constant loss rate have negligible influence on the later storm peaks (from Jan 10 and later). This might be because these events primarily act as deficit-filling storms rather than post-saturation storms. The soil moisture deficit at the start of these later events might be relatively large, and the rainfall depths and intensities are modest. Consequently, most of the rainfall is used to replenish soil storage. Since the Deficit & Constant method assumes all rainfall infiltrates while the soil moisture deficit remains, the constant loss rate is not applied until

the deficit is fully filled. By this point, the remaining rainfall is minimal, and intensities are low. As a result, the small amount of rainfall under saturated conditions might have led to nearly identical excess precipitation across all conditions (-40%, -20%, +20%, and +40%), and which after routing yielded similar hydrograph peaks at later events.



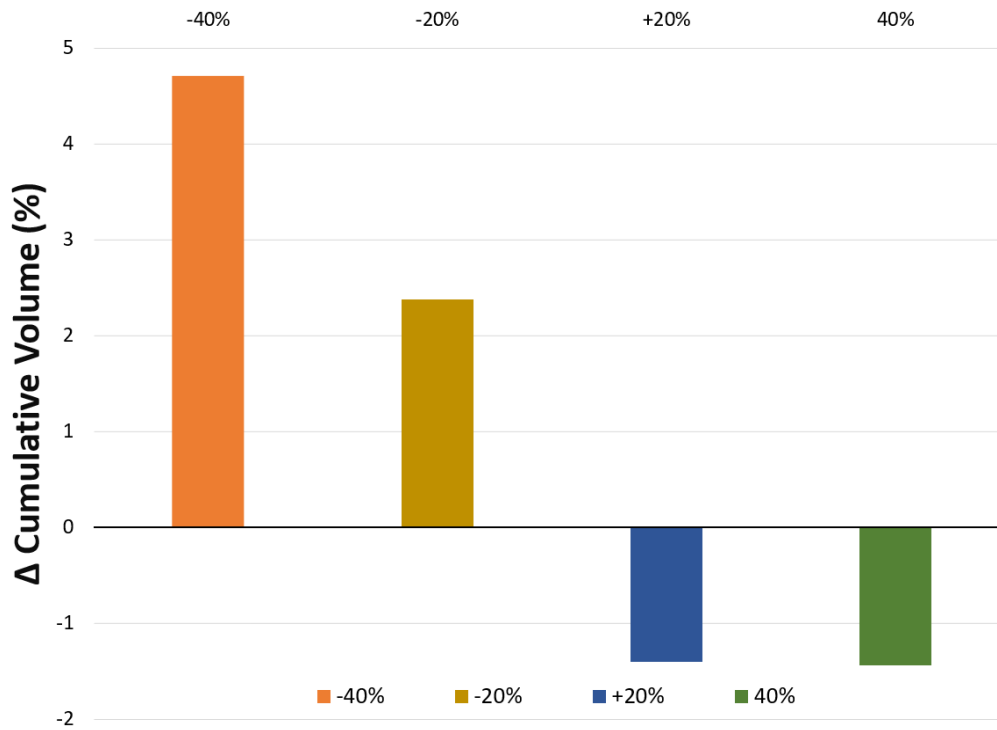
**Figure 21: Sensitivity analysis of simulated Total inflow at BCR for variations in Loss Parameter: Constant Rate**

Figure 22 shows that reducing the constant loss rate (i.e. allowing less infiltration) clearly degrades the model's efficiency: the NSE drops by approximately 2–3% under a -20% parameter change, and by nearly 6% under a -40% change. In contrast, increasing the loss rate (more infiltration) has very less effect on NSE. NSE does not improve meaningfully in this scenario because the hydrograph shape and volume might remain virtually unchanged (Figure 21) and any extra infiltrative capacity goes unused given the storm intensities, yielding diminishing returns.



**Figure 22: Sensitivity analysis of HEC-HMS Loss Parameter (Constant Rate) relative to baseline Total inflow in terms of NSE at BCR.**

Figure 23 shows the change in cumulative volume when constant rate is changed from -40 to +40%. As expected, decreasing the loss rate introduces an increase in cumulative volume, because the lower percolation capacity causes a larger fraction of rainfall to appear as surface runoff in each event. In contrast, increasing the loss rate above the baseline produces a modest decrease in cumulative volume, since more rainfall is removed by infiltration.



**Figure 23: Sensitivity analysis of HEC-HMS Loss Parameter (Constant Rate) relative to baseline Total inflow in terms of Cumulative Runoff Volume at BCR.**

### 3.1.3.3 Sensitivity to Transform Method: Number of cores

Table 12 indicates that all simulations produced virtually identical discharge hydrographs and other hydrologic outputs, indicating that increasing the number of processing cores did not alter model accuracy. However, the simulation time changed markedly as more cores were employed, with the 8-core run completing much faster than the 4-core and 16-core runs. These results demonstrate that a higher number of cores does not necessarily yield faster performance, and it is therefore important to test different levels of parallelization to ensure efficient hydrologic modeling without compromising the fidelity of the results.

**Table 12: Comparison of Total inflow error and simulation time for different levels of parallelization in HMS Baseline Condition at Bent Creek Road (BCR) monitoring site.**

Number of Cores	NSE <sub>Discharge</sub>	Simulation Time, minutes
4	0.844	99
8	0.844	77
16	0.844	90

## 3.2 HEC-RAS Results

Similar to the HEC-HMS Result Section, this section also includes calibration and validation results, along with a limited sensitivity analysis for the model parameters in HEC-RAS. The calibration and validation timeframe and rain data were similar to what was used for HEC-HMS.

### 3.2.1 Calibration Results

This section presents calibration results for HEC-RAS rain-on-grid (RoG) configurations using two solvers: the full Shallow Water Equations (SWE) and the simplified 2D Diffusion Wave formulation. The latter is analogous to the solver used in the HEC-HMS 2D model. Calibration in HEC-RAS was performed only for the Diffusion Wave solver and focused on a smaller set of parameters than in HEC-HMS, primarily adjusting Manning’s roughness for channels and floodplains, modifying loss parameters, and refining breaklines and local terrain in critical areas. In contrast, HEC-HMS calibration relied mainly on hydrologic parameters, particularly manual adjustment of baseflow parameters, and other common parameters between models like loss parameters were not further tuned within HEC-HMS.

Depth, velocity, and discharge hydrographs at the HAM and BCR monitoring sites generated from HEC-RAS baseline model are presented together with their performance metrics (NSE, RMSE, and R<sup>2</sup>). The RAS-SWE scenario was generated from the calibrated RAS Diffusion

Wave model by changing only the numerical solver to the full SWE while keeping all other model parameters and settings constant, so the SWE results should be interpreted as a solver-sensitivity test rather than a separately calibrated configuration.

### 3.2.1.1 Depth Hydrograph

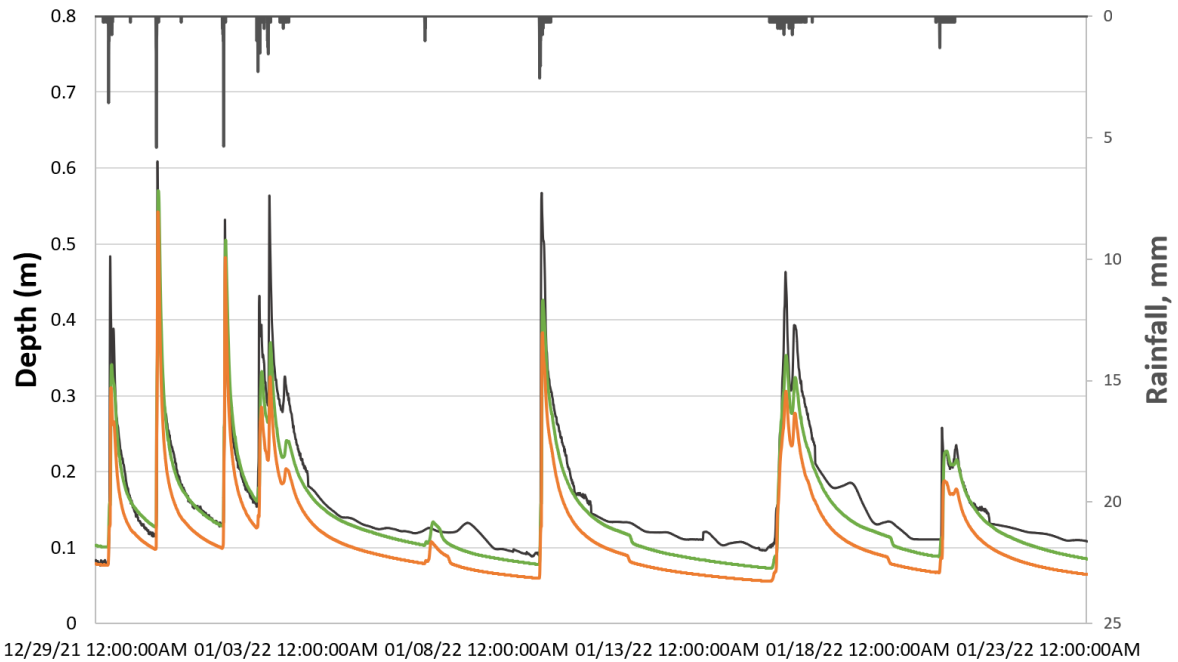
Table 13 shows that for this watershed, HEC-RAS using the calibrated 2D Diffusion Wave solver shows good performance in terms of depth hydrograph compared to using Full Shallow Water Equation.

**Table 13: Comparison of depth error for scenarios in HEC-RAS using two different solvers for Hamilton (HAM) and Bent Creek Road (BCR) monitoring sites.**

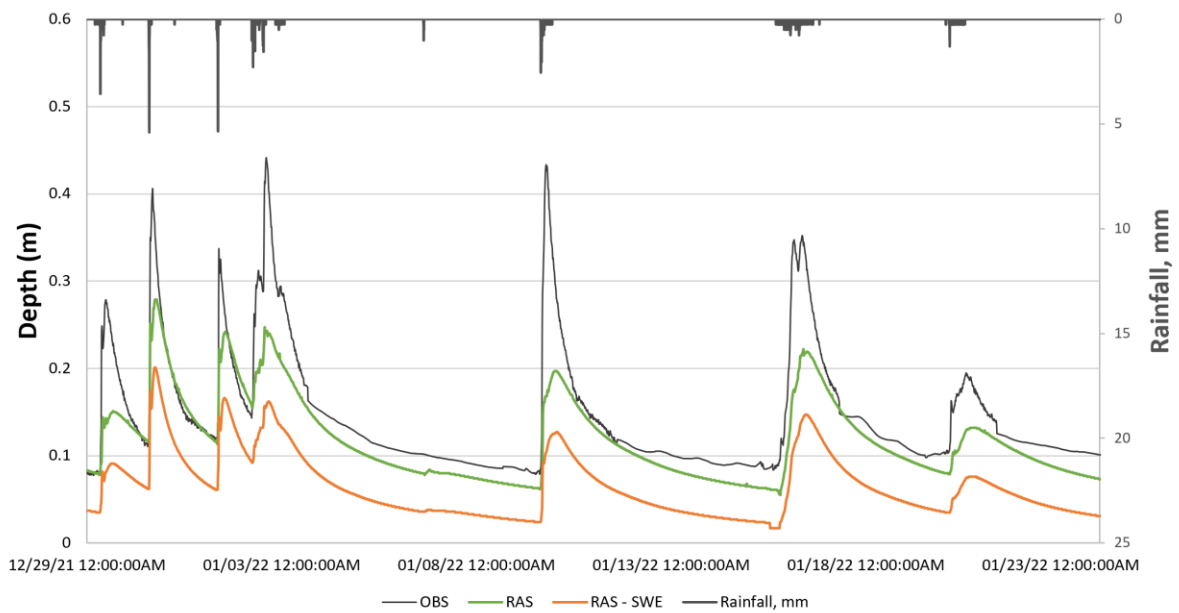
RAS-Scenario	NSE <sub>Depth</sub>		R <sup>2</sup> <sub>Depth</sub>		RMSE <sub>Depth</sub> (m)	
	HAM	BCR	HAM	BCR	HAM	BCR
RAS	0.82	0.59	0.88	0.78	0.03	0.04
RAS - SWE	0.48	-0.69	0.9	0.8	0.05	0.09

Figure 24 shows that under identical terrain, mesh, loss method, and land cover scenarios, the two solvers produce different hydrographs at both stations. In each station, the trends in the rising and falling of the hydrographs are similar in both solvers; however, the model using the full shallow water equations fails to achieve the base water level at each station, with the effect becoming more prominent as we move further downstream from HAM to BCR. This might be because diffusion wave solution tend to move water more slowly and spreading it out in time and to move the same volume with slower velocities, the system often compensated by holding more water, giving higher depths compared to SWE. The earlier literature by (Bragg et al., 2025) in the same watershed, calibrated using full shallow water equation showed satisfactory results, however,

required a huge effort in adjusting the cross-sections of DEM and inclusion of low flow discharge through internal boundary conditions to match the baseline depths or velocities.



(a)



(b)

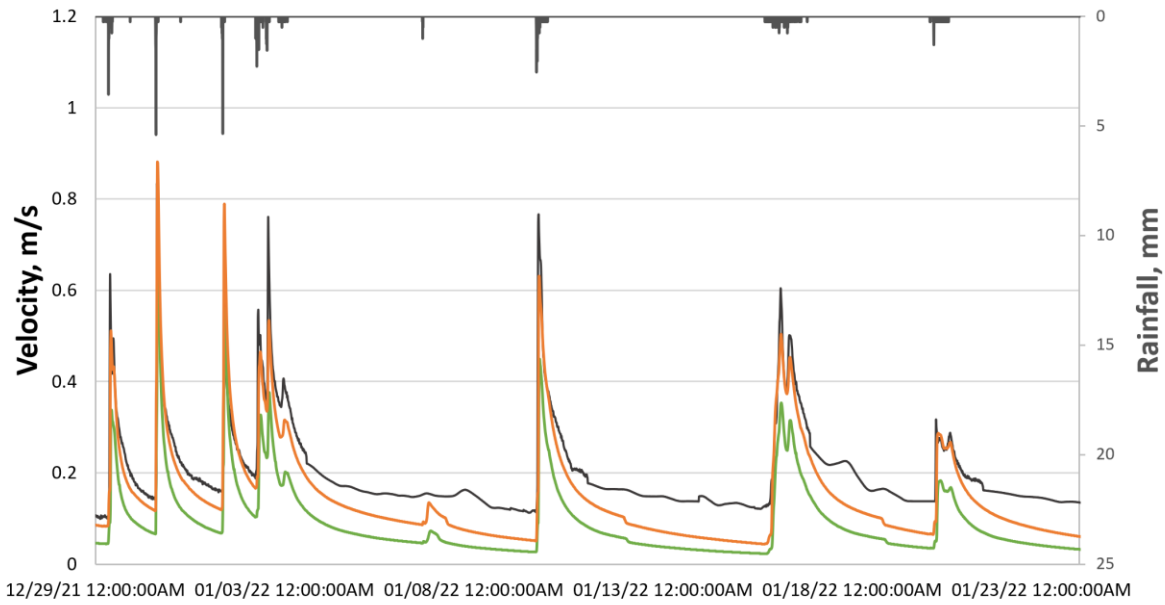
**Figure 24: Comparison of Depth Hydrographs for Calibration Period in HEC-RAS at (a) HAM and (b) BCR**

### 3.2.1.2 Velocity Hydrograph

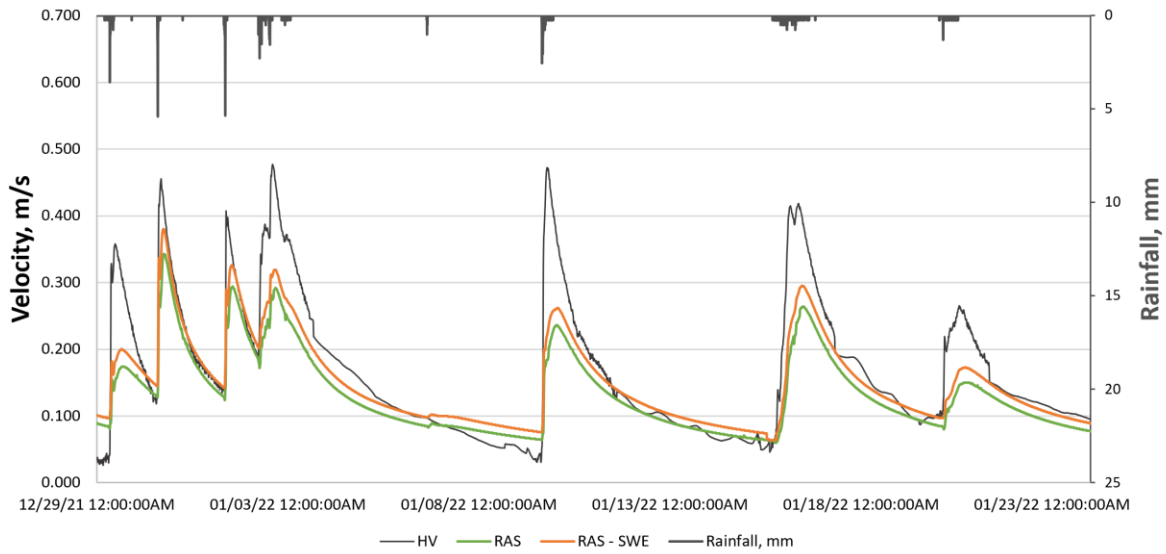
Table 14 shows the performance metrics for each scenario in HEC-RAS for velocity hydrograph. The model with SWE seems to give better results here due to the base velocity from RAS - SWE being higher than RAS model, bringing it closer to the observed base velocity (Figure 25). Contrary to depth hydrograph, velocity hydrograph generated from RAS- SWE are yielding higher values than similar RAS model for the same reason discussed above in the depth hydrograph section 3.2.1.1. The offset in the HAM section for base velocity is visible even in HEC-RAS Scenarios for the same reason discussed in HEC-HMS Section 3.1.1.2.

**Table 14: Comparison of velocity error for scenarios in HEC-RAS using two different solvers for Hamilton (HAM) and Bent Creek Road (BCR) monitoring sites.**

RAS-Scenario	NSE <sub>Velocity</sub>		R <sup>2</sup> <sub>Velocity</sub>		RMSE <sub>Velocity</sub> (m/s)	
	HAM	BCR	HAM	BCR	HAM	BCR
RAS	0.43	0.64	0.87	0.86	0.11	0.06
RAS - SWE	0.54	0.77	0.9	0.88	0.06	0.05



(a)



(b)

**Figure 25: Comparison of Velocity Hydrographs for Calibration Period in HEC-RAS at (a) HAM and (b) BCR**

### 3.2.1.3 Discharge Hydrograph

In terms of error metrics as shown in Table 15, discharge hydrograph generated from the application of the shallow water equation is slightly better than that from the diffusion wave. However, if we see the hydrograph (Figure 26), the difference between them is negligible compared to what was observed in depth and velocity hydrographs. This behavior likely reflects how the two HEC-RAS 2D solvers treat the governing equations: both options use the same continuity (mass) equation, so they route nearly the same total runoff volume from a given rainfall input and therefore produce very similar discharge hydrographs at the outlet, whereas they differ in the momentum formulation, with the shallow water solver retaining the inertial terms and the diffusion wave solver neglecting them, which leads to the larger differences as seen in the depth and velocity hydrographs (Figures 24 and 25).

**Table 15: Comparison of Total inflow error for scenarios in HEC-RAS using two different solvers for Bent Creek Road (BCR) monitoring site**

RAS-Scenario	$NSE_{Discharge}$	$R^2_{Discharge}$	$RMSE_{Discharge}$ (m <sup>3</sup> /s)
RAS	0.25	0.72	0.25
RAS - SWE	0.28	0.75	0.25

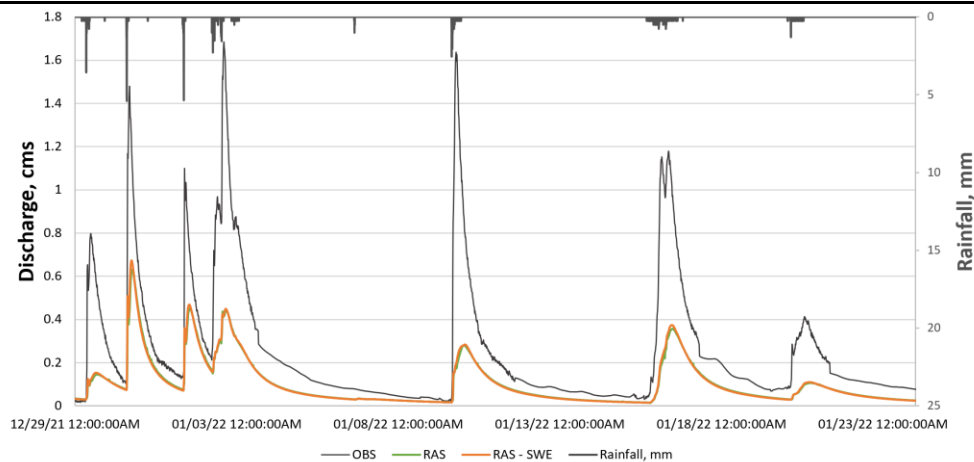
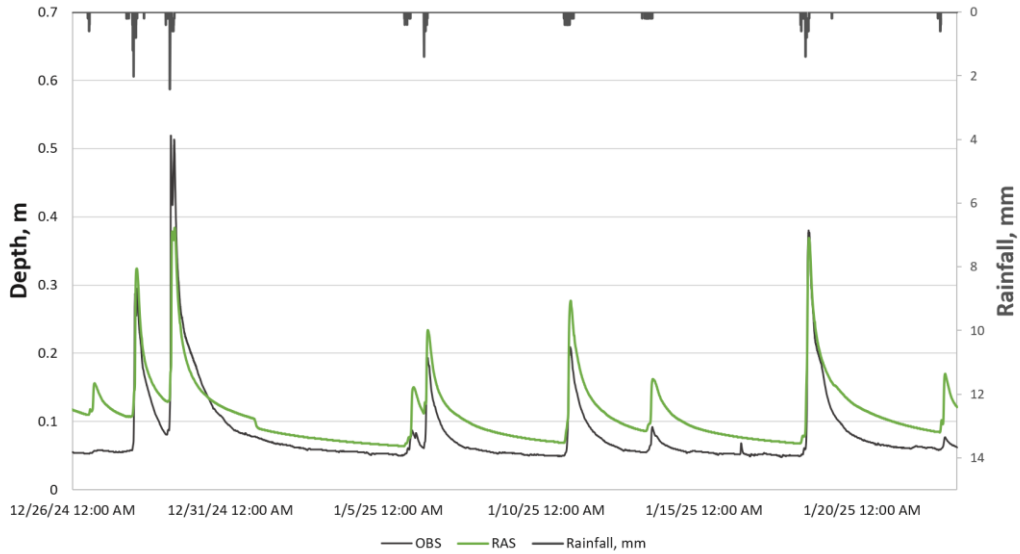


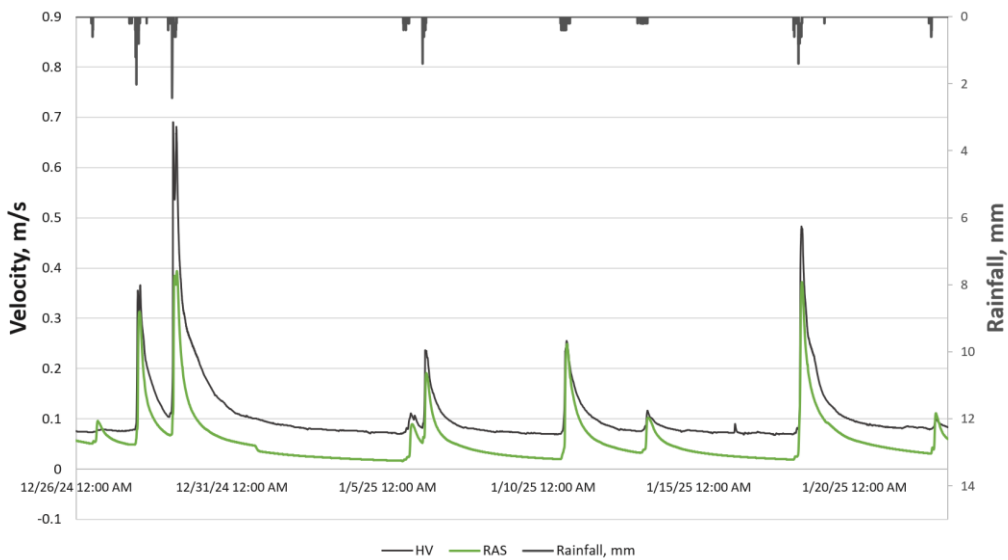
**Figure 26: Comparison of Total inflow Hydrographs at BCR for Calibration Period in HEC-RAS**

### 3.2.2 Validation Results

For Validation, HEC-RAS also performed good for depth and velocity hydrographs as shown by Table 16. But Figure 27 shows the offset in the baseline values in both depth and velocity hydrographs.



(a)



(b)

**Figure 27: Depth and Velocity hydrographs at HAM for validation period using HEC-RAS**

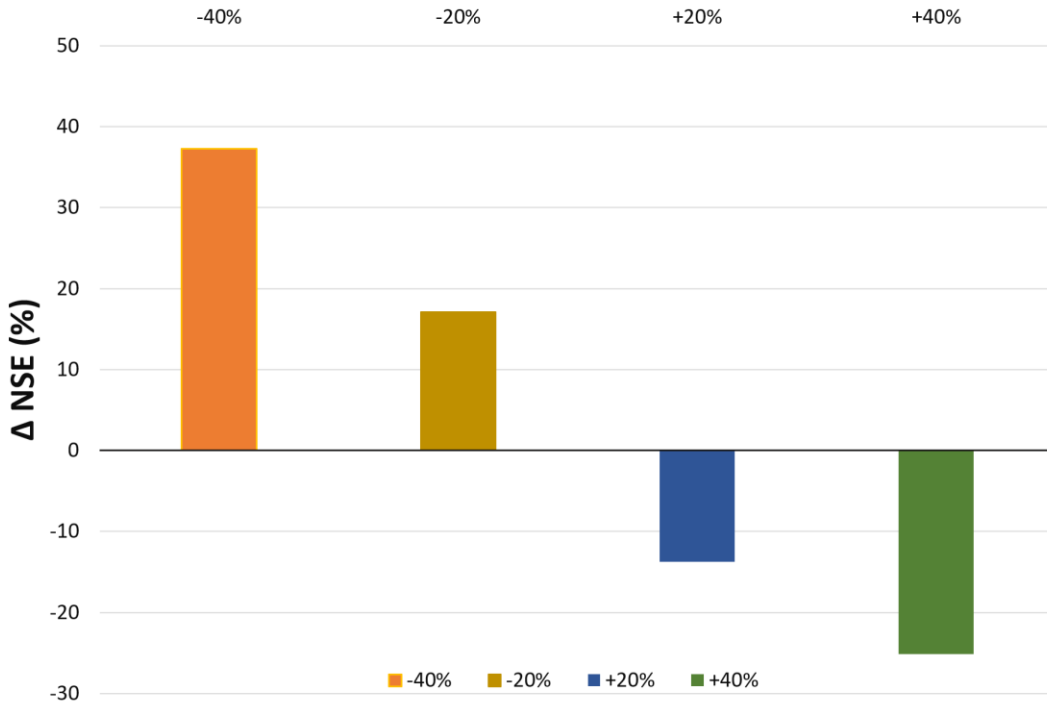
**Table 16: Error metrics for Validation at HAM using HEC-RAS**

HMS-Scenario	NSE	R <sup>2</sup>	RMSE
HMS - BF (Depth)	0.75	0.85	0.03 m
HMS - BF (Velocity)	0.55	0.86	0.06 m/s

### 3.2.3 Sensitivity Analysis in HEC- RAS

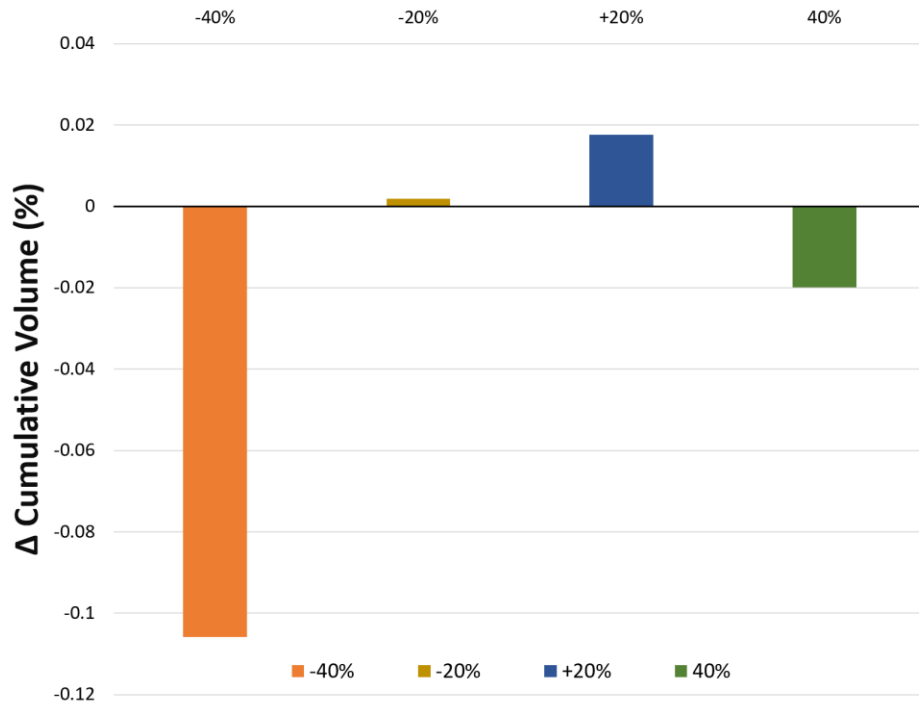
#### 3.2.3.1 Mannings Roughness

Figure 28 shows that varying Mannings roughness significantly changes the model’s efficiency, even a  $\pm 20\%$  variation is causing huge change in NSE, in the range of  $\pm 15\%$ . This indicates that Mannings roughness is the most sensitive parameter in rain-on-grid models.



**Figure 28: Sensitivity analysis of Mannings roughness coefficient relative to HEC-RAS baseline scenario for Total inflow in terms of change in NSE at BCR.**

Figure 29 shows the change in cumulative volume when Mannings roughness coefficient is changed from -40 to +40%. The difference in the volume is very minimal, which signifies the Mannings roughness, although it play role in shaping the hydrograph, it has minimum sensitivity in terms of volume change.



**Figure 29: Sensitivity analysis of Mannings roughness coefficient relative to HEC-RAS baseline scenario in terms of change in cumulative volume at BCR.**

### 3.2.3.2 Spatial Discretization

The results in Figure 30 and Table 17 show that using either a finer or a coarser grid had a negligible effect on the simulated hydrographs, indicating that the coarser grid size was adequate for this modeling application. At this scale, grid resolution was not a major factor affecting hydrograph accuracy. It is important to note that grid resolution was modified only for the overland mesh and not for areas refined using breaklines and localized refinements. The finer configuration with 60-m cells produced approximately 15k grid cells, while the coarser 120-m configuration

produced about 14.5k cells. The overall mesh density was influenced far more by breaklines and stream-aligned refinements than by the overland cell size alone. Had the grid resolution been altered across the breaklines, the results would likely have been different.

**Table 17: Error metrics for Validation at HAM using HEC-RAS**

RAS-Scenario	$NSE_{Discharge}$	$R^2_{Discharge}$	$RMSE_{Discharge}$ (m <sup>3</sup> /s)
RAS	0.25	0.72	0.25
RAS – Low Resolution	0.25	0.71	0.25

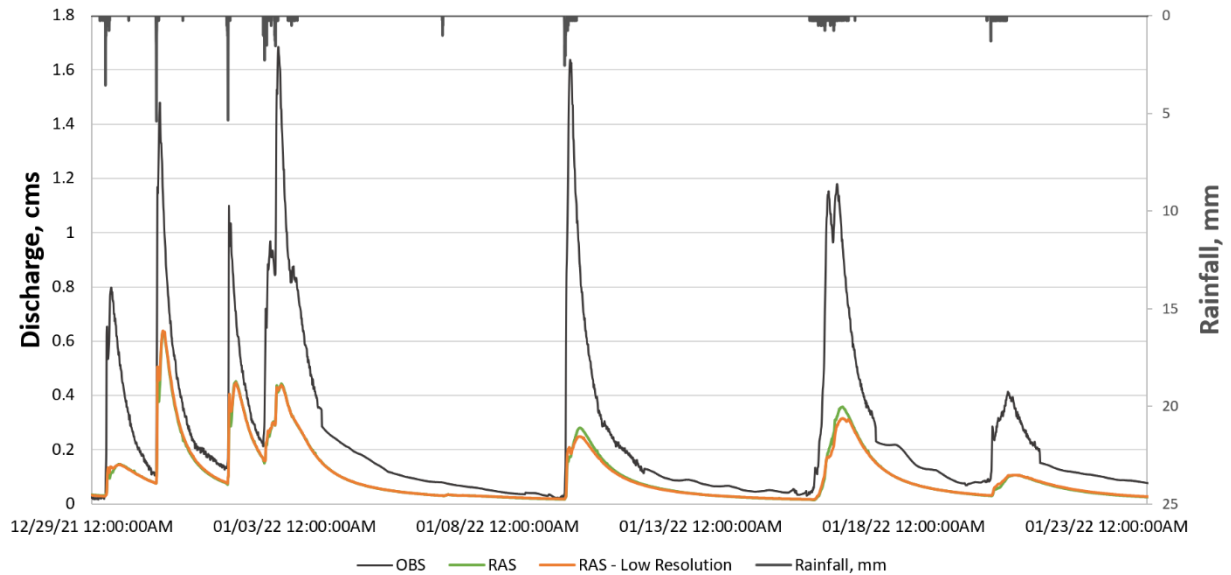


**Figure 30: Sensitivity analysis of spatial discretization to Total inflow hydrograph at BCR for RAS model.**

### **3.3 Comparative Analysis between HEC-RAS & HEC-HMS RoG Simulations**

This section compares the rain-on-grid (RoG) simulations generated in HEC-RAS and HEC-HMS using the same terrain, unstructured mesh, and rainfall, focusing on how different model setups and loss formulations affect discharge hydrographs, cumulative runoff volume, and runoff coefficients in a catchment. For comparison under identical conditions, the HEC-RAS scenario using the 2D diffusion wave solver (RAS) is only considered, consistent with the method employed in HEC-HMS.

#### **3.3.1 Comparison using Deficit and Constant loss method.**

Figure 31 shows the discharge hydrographs generated by HEC-RAS and HEC-HMS using the Deficit and Constant loss method. Among the three configurations, the HEC-HMS simulation with the linear reservoir baseflow component (HMS-BF) reproduces the observed stream discharge most closely throughout the period. HMS-BF captures the sharp peaks during storm events, maintains flow during inter-event periods, and preserves flow volume over the long term. In contrast, the HMS-No BF and HEC-RAS simulations do not incorporate groundwater return flow, so any infiltrated rain is treated as a permanent loss from the surface system. As a result, their hydrographs recede toward near-zero flow soon after rainfall ends and underestimate the observed discharge between events. Because HMS-No BF and HEC-RAS share the same mesh, terrain, loss method, and 2D diffusive wave transform, their simulated hydrographs are broadly similar. The small differences that are visible likely arise from software-specific numerical implementations, including details of rainfall interpolation, and internal handling of cell-averaged quantities.

Similar behavior was seen in the velocity and depth hydrographs, where the HEC-HMS model with baseflow (HMS – BF) shows better alignment with the observed hydrograph than HEC-RAS (RAS) and HEC-HMS (HMS – No BF) models. (see Figures 12-13, 24-25).

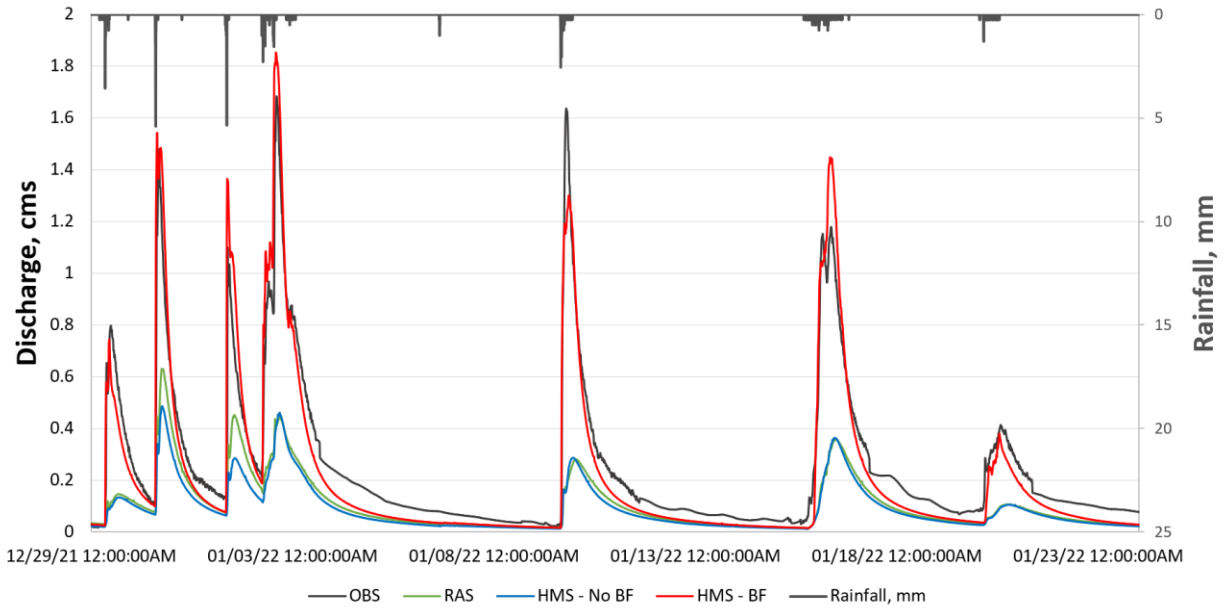


**Figure 31: Comparison of Discharge Hydrograph between HEC-HMS and HEC-RAS at BCR using Deficit and Constant Loss Method**

### 3.3.2 Comparison using SCS CN loss method

For all hydrographs, depth, velocity and discharge in Figure 32 using CN simulations, similar trends can be visualized. The two HEC-HMS runs behave almost identically and both clearly overshoot the observed peaks after the first major storm sequence, whereas the RAS - CN run underestimates them.

The high peaks in the later storms might be due to the SCS CN method treats the entire year’s rainfall as one cumulative event. As rainfall accumulates, infiltration approaches the maximum retention (S) and then stops, causing subsequent rainfall to become almost entirely

direct runoff. Since there's no soil drying or evaporation between events, the soil cannot recover its storage capacity. This results in early storms having reasonable hydrographs, but later storms producing exaggerated peaks with almost all rainfall becoming runoff, leading to an unrealistic water balance as depicted in Figure 32.

However, no such spikes are visible in later storms in HEC-RAS. This might be because HEC-RAS includes a mechanism to reset infiltration parameters at regular intervals (e.g., in this study, every 24 hours), nearly treating each storm as a separate event as mentioned in (HEC-RAS Hydraulic Reference Manual,2025). As a result, the model avoids the cumulative buildup of rainfall that leads to high peaks in CN-based simulations, giving close match to observed depth and velocity over the long run as shown in Figure 32 (a,b). However, the total runoff volume from this setup is still lower than observed (Figure 32 (c)). This is likely due to the lack of a loss recovery option, leading to underestimation of cumulative runoff.

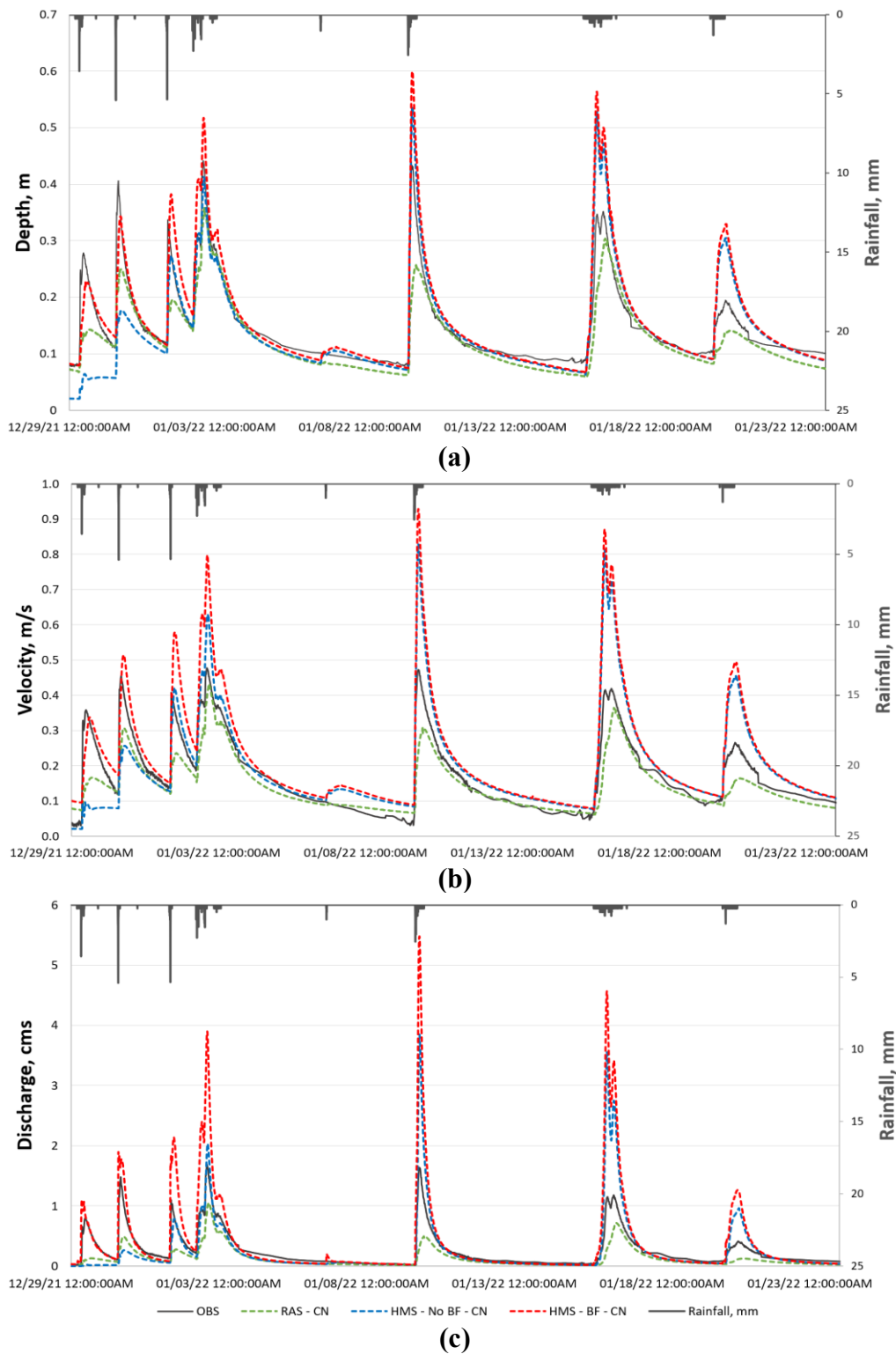
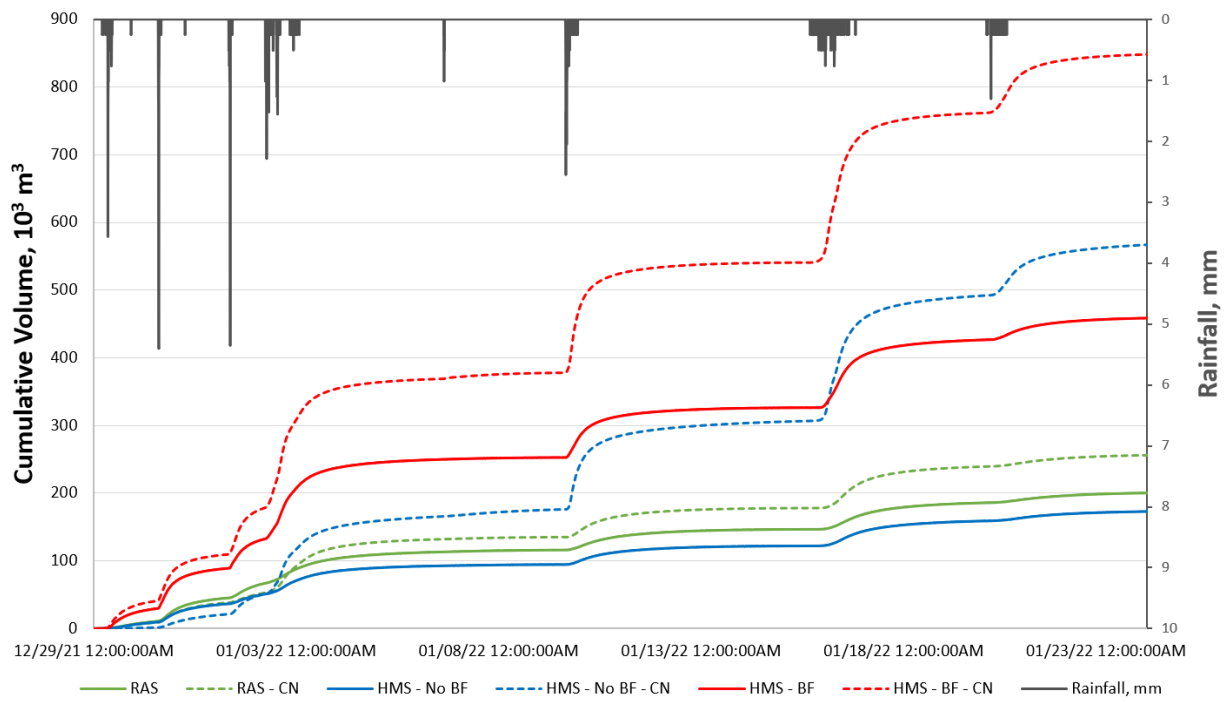


**Figure 32: Comparison of (a) Depth and (b) Velocity and (c) Total inflow Hydrographs between HEC-HMS and HEC-RAS at BCR monitoring site using CN Loss Method**

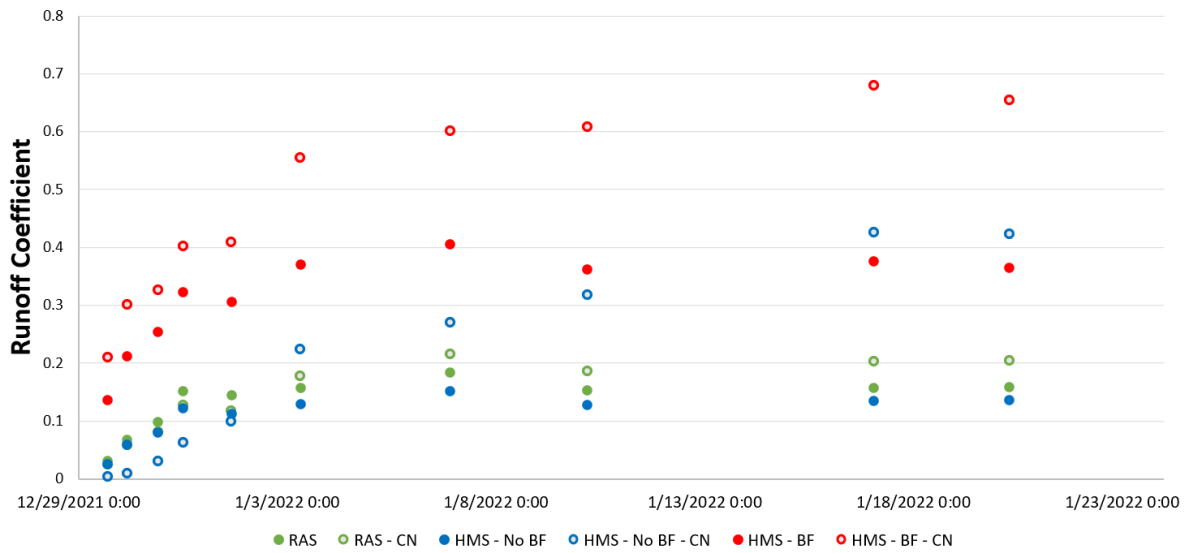
### 3.3.3 Cumulative Volume

The cumulative runoff volume curves (Figure 33 (a)) reveal clear differences between the RAS and HMS models across the range of configurations. Enabling baseflow in HEC-HMS introduces a continuous groundwater contribution, which substantially increases the cumulative volume curves. Without baseflow, HEC-RAS generally produces less runoff volume than HEC-HMS for a given loss method. The loss method also strongly influences runoff volume: the SCS Curve Number method produces higher cumulative runoff than the Deficit & Constant method in both models; however, the difference is greater in HEC-RAS than in HEC-HMS. This is likely because the software handles soil moisture settings differently for the same CN grids.

The time-varying runoff coefficient (Figure 33 (b)) shows the dynamic runoff response, which differs between models and loss methods. All scenarios exhibit low initial runoff coefficients at the onset of rainfall, as the dry soil infiltrates a large portion of the early precipitation. During each rainfall event, the runoff coefficient rises non-linearly. The CN-based simulations reach a higher peak runoff coefficient than their Deficit & Constant counterparts, particularly in prolonged storms. This is likely because once the CN loss method's initial retention is satisfied, additional rainfall is converted mainly to runoff, causing the coefficient to surge toward a higher value. In contrast, the Deficit & Constant method continues to infiltrate at a constant rate even after saturation, which moderates the rise in the runoff fraction. Baseflow effects are also clearly reflected in the trends of the runoff coefficient.



(a)



(b)

**Figure 33: Comparison of (a) Cumulative runoff volume and (b) runoff coefficients at BCR monitoring site**

## Chapter 4: Discussion and Limitations

### 4.1 Discussion

The objective of this study was to understand the hydrology of the MMC Watershed by evaluating how the rain-on-grid approach performs in HEC-HMS and HEC-RAS and understand how each model responds under different configuration setups. Although both models produced satisfactory to very good depth and velocity results based on NSE classifications, their outputs displayed clear differences when the model configurations were varied.

In our study, one of the most important distinctions between HEC-HMS 2D and HEC-RAS 2D in continuous rain-on-grid simulations is how baseflow is treated. HEC-HMS includes explicit baseflow modules using linear reservoir baseflow method, while HEC-RAS 2D in rain-on-grid mode represents only surface processes. In our simulations, routing a portion of infiltrated water to the surface as baseflow in HEC-HMS produced hydrographs with a more realistic recession limb and cumulative runoff volume between events. When the same watershed was simulated with HEC-RAS 2D using only surface runoff, inter-event flows were underpredicted. This contrast gives an insight on a broader limitation when hydraulic models such as HEC-RAS are applied to long-term watershed simulation. Although these models are highly effective for representing flood wave propagation, spatially distributed inundation, and peak timing, they lead to biased water balances and unrealistic low flow conditions. Our findings are consistent with recent studies that emphasize the importance of representing groundwater in continuous modelling. Bragg et al. (2025), for example, compared scenarios with and without a groundwater module in a semi-urban watershed using SWMM and showed that including a baseflow component substantially improved the overall water balance. Similarly, Holberg, (2015) reported that combining a soil moisture

accounting loss method with a linear reservoir baseflow option in HEC-HMS yielded more realistic runoff volumes and recession behavior. Together, these results indicate that explicit baseflow representation is a key requirement for extending rain-on-grid frameworks beyond event-based flood analysis toward continuous watershed simulation.

One critical factor affecting our results was the choice of infiltration model for continuous simulation. Although a similar study by Fanta & Tadesse (2022) reported good long-term performance using the SCS -CN method, our HEC-HMS runs with SCS-CN produced reasonable agreement for the first few storms but increasingly overpredicted runoff in later events. We attribute this discrepancy to the event-based nature of SCS-CN, which in HEC-HMS effectively treats a sequence of storms as a single event and does not maintain a dynamic soil moisture store that can be depleted and then rebuilt between storms. In reality, soils lose water through drainage and evapotranspiration during dry intervals, and because SCS-CN in HEC-HMS does not carry soil moisture forward or apply evapotranspiration to a continuous soil store, the catchment remains unrealistically wet, leading to excess runoff in successive storms. This limitation is consistent with the HEC-HMS user manual, which recommends SCS-CN for event simulations rather than for continuous applications. In our HEC-RAS 2D runs, resetting the initial soil moisture conditions between events partially mitigated this problem and improved hydrograph shape, but the cumulative runoff volumes were still biased. To address this, we adopted the Deficit and Constant (D&C) loss method in HEC-HMS, coupled with an evapotranspiration model, which provided more realistic behavior for continuous simulations. With D&C, the soil moisture deficit was reduced during storms and gradually rebuilt during dry periods, and the resulting hydrographs showed more consistent timing and magnitude across sequences of storms. This continuous accounting also clarified the separation between surface runoff routing and baseflow generation.

When we first applied D&C without an explicit baseflow component, the modeled peaks and recessions remained too low and slightly steep compared with observations, but introducing a linear reservoir to represent delayed subsurface flow improved the agreement with observed flow as discussed earlier. Overall, these results suggest that in fully distributed rain-on-grid simulations, hydrograph realism is controlled largely by the loss formulation, its ability to store soil moisture state, and an appropriate baseflow representation rather than by the routing scheme alone. In our study, using a loss method designed for continuous simulation such as D&C together with an explicit baseflow reservoir was necessary to reproduce both storm peaks and inter-event baseflow, which is consistent with the conclusions of Odey & Cho (2025) for long-term HEC-HMS applications.

Our results indicate that the event-scale runoff coefficients computed from the continuous HEC-HMS 2D simulations varied from storm to storm in response to antecedent soil moisture and storm intensity. Before larger storm events, the soil-moisture accounting module indicated higher saturation, which led to higher runoff efficiency. This behavior is consistent with previous PCSWMM applications in the Moore's Mill Creek watershed, which calculated time-varying runoff coefficients and reported a systematic increase in runoff fraction as the catchment became progressively wetter, similar to the pattern observed in our simulations (Bragg et al., 2025). Compared with HEC-HMS 2D results, the PCSWMM models tend to produce somewhat higher runoff coefficients; however, these differences are likely influenced by differences in model configuration, loss methods, calibration strategy, and monitoring locations, so a strict one-to-one comparison is not possible. Xu et al. (2024) also examined tens of thousands of rainfall–runoff events in the Ohio River region and found that the same watershed can generate a small runoff fraction during one storm and a much larger fraction during a subsequent storm when the soil is

wet, further reinforcing that runoff coefficients are highly event-dependent. In contrast, design approaches that rely on a single runoff coefficient for each land-use category, such as the traditional Rational Method, cannot represent this dependence on antecedent conditions and storm sequencing, a limitation that is also acknowledged in the WSDOT Hydraulics Manual (2025).

In addition, different scenarios in this study showed that the use of the SCS-CN loss method (HMS – No BF – CN, HMS – BF – CN, RAS – CN) consistently yielded higher cumulative volumes and higher event runoff coefficients than the corresponding Deficit and Constant runs, which indicates a lower effective infiltration capacity in the CN based formulations. However, since CN in this study were not calibrated, but imported directly from the QGIS CN look up values, it might be inappropriate to conclude about this. Furthermore, turning on the baseflow module (HMS – BF and HMS – BF – CN) further increased both cumulative discharge and event runoff coefficients compared with the no baseflow cases, because groundwater discharge also added to stormflow volume. Taken together, these patterns also show that the effective runoff coefficient in this semi urban catchment is a dynamic outcome of antecedent soil moisture, baseflow state, rainfall intensity, and the chosen loss formulation, rather than an intrinsic constant tied only to land use.

## **4.2 Limitations**

Even though HEC-HMS and HEC-RAS were configured with the same rain-on-grid configuration, unstructured mesh, and closely aligned solver settings, the comparison is still shaped by the coverage and quality of the data available for calibration and evaluation. Discharge was measured only at the outlet near Bent Creek Road (BCR), so both models were ultimately tuned and compared on a single hydrograph. Within the interior of the mesh, we evaluated model

behavior at Hamilton using depth and velocity time series rather than discharge. Those internal checks are valuable, but they do not provide a full stage–discharge relationship or an independent volumetric constraint. As a result, it remains possible for parameter sets to reproduce the BCR discharge record while routing water somewhat differently within the basin. A second gauged outlet, with a separate junction point at the HAM station and its own rating curve and flow record, would strengthen the calibration by ensuring consistency in recession behavior and cumulative volume at more than one location.

The observations used to construct and interpret discharge also carry uncertainty. Any rating curve derived from a finite number of paired stage and velocity measurements carries non-trivial error, particularly at high flows and on the recession limb. Studies of rating curves in river networks show that both low and high flows can be substantially uncertain even when the underlying stage data are accurate (Jalbert et al., 2011). At HAM and BCR, the velocity data used to support head–velocity relationships are sensitive to the behavior of the acoustic Doppler area–velocity sensor, whose performance depends on the presence of suspended particles and bubbles to scatter the acoustic signal (Rehmel, 2007). Such devices can underestimate or produce noisier velocities when suspended sediment concentrations are low or when flow conditions deviate from the ideal sampling geometry. Furthermore, periods of partial fouling or misalignment can reduce confidence in the depth–velocity relationship, especially during small events and late recessions when the signal is weakest. Small timing offsets among stage and velocity loggers add an additional layer of uncertainty to peak timing and rising-limb shape.

Uncertainty in the rainfall is another important limitation. The spatial variability of rainfall is widely recognized as a dominant source of error in flood and runoff modeling (Arnaud et al.,

2011). In this study, the limited spatial coverage means that subcatchment-scale gradients and short-duration intensity peaks may not be fully captured, as was seen in the BCR validation phase. Because both HEC-HMS and HEC-RAS used the same gridded rainfall inputs, any bias in storm structure, timing, or magnitude is inherited by both configurations. In addition to the spatial data coverage, instrumentation in this study was also sensitive to environmental conditions. Moore (2016) reported that HOBO U20 pressure loggers exhibit temperature-dependent drift, meaning the recorded pressure (and thus water level) can gradually deviate from actual conditions as temperature changes. In our deployments, temperature appeared to affect the rain gauges as well, because the units were more likely to shut down early or produce missing records during periods of very high or very low air temperature.

Terrain and elevation data introduce additional, shared uncertainty. Flood and runoff models are highly sensitive to the quality of the digital elevation model (DEM), including its resolution, vertical accuracy, and ability to represent small features such as low berms, roadway crowns, and shallow swales. In this work, the unstructured mesh was derived from an existing DEM that does not fully capture bathymetry below the water surface and may smooth or omit microtopography that influences connectivity and floodplain storage. Vertical-datum inconsistencies between the DEM, surveyed control points, and sensor reference elevations can shift absolute water levels by several centimeters, which is enough to change the onset of overbank flow and the apparent match to observed stages. Since both HEC-HMS and HEC-RAS share this geometric foundation, agreement between the two models at certain locations may reflect common topographic limitations rather than precise representation of field conditions.

Finally, the interpretation of the calibrated models is constrained by equifinality, the idea that many different parameter sets and sometimes different model structures can produce similarly acceptable simulations when compared against limited data. With only one discharge gauge at BCR, multiple combinations of loss parameters, transform parameters, and baseflow settings in HEC-HMS can reproduce the outlet hydrograph while implying different balances between rapid runoff and delayed groundwater contributions. The identical mesh and solver settings help isolate the added value of explicit baseflow representation, but they do not remove the non-uniqueness imposed by sparse observations, uncertain rainfall, and elevation errors.

## Chapter 5: Conclusions and Recommendations

### 5.1 Conclusions

Overall, HEC-HMS 2D demonstrated significant advantages in simulating continuous hydrological processes, primarily due to its ability to represent baseflow (groundwater contributions). Incorporating a simple linear reservoir baseflow in HEC-HMS greatly improved the simulation of inter-event flows and resulted in more realistic hydrograph recessions and cumulative runoff volume. In contrast, HEC-RAS 2D, which lacks an explicit groundwater component, underpredicted inter-event flows and caused the hydrograph to recede too quickly, resulting in a lower cumulative runoff volume over time. In principle, a modeler could attempt to mimic baseflow in HEC-RAS 2D using low-flow boundary conditions or distributed lateral inflows, but under the comparable set of assumptions and parameter choices tested here, the rain-on-grid RAS simulations did not match the observed inter-event response. As a result, the explicit baseflow mechanism in HEC-HMS, when calibrated together with more sensitive hydrologic parameters like loss parameters, baseflow fraction and Manning's roughness for the channel and floodplain, provided a more consistent representation of both flood peaks and low flows and a more balanced water budget than HEC-RAS 2D.

Notably, the choice of loss/infiltration method in HEC-HMS was crucial: for continuous multi-event simulation, the simple SCS-CN method proved inadequate, as it does not reset soil moisture between events. Instead, a continuous loss model such as the Deficit-and-Constant method was necessary to realistically represent infiltration and runoff generation over weeks of rainfall. This underscores the importance of selecting the appropriate loss model based on the

simulation goal. SCS-CN is best suited for event-based modeling, while continuous simulations require methods that account for infiltration capacity recovery between storms.

The dynamic runoff response further illustrated that runoff coefficients in the watershed are not constant. The effective runoff percentage varied between storms, depending on soil saturation and rainfall patterns. This variability, captured naturally by the hydrologic model, emphasizes the advantage of using a physics-based simulation over simpler methods like the Rational method, which assumes a fixed runoff coefficient for a given land use.

In summary, this research demonstrated that the improved 2D rain-on-grid module in HEC-HMS provides significant benefits over HEC-RAS 2D for simulating rainfall-runoff processes in a semi-urban watershed. HEC-HMS 2D offered a more complete hydrological representation by accounting for infiltration and groundwater flow, leading to a more accurate continuous simulation of the hydrograph, particularly in terms of volume and recession, without sacrificing accuracy in peak flows or timings. While HEC-RAS 2D remains a powerful hydraulic model that excels at detailed spatial flood dynamics and peak timing, it showed clear limitations for continuous hydrologic prediction due to its lack of a baseflow mechanism. For applications requiring modeling beyond single storm events, such as water resource assessments, baseflow-dominated low-flow analysis, or long-term watershed simulations, HEC-HMS 2D appears to be the more suitable and powerful model.

## **5.2 Recommended Future Investigations**

While this thesis focused on a one-month period and a single watershed configuration, several opportunities exist to extend and generalize the findings.

- Future studies should apply the HEC-HMS 2D and HEC-RAS 2D comparison over longer periods (multiple months or years) and across different seasonal conditions. This would test the stability and transferability of calibrated parameters, such as baseflow coefficients and transform method settings, over time and ensure that the conclusions hold under varying weather patterns or climate conditions.
- Exploring coupling strategies between the two models could yield the best of both worlds. For example, one could use HEC-HMS 2D as a hydrologic preprocessor to generate runoff hydrographs (including baseflow) for each subbasin, then use those as boundary conditions in HEC-RAS 2D for detailed hydraulic routing through the river network. Alternatively, HEC-RAS 2D could be enhanced by adding spatially distributed lateral inflows that mimic groundwater contributions, improving its continuous simulation without full coupling to see if this setup outperforms over full rain-on-grid.
- Assessing the sensitivity of the model comparisons to different rainfall inputs and temporal scales would be valuable. Using alternative rainfall products (e.g., radar-based estimates or different gridded precipitation datasets) and experimenting with different temporal aggregation (time-step sizes) could help distinguish input data uncertainty from model structural differences.
- Future research should consider increasing the spatial complexity of the HEC-HMS model by subdividing the watershed into multiple sub-basins or internal elements. In the current study, flows were primarily evaluated at the watershed outlet. By introducing more sub-basins and junctions, one could evaluate the models' ability to simulate distributed flows at interior locations, not just at a single outlet. This would determine whether HEC-HMS 2D can effectively represent the spatial distribution of runoff generation across a larger

network and whether HEC-RAS 2D might perform differently when multiple inflow points are considered. It is also worth exploring the performance trade-offs between a fully 2D modeling approach (rainfall on a gridded surface, as done here) and a more traditional semi-distributed approach in HEC-HMS (where each sub-basin is treated with lumped parameters and an empirical unit hydrograph). Comparing these methods could reveal whether the 2D explicit routing offers significant accuracy or insight to justify its higher computational cost, or if a calibrated semi-distributed model can achieve similar results more efficiently.

- Evaluating alternative model components and representations will further strengthen the conclusions. Testing different loss models (such as Green-Ampt infiltration or the Soil Moisture Accounting method) in HEC-HMS would help determine if the advantages observed with the Deficit-and-Constant method are generalizable. Likewise, incorporating more detailed soil or land cover representations could help assess whether the findings related to roughness sensitivity and grid resolution hold under varied conditions. Sixth, scaling up the modeling framework to larger or more complex watersheds would test the feasibility and practicality of using HEC-HMS 2D for large watersheds. If the approach remains accurate and computationally practical for a full watershed or a basin with many sub-catchments, it suggests strong potential for real-world operational use. Conversely, challenges at larger scales, such as longer run times or calibration difficulties, would provide valuable insight for model developers and users.
- Finally, a natural extension of this work is to connect hydrologic simulations with sediment transport or water quality analyses. Improved flow simulation in both time and space could enhance sediment modeling, as knowing where and when water is flowing allows for better

predictions of erosion, sediment yield, and deposition patterns. Earlier exploratory modeling in this watershed suggested that spatially distributed models can help identify hotspots for erosion and deposition. Incorporating a sediment transport component could validate whether the flows generated by the hydrologic model translate into realistic sediment movement. This would add a valuable dimension to the analysis and support decision-making for watershed management in MMC, such as identifying priority areas for erosion control or understanding how storm events and baseflow conditions contribute to sediment delivery.

## References

- Acer Engineering, LLC. 2008. Moore's Mill Creek Watershed Management Plan Lee County, Alabama. Atlanta, GA: Acer Environmental, Inc.
- Alabama Department of Environmental Management. 2024b. "Alabama's Water Quality Assessment and Listing Methodology." Accessed November 24, 2025. <https://adem.alabama.gov/programs/water/wquality/2024WAM.pdf>
- Arnaud, P., Lavabre, J., Fouchier, C., Diss, S., & Javelle, S. P. (2011). Sensibilité des modèles hydrologiques aux incertitudes dues à l'information pluviométrique. *Hydrological Sciences Journal*, 56(3), 397–410. <https://doi.org/10.1080/02626667.2011.563742;WGROU:STRING:PUBLICATION>
- Beven, K. (1989). Changing ideas in hydrology — The case of physically-based models. *Journal of Hydrology*, 105(1–2), 157–172. [https://doi.org/10.1016/0022-1694\(89\)90101-7](https://doi.org/10.1016/0022-1694(89)90101-7)
- Bragg, M. A. (2025). *Modeling hydrology and water quality in Moore's Mill Creek using the Storm Water Management Model (SWMM)*. <https://etd.auburn.edu/handle/10415/9693>
- Bragg, M. A., Poudel, A., & Vasconcelos, J. G. (2025). Comparing SWMM and HEC-RAS Hydrological Modeling Performance in Semi-Urbanized Watershed. *Water* 2025, Vol. 17, Page 1331, 17(9), 1331. <https://doi.org/10.3390/W17091331>
- Bratton, A. (2017). *A comparison of 1D and 2D HEC-RAS models of the napa river through the city of St. Helena, California*. <https://scholarworks.calstate.edu/concern/projects/pc289r04z>
- City of Auburn (COA). 2025. *City of Auburn Map*. Retrieved November 24, 2025, from <https://webgis.auburnalabama.org/coamap/>

- City of Auburn Dashboard, COA (2025). *Watershed - City of Auburn*. Retrieved November 20, 2025, from <https://www.auburnal.gov/water-resource-management/watershed/>
- Costabile, P., Costanzo, C., Ferraro, D., & Barca, P. (2021). Is HEC-RAS 2D accurate enough for storm-event hazard assessment? Lessons learnt from a benchmarking study based on rain-on-grid modelling. *Journal of Hydrology*, *603*, 126962.  
<https://doi.org/10.1016/J.JHYDROL.2021.126962>
- Costabile, P., Macchione, F., Natale, L., & Petaccia, G. (2015). Flood mapping using LIDAR DEM. Limitations of the 1-D modeling highlighted by the 2-D approach. *Natural Hazards* *2015 77:1*, *77*(1), 181–204. <https://doi.org/10.1007/S11069-015-1606-0>
- Ennouini, W., Fenocchi, A., Petaccia, G., Persi, E., & Sibilla, S. (2024). A complete methodology to assess hydraulic risk in small ungauged catchments based on HEC-RAS 2D Rain-On-Grid simulations. *Natural Hazards* *2024 120:8*, *120*(8), 7381–7409.  
<https://doi.org/10.1007/S11069-024-06515-2>
- Fanta, S. S., & Tadesse, S. T. (2022). Application of HEC–HMS for runoff simulation of Gojeb Watershed, Southwest Ethiopia. *Modeling Earth Systems and Environment* *2022 8:4*, *8*(4), 4687–4705. <https://doi.org/10.1007/S40808-022-01397-4>
- Fernando, L., & Galvis, C. (2023). *Effect of hydrologic and hydraulic calculation approaches on pier scour estimates*. <https://etd.auburn.edu/handle/10415/9073>
- GSHHA (2025). *Gridded Surface Subsurface Hydrologic Analysis (GSSHA) model - Engineering With Nature*. Retrieved November 10, 2025, from <https://ewn.erd.c.dren.mil/tools/gridded-surface-subsurface-hydrologic-analysis-gssha-model/>

HEC-HMS Technical Reference Manual (2025). Retrieved November 21, 2025, from <https://www.hec.usace.army.mil/confluence/hmsdocs/hmstrm>

HEC-HMS User's Manual (2025). Retrieved November 10, 2025, from <https://www.hec.usace.army.mil/confluence/hmsdocs/hmsum/latest>

HEC-RAS. Retrieved November 20, 2025, from <https://www.hec.usace.army.mil/software/hecras/>

HEC-RAS Hydraulic Reference Manual (2025). Retrieved November 24, 2025, from <https://www.hec.usace.army.mil/confluence/rasdocs/ras1dtechref/latest>

Holberg, J. (2015). Downward model development of the soil moisture accounting loss method in HEC-HMS: Revelations concerning the soil profile. *Open Access Theses*. [https://docs.lib.purdue.edu/open\\_access\\_theses/501](https://docs.lib.purdue.edu/open_access_theses/501)

Hossain, S., Hewa, G. A., & Wella-Hewage, S. (2019). A Comparison of Continuous and Event-Based Rainfall–Runoff (RR) Modelling Using EPA-SWMM. *Water* 2019, Vol. 11, Page 611, 11(3), 611. <https://doi.org/10.3390/W11030611>

Jalbert, J., Mathevet, T., & Favre, A. C. (2011). Temporal uncertainty estimation of discharges from rating curves using a variographic analysis. *Journal of Hydrology*, 397(1–2), 83–92. <https://doi.org/10.1016/J.JHYDROL.2010.11.031>

Jones, J. A. A. (2014). Global hydrology: Processes, resources and environmental management. *Global Hydrology: Processes, Resources and Environmental Management*, 1–399. <https://doi.org/10.4324/9781315844398>

- Kampf, S. K., & Burges, S. J. (2007). Parameter estimation for a physics-based distributed hydrologic model using measured outflow fluxes and internal moisture states. *Water Resources Research*, 43(12), 12414. <https://doi.org/10.1029/2006WR005605>
- Khakbaz, B., Imam, B., Hsu, K., & Sorooshian, S. (2012). From lumped to distributed via semi-distributed: Calibration strategies for semi-distributed hydrologic models. *Journal of Hydrology*, 418–419, 61–77. <https://doi.org/10.1016/J.JHYDROL.2009.02.021>
- Machado, R. E., Cardoso, T. O., & Mortene, M. H. (2022). Determination of runoff coefficient (C) in catchments based on analysis of precipitation and flow events. *International Soil and Water Conservation Research*, 10(2), 208–216. <https://doi.org/10.1016/J.ISWCR.2021.09.001>
- MIKE SHE (2025). *MIKE SHE | Integrated Hydrological Modelling Software*. Retrieved November 10, 2025, from <https://www.dhigroup.com/technologies/mikepoweredbydhi/mike-she>
- Miller, M. P., Buto, S. G., Susong, D. D., & Rumsey, C. A. (2016). The importance of base flow in sustaining surface water flow in the Upper Colorado River Basin. *Water Resources Research*, 52(5), 3547–3562. <https://doi.org/10.1002/2015WR017963;REQUESTEDJOURNAL:JOURNAL:19447973;ISSUE:ISSUE:DOI>
- Moore, M. 2016. “Measuring and modeling stormwater runoff from an interstate in a rural/forested watershed.” Ph.D. Dissertation, Auburn University.
- Moriasi, D. N., Arnold, J. G., Liew, M. W. Van, Bingner, R. L., Harmel, R. D., & Veith, T. L. (2007). Model Evaluation Guidelines for Systematic Quantification of Accuracy in Watershed

Simulations. *Transactions of the ASABE*, 50(3), 885–900.

<https://doi.org/10.13031/2013.23153>

Odey, G., & Cho, Y. (2025). Event-Based vs. Continuous Hydrological Modeling with HEC-HMS:

A Review of Use Cases, Methodologies, and Performance Metrics. *Hydrology*, 12(2).

<https://doi.org/10.3390/HYDROLOGY12020039/S1>

Onset (2025). *Onset HOBO and InTemp Data Loggers*. Retrieved November 20, 2025, from

[https://www.onsetcomp.com/?srsltid=AfmBOorbxiHzlTKpmW\\_POymI1Iao2jlyFXSprb9ajIyFCUfbSGXpskq9](https://www.onsetcomp.com/?srsltid=AfmBOorbxiHzlTKpmW_POymI1Iao2jlyFXSprb9ajIyFCUfbSGXpskq9)

Reed, S., Koren, V., Smith, M., Zhang, Z., Moreda, F., Seo, D. J., Arnold, J., Bandaragoda, C.,

Bingeman, A., Bras, R., Butts, M., Carpenter, T., Cui, Z., Diluzio, M., Georgakakos, K., Gaur,

A., Guo, J., Gupta, H., Hogue, T., ... Woods, R. (2004). Overall distributed model intercomparison project results. *Journal of Hydrology*, 298(1–4), 27–60.

<https://doi.org/10.1016/J.JHYDROL.2004.03.031>

Rehmel, M. (2007). Application of Acoustic Doppler Velocimeters for Streamflow Measurements.

*Journal of Hydraulic Engineering*, 133(12), 1433–1438.

[https://doi.org/10.1061/\(ASCE\)0733-9429\(2007\)133:12\(1433\)](https://doi.org/10.1061/(ASCE)0733-9429(2007)133:12(1433))

Sahu, M. K., Shwetha, H. R., & Dwarakish, G. S. (2023). State-of-the-art hydrological models and

application of the HEC-HMS model: a review. *Modeling Earth Systems and Environment*

2023 9:3, 9(3), 3029–3051. <https://doi.org/10.1007/S40808-023-01704-7>

- Sánchez-Gómez, A., Schürz, C., Molina-Navarro, E., & Bieger, K. (2024). Groundwater modelling in SWAT+: Considerations for a realistic baseflow simulation. *Groundwater for Sustainable Development*, 26. <https://doi.org/10.1016/J.GSD.2024.101275>
- Singh, W. R., & Jain, M. K. (2015). Continuous Hydrological Modeling using Soil Moisture Accounting Algorithm in Vamsadhara River Basin, India. *Journal of Water Resource and Hydraulic Engineering*, 4(4), 398–408. <https://doi.org/10.5963/JWRHE0404011>
- US Climate Data (2025). *Auburn climate: Weather Auburn & temperature by month*. Retrieved December 7, 2025, from <https://en.climate-data.org/north-america/united-states-of-america/alabama/auburn-17365/>
- USDA: NRCS: Geospatial Data Gateway (2025). Retrieved November 24, 2025, from <https://datagateway.nrcs.usda.gov/GDGHome.aspx>
- USDA Natural Resources Conservation Service (2015). Soil Survey Geographic Database (SSURGO). Natural Resources Conservation Service, United States Department of Agriculture. Dataset. <https://doi.org/10.15482/USDA.ADC/1242479>
- U.S. Department of Agriculture. 2024. Soil Survey Geographic Database (SSURGO). Accessed February 28, 2025: <https://doi.org/10.15482/USDA.ADC/1242479>
- U.S. Geological Survey. 2024. Annual National Land Cover Database. Accessed on February 28, 2025. <https://www.usgs.gov/centers/eros/science/annual-national-land-cover-database>
- U.S. Geological Survey. 2019. *What is Hydrology?* | *U.S. Geological Survey*. (2019). Retrieved November 8, 2025, from <https://www.usgs.gov/water-science-school/science/what-hydrology>

- Vasconcelos, J. G., Fang, X., Geller, V. G., Nicolaico, G. G., & Reyes, E. M. (2023). Resilient Design with Distributed Rainfall-Runoff Modeling. *Resilient Design with Distributed Rainfall-Runoff Modeling*. <https://doi.org/10.17226/27051>
- Web Soil Survey (2025). Retrieved November 24, 2025, from [https://websoilsurvey.nrcs.usda.gov/app/HomePage.htm?TARGET\\_APP=Web\\_Soil\\_Surv](https://websoilsurvey.nrcs.usda.gov/app/HomePage.htm?TARGET_APP=Web_Soil_Surv)
- Wolff-Piggott, B., & Gorgens, A. H. M. *Demonstrating the potential of GIS technology in hydrosalinity modelling through interfacing the DISA model and a GIS EXECUTIVE SUMMARY Background*.
- Xiao, H. (2022). *Evaluating alternatives for the implementation of Curve Number in SWMM for an urbanized watershed*.
- Xiao, H., & Vasconcelos, J. G. (2022). Evaluating Curve Number Implementation Alternatives for Peak Flow Predictions in Urbanized Watersheds Using SWMM. *Water* 2023, Vol. 15, Page 41, 15(1), 41. <https://doi.org/10.3390/W15010041>
- Xu, T., Li, P. C., & Merwade, V. (2024). Analysis of short- and long-term controls on the variability of event-based runoff coefficient. *Journal of Hydrology: Regional Studies*, 56, 101993. <https://doi.org/10.1016/j.ejrh.2024.101993>
- Zeiger, S. J., & Hubbart, J. A. (2021). Measuring and modeling event-based environmental flows: An assessment of HEC-RAS 2D rain-on-grid simulations. *Journal of Environmental Management*, 285, 112125. <https://doi.org/10.1016/J.JENVMAN.2021.112125>

Zhang, Z. (2025). Performance of long-term continuous hydrological models in fluvial flow simulation in a large-scale river basin. *Scientific Reports* 2025 15:1, 15(1), 1–16.  
<https://doi.org/10.1038/s41598-025-06387-x>

## Appendix A: CN Look Up Table

NLCD Value	NLCD Land Cover Classification	Hydrological Soil Group			
		A	B	C	D
11	Open Water	100	100	100	100
12	Perennial Ice/Snow	100	100	100	100
21	Developed, Open	52	68	78	84
22	Low Intensity Development	81	88	90	93
23	Medium Intensity Development	84	89	93	94
24	High Intensity Development	88	92	93	94
31	Barren Land	70	81	88	92
41	Deciduous Forest	45	66	77	83
42	Evergreen Forest	30	55	70	77
43	Mixed Forest	36	60	73	79
51	Dwarf Scrub	33	42	55	62
52	Shrub	33	42	55	62
71	Grassland	47	63	75	85
72	Sedge	47	63	75	85
73	Lichens	74	74	74	74
74	Moss	79	79	79	79
81	Pasture	40	61	73	79
82	Cropland	62	74	82	86
90	Woody Wetland	86	86	86	86
95	Emergent Wetlands	80	80	80	80

## Appendix B: Python Code for Rain Data Extraction from COA

```
12 import os
13 import sys
14 import json
15 import requests
16 import pandas as pd
17 from pathlib import Path
18 from datetime import datetime, timezone
19 from zoneinfo import ZoneInfo
20
21 # -----
22 # Configuration
23 # -----
24 URL = "https://www.licor.cloud/api/dashboard/public/query"
25 DASHBOARD_ID = "52f7495a-bd9c-48ff-a568-20431bc95b60"
26 METRIC_NAME = "com.onset.sensordata.rain_us"
27 DATACHANNEL_ID = "b41b722b-ed1a-4295-94b2-22c3847837e9"
28
29 # Optional: set LICOR_COOKIE in your environment
30 # PowerShell: $env:LICOR_COOKIE = "li_security=...; other=..."
31 # CMD:       setx LICOR_COOKIE "li_security=...; other=..."
32 COOKIE = os.environ.get("LICOR_COOKIE", "").strip()
33
34 LOCAL_TZ_NAME = "America/Chicago"
35 LOCAL_TZ = ZoneInfo(LOCAL_TZ_NAME)
36
37 # Output base: auto-detect Box folder under current user profile
38 def _detect_box_root() -> Path:
39     home = Path.home()
40     candidates = [
41         home / "Box",
42         home / "Box Sync",
43         home / "Box Drive",
44         home / "Box" / "Drive",      # some enterprise installs
45     ]
46     for p in candidates:
47         if p.exists():
48             return p
49     # Fallback to Documents if no Box path found
50     return home / "Documents" / "Box_Fallback"
51
52 BOX_ROOT = _detect_box_root()
53
54 # Your desired subpath
55 OUT_DIR = BOX_ROOT / "Vasconcelos Group Contributions" / "Ashmita Poudel" / "Data" / "COA"
--
```

```

    HEADERS = {
        "accept": "application/json, text/plain, */*",
        "content-type": "application/json",
        "origin": "https://www.licor.cloud",
        "referer": f"https://www.licor.cloud/dashboards/public/{DASHBOARD_ID}/true",
        "user-agent": "python-requests",
    }
    if COOKIE:
        HEADERS["cookie"] = COOKIE

# -----
# Helpers
# -----
def to_epoch_ms(dt_utc: datetime) -> int:
    if dt_utc.tzinfo is None:
        raise ValueError("to_epoch_ms expects an aware datetime in UTC")
    return int(dt_utc.timestamp() * 1000)

def build_body_absolute(start_utc: datetime, end_utc: datetime) -> dict:
    """
    Build the absolute-time query body at 5-minute sampling.
    End is exclusive as per typical time-range conventions.
    """
    return {
        "id": DASHBOARD_ID,
        "query": {
            "limit": 10000, # ~6,336 points for this range at 5-min sampling
            "metrics": [{
                "aggregators": [{
                    "name": "avg",
                    "align_start_time": False,
                    "sampling": {"value": 5, "unit": "minutes"}
                }],
                "name": METRIC_NAME,
                "exclude_tags": True,
                "group_by": [],
                "tags": {"dataChannel": [DATACHANNEL_ID]},
            }],
        "start_absolute": to_epoch_ms(start_utc),
        "end_absolute": to_epoch_ms(end_utc),
    }
}

```

```

def fetch_absolute(start_utc: datetime, end_utc: datetime) -> list[dict]:
    body = build_body_absolute(start_utc, end_utc)
    try:
        r = requests.post(URL, headers=HEADERS, json=body, timeout=60)
    except requests.RequestException as e:
        raise SystemExit(f"Network error calling Li-Cor API: {e}") from e

    # Helpful diagnostics on failures
    if r.status_code >= 400:
        detail = r.text
        try:
            detail = json.dumps(r.json(), indent=2)
        except Exception:
            pass
        raise SystemExit(
            f"Li-Cor API returned HTTP {r.status_code}.\n"
            f"Response body:\n{detail}"
        )

    try:
        data = r.json()
    except ValueError as e:
        raise SystemExit(f"Invalid JSON from API: {e}\nRaw text:\n{r.text[:1000]}") from e

    rows = []
    for q in data.get("queries", []):
        for res in q.get("results", []):
            for ts_ms, val in res.get("values", []):
                ts = datetime.fromtimestamp(ts_ms / 1000, tz=timezone.utc)
                rows.append({"timestamp_utc": ts, "value": val})

    return rows

def ensure_out_dir(path: Path) -> None:
    try:
        path.mkdir(parents=True, exist_ok=True)
    except PermissionError as e:
        raise SystemExit(
            f"Permission denied creating output folder:\n {path}\n"
            "Choose a folder you own, or run the IDE with sufficient rights."
        ) from e

```

```

# -----
# Main
# -----
def main():
    # Date range in local time:
    # Start: 2025-06-07 00:00 local, inclusive
    # End:   2025-06-29 00:00 local, exclusive
    start_local = datetime(2025, 6, 7, 0, 0, tzinfo=LOCAL_TZ)
    end_local   = datetime(2025, 6, 29, 0, 0, tzinfo=LOCAL_TZ)

    start_utc = start_local.astimezone(timezone.utc)
    end_utc   = end_local.astimezone(timezone.utc)

    print(f"Querying {METRIC_NAME}")
    print(f"Local window: {start_local} to {end_local} ({LOCAL_TZ_NAME}, end exclusive)")
    print(f"UTC window:   {start_utc} to {end_utc} (end exclusive)")

    rows = fetch_absolute(start_utc, end_utc)
    df = pd.DataFrame(rows).sort_values("timestamp_utc")

    if df.empty:
        print("No data returned for the specified range.")
        return

    # Add a local-time convenience column
    df["timestamp_local"] = df["timestamp_utc"].dt.tz_convert(LOCAL_TZ_NAME)

    # Prepare output
    ensure_out_dir(OUT_DIR)
    out_path = OUT_DIR / f"Lake_Ogeltree_rain_5min_{start_local.date()}_to_{end_local.date()}.csv"

    df.to_csv(out_path, index=False)
    print(f"Saved {len(df)} rows to {out_path}")

    # Optional: quick preview
    print(df.head(3).to_string(index=False))

if __name__ == "__main__":
    try:
        main()
    except KeyboardInterrupt:
        sys.exit(130)

```

## Appendix C: VBA Code for Error Metrics

```
' Calculate RMSE and NSE

Public Function CalcRMSE(ObsRange As Range, SimRange As Range, Optional NumParameters As Long = 0) As Double

    Dim i As Long
    Dim n As Long
    Dim obsSum As Double, obsMean As Double
    Dim numeratorRMSE As Double, denominatorRMSE As Double
    Dim obsVal As Variant, simVal As Variant
    Dim calculatedRMSE As Double

    ' Check that ranges are the same size
    If ObsRange.Count <> SimRange.Count Then
        CalcRMSE = CVErr(xlErrValue)
        Exit Function
    End If

    n = ObsRange.Count

    ' Calculate RMSE (Root Mean Square Error)
    For i = 1 To n
        obsVal = ObsRange.Cells(i, 1).Value
        simVal = SimRange.Cells(i, 1).Value
        If IsNumeric(obsVal) And IsNumeric(simVal) Then
            numeratorRMSE = numeratorRMSE + (obsVal - simVal) ^ 2
        End If
    Next i

    Dim denomRMSE As Long
    denomRMSE = n - NumParameters
    If denomRMSE <= 0 Then
        calculatedRMSE = CVErr(xlErrDiv0)
    Else
        calculatedRMSE = Sqr(numeratorRMSE / denomRMSE)
    End If

    ' Return RMSE
    CalcRMSE = calculatedRMSE
End Function
```

---

```

Public Function NSE(ObsRange As Range, SimRange As Range) As Double
    Dim i As Long
    Dim n As Long
    Dim obsSum As Double, obsMean As Double
    Dim numeratorNSE As Double, denominatorNSE As Double
    Dim obsVal As Variant, simVal As Variant
    Dim calculatedNSE As Double

    ' Check that ranges are the same size
    If ObsRange.Count <> SimRange.Count Then
        NSE = CVErr(xlErrValue)
        Exit Function
    End If

    n = ObsRange.Count

    ' Calculate mean of observed values for NSE
    For i = 1 To n
        obsVal = ObsRange.Cells(i, 1).Value
        If IsNumeric(obsVal) Then obsSum = obsSum + obsVal
    Next i
    obsMean = obsSum / n

    ' Calculate numerator and denominator for NSE
    For i = 1 To n
        obsVal = ObsRange.Cells(i, 1).Value
        simVal = SimRange.Cells(i, 1).Value
        If IsNumeric(obsVal) And IsNumeric(simVal) Then
            ' NSE calculation
            numeratorNSE = numeratorNSE + (obsVal - simVal) ^ 2
            denominatorNSE = denominatorNSE + (obsVal - obsMean) ^ 2
        End If
    Next i

    ' Calculate NSE (Nash-Sutcliffe Efficiency)
    If denominatorNSE = 0 Then
        calculatedNSE = CVErr(xlErrDiv0)
    Else
        calculatedNSE = 1 - (numeratorNSE / denominatorNSE)
    End If

    ' Return NSE
    NSE = calculatedNSE
End Function

```